

PREDICTION OF WAVE FORCES FROM
NONLINEAR RANDOM SEA SIMULATIONS

By

ROBERT TURNER HUDSPETH

A DISSERTATION PRESENTED TO THE GRADUATE COUNCIL OF
THE UNIVERSITY OF FLORIDA
IN PARTIAL FULFILLMENT OF THE REQUIREMENTS FOR THE
DEGREE OF DOCTOR OF PHILOSOPHY

UNIVERSITY OF FLORIDA

1974

*To Alexander Robert,
the personification of convolution
between a filtered response to a
forced input.*

ACKNOWLEDGMENTS

To my wife, Heide, I owe my sincerest appreciation for her encouragement, patience, and understanding during the years of study which were required to prepare this dissertation. I cannot adequately express my deep gratitude for her companionship and concern during this period as a student-wife.

I owe an equally sincere debt of appreciation to the members of my graduate supervisory committee who have contributed individually and collectively to my interest in and understanding of the physics of coastal processes. Professor R. G. Dean, Department of Civil and Coastal Engineering, served as chairperson and he provided, through his extensive experience and knowledge of wave hydromechanics, enormous insight and assistance in reducing complex problems to relatively tractable solutions having engineering applications. Professor O. H. Shemdin, Department of Civil and Coastal Engineering, and Director, Coastal Engineering Laboratory, has been both counselor and friend. Professor Z. R. Pop-Stojanovic, Department of Mathematics, demonstrated an exceptional facility for transforming the complex mathematics of stochastic processes and random functions into engineering applications.

Professor C. P. Luehr, Department of Mathematics, served on the committee during the early stages and provided much-needed assistance in understanding the mathematical physics of boundary value problems. Professor Ü. Ünluata, Department of Civil and Coastal Engineering, was responsible for leading me to several important references and for providing alternate methods of solutions. As will become obvious to the reader, I have drawn heavily from the publications of Dr. L. E. Borgman in addition to numerous personal discussions with him. I am indebted to Dr. Dean for making these exchanges, *vis-a-vis*, possible. The numerical statistical results which are presented were obtained from a computer program provided by Dr. Borgman.

This study was co-sponsored by the Coastal Engineering Research Center, Department of the Army, and by a Joint Petroleum Industry Wave Force Project. Dr. F. Hsu, AMOCO Production Company, served as Project Manager for the petroleum industry and I have benefited immensely from many discussions with him which have stimulated my interest in this topic. Dr. J. H. Schaub, Chairperson, Department of Civil and Coastal Engineering, and Professor B. D. Spangler, Department of Civil and Coastal Engineering, were most generous in providing funds for computer time and in providing counseling assistance.

Mrs. Evelyn Hill did an exceptional job of typing the original rough draft as well as paying meticulous attention to the details and regulations required for completing degree

work and for ensuring that I met these requirements on time. In typing the rough draft, Mrs. Hill was cheerfully and ably assisted by Mrs. Marilyn Morrison, Tena Jones and Miss Carol Miller. The excellently prepared figures were drafted by Ms. Ferris Stepan and Ms. Denise Frank, frequently under critical time constraints. The final copy was typed with remarkable speed and accuracy, considering the number of equations involved, by Mrs. Elizabeth Godey.

Finally, but quite possibly most importantly, I gratefully acknowledge the assistance, camaraderie, and criticism of my fellow graduate students who, along with Dr. Dean, always managed to somehow find the time and the interest to lend assistance and support when they were required the most.

TABLE OF CONTENTS

	Page
ACKNOWLEDGMENTS	iii
LIST OF TABLES	viii
LIST OF FIGURES	ix
ABSTRACT	xiii
 CHAPTER	
1 INTRODUCTION	1
1. Related Previous Studies	2
2. Linear Superposition and Nonlinear Wave-Wave Interactions	9
3. Simulating Wave Forces by the Digital Linear Filter Technique	16
2 THEORY OF RANDOM NONLINEAR WAVE-WAVE INTERACTIONS	18
1. Random Differential Equations	19
2. Introduction to Random Functions	22
3. Trivariate Function	29
4. Nonlinear Wave-Wave Interactions Correct to Second Perturbation Order	33
5. The Bispectrum	49
6. Second Perturbation Order Spectra	52
3 APPLICATIONS OF NONLINEAR RANDOM SEA SIMULATIONS	57
1. Fourier Series Approximations of the Random Measure	58
2. Fast Fourier Transform (FFT)	63
3. The Bretschneider Spectrum and the Phillips Equilibrium Spectrum	66
4. Hurricane Carla Data (September 8-10, 1961)	73
5. Comparison of Sea Surface Realizations	77
6. Digital Linear Filter	104
7. Comparison of Pressure Forces	114

TABLE OF CONTENTS (continued)

	Page
CHAPTER	
4 CONCLUSIONS AND RECOMMENDATIONS	134
1. Random Sea Simulations Correct to Second Perturbation Order	134
2. Wave Induced Pressure Forces on a Vertical Piling Computed by Digital Linear Filter with "Stretched" Vertical Coordinate	136
3. Recommendations for Additional Applications	139
APPENDIX	
A THE FOUR-PRODUCT MOMENT FOR A GAUSSIAN VARIATE	142
B ALTERNATE QUADRATIC FILTER	145
C EFFECT OF THE HORIZONTAL SPATIAL SEPARATION BETWEEN WAVE STAFF AND INSTRUMENTED PILING ON THE EVALUATION OF PRESSURE FORCE COEFFI- CIENTS	148
LIST OF REFERENCES	156
BIOGRAPHICAL SKETCH	167

LIST OF TABLES

Table		Page
3.1	Rate of Convergence and Final RMS Error Computed for the Best Least-Squares Fit to Measured Spectra from Hurricane Carla for $M_C = 305$	71
3.2	Characteristics of Hurricane Carla Records	75
3.3	Impulse Response Coefficients for Horizontal Velocity Field with Stretched Vertical Coordinate ($h = 99$ ft.)	113
3.4	Drag and Modified Inertia Force Coeffi- cients for Resultant Pressure Forces	114
3.5	Comparison Between Measured and Simulated Pressure Forces at 55 foot Dynamometer Elevation from Hurricane Carla	124
3.6	Statistics of Measured and Simulated Pressure Force Spectra from Hurricane Carla	131

LIST OF FIGURES

Figure	Page
3.1 Smoothed Measured Spectrum and Bretschneider Spectrum of Equal Variance and Best Least-Squares Fit to Peak Frequency for $M_c = 305$ for Record No. 06885/1	78
3.2 Smoothed Measured Spectrum and Bretschneider Spectrum of Equal Variance and Best Least-Squares Fit to Peak Frequency for $M_c = 305$ for Record No. 06886/1	79
3.3 Smoothed Measured Spectrum and Bretschneider Spectrum of Equal Variance and Best Least-Squares Fit to Peak Frequency for $M_c = 305$ for Record No. 06886/2	80
3.4 Smoothed Measured Spectrum and Bretschneider Spectrum of Equal Variance and Best Least-Squares Fit to Peak Frequency for $M_c = 305$ for Record No. 06887/1	81
3.5 Cumulative Probability Distributions for the Normalized Measured Realization and the Linear and Nonlinear Simulated Realizations for Record No. 06885/1	85
3.6 Cumulative Probability Distributions for the Normalized Measured Realization and the Linear and Nonlinear Simulated Realizations for Record No. 06886/1	86
3.7 Cumulative Probability Distributions for the Normalized Measured Realization and the Linear and Nonlinear Simulated Realizations for Record No. 06886/2	87
3.8 Cumulative Probability Distributions for the Normalized Measured Realization and the Linear and Nonlinear Simulated Realizations for Record No. 06887/1	88
3.9 Second Order Spectra Computed from Smoothed Measured Spectrum and from Bretschneider Spectrum for Record No. 06885/1	90

LIST OF FIGURES (continued)

Figure		Page
3.10	Second Order Spectra Computed from Smoothed Measured Spectrum and from Bretschneider Spectrum for Record No. 06886/1	91
3.11	Second Order Spectra Computed from Smoothed Measured Spectrum and from Bretschneider Spectrum for Record No. 06886/2	92
3.12	Second Order Spectra Computed from Smoothed Measured Spectrum and from Bretschneider Spectrum for Record No. 06887/1	93
3.13	Ensemble Comparison Between Measured Realization and Linear and Nonlinear Realizations Simulated from Smoothed Measured Spectrum from Record No. 06885/1	96
3.14	Ensemble Comparison Between Measured Realization and Linear and Nonlinear Realizations Simulated from Smoothed Measured Spectrum from Record No. 06886/1	97
3.15	Ensemble Comparison Between Measured Realization and Linear and Nonlinear Realizations Simulated from Smoothed Measured Spectrum from Record No. 06886/2	98
3.16	Ensemble Comparison Between Measured Realization and Linear and Nonlinear Realizations Simulated from Smoothed Measured Spectrum from Record No. 06887/1	99
3.17	Ensemble Comparison Between Measured Realization and Linear and Nonlinear Realizations Simulated from Bretschneider Spectrum from Record No. 06885/1	100
3.18	Ensemble Comparison Between Measured Realization and Linear and Nonlinear Realizations Simulated from Bretschneider Spectrum from Record No. 06886/1	101
3.19	Ensemble Comparison Between Measured Realization and Linear and Nonlinear Realizations Simulated from Bretschneider Spectrum from Record No. 06886/2	102

LIST OF FIGURES (continued)

Figure		Page
3.20	Ensemble Comparison Between Measured Realization and Linear and Nonlinear Realizations Simulated from Bretschneider Spectrum from Record No. 06887/1	103
3.21	Comparison of Horizontal Kinematic Fields and Pressure Forces Computed by Digital Linear Filter Technique from Skewed and Nonskewed Strictly Periodic Waves	117
3.22	Comparison of Horizontal Kinematic Fields and Pressure Forces Computed by Digital Linear Filter Technique from Skewed and Nonskewed Strictly Periodic Waves	118
3.23	Comparison Between Measured and Predicted Pressure Force Spectra from Record No. 06885/1	120
3.24	Comparison Between Measured and Predicted Pressure Force Spectra from Record No. 06886/1	121
3.25	Comparison Between Measured and Predicted Pressure Force Spectra from Record No. 06886/2	122
3.26	Comparison Between Measured and Predicted Pressure Force Spectra from Record No. 06887/1	123
3.27	Cumulative Probability Distributions of Measured and Predicted Pressure Force Realizations from Record No. 06885/1	126
3.28	Cumulative Probability Distributions of Measured and Predicted Pressure Force Realizations from Record No. 06886/1	127
3.29	Cumulative Probability Distributions of Measured and Predicted Pressure Force Realizations from Record No. 06886/2	128
3.30	Cumulative Probability Distributions of Measured and Predicted Pressure Force Realizations from Record No. 06887/1	129

LIST OF FIGURES (continued)

Figure	Page
C.1 Orientation of Wave Staff and Instrumented Piling for Wave Project II	149
C.2 Effect of Dimensionless Wave Staff-Instrumented Piling Separation Distance on Drag Coefficients Determined from the Morison Equation with Linear Theory Kinematics (L = linear theory wavelength)	154
C.3 Effect of Dimensionless Wave Staff-Instrumented Piling Separation Distance on Inertia Coefficients Determined from the Morison Equation with Linear Theory Kinematics (L = linear theory wavelength)	155

Abstract of Dissertation Presented to the Graduate Council
of the University of Florida in Partial Fulfillment of the
Requirements for the Degree of Doctor of Philosophy

PREDICTION OF WAVE FORCES FROM
NONLINEAR RANDOM SEA SIMULATIONS

By

Robert Turner Hudspeth

December, 1974

Chairperson: Dr. Robert G. Dean

Major Department: Civil and Coastal Engineering

The nonlinear boundary value problem for the propagation of random surface gravity waves in an ocean of finite depth is solved correct to second order in perturbation parameter. A nonlinear second order interaction kernel is obtained which results in nonlinear spectral corrections to a linear Gaussian sea spectrum at frequencies which are the sums and differences of the interacting frequencies of the linear spectrum. The trivariate function is shown to be a closed statistical measure of the second order nonlinearities and the coarse measure of the trivariate function, i.e., the skewness, is used to determine the magnitude of the second order nonlinear contributions. An algorithm is presented for simulating a time sequence of nonlinear random surface gravity waves correct to second order by employing the fast Fourier transform.

The normalized cumulative probability distributions of linear and nonlinear simulated realizations are compared with

measured hurricane-generated realizations recorded during Hurricane Carla in the Gulf of Mexico by Wave Force Project II. The simulations are synthesized from a smoothed measured spectrum and from a Bretschneider spectrum having equal variance and best least-squares fit to the smoothed measured spectrum in order to demonstrate the effect of spectral shape and phase angles in random simulations in addition to establishing the applicability of the Bretschneider spectrum for design.

Resultant wave forces at the 55 foot dynamometer elevation are predicted from both the linear and nonlinear simulations synthesized from both spectra. Kinematic fields are computed by the digital linear filter technique modified by a vertical coordinate stretching function and are used in the Morison equation with Dean and Aagaard drag and modified inertia coefficients. Normalized cumulative probability distributions and wave force spectra of the simulated forces are compared with measured wave force realizations and with wave force realizations predicted by filtering the measured sea surface realization.

CHAPTER 1

INTRODUCTION

As the design of offshore permanent pile-supported structures moves beyond the four hundred foot bottom contour into regions of greater depth and as the mathematical models which describe the compliant nature of the pile-soil interaction become more sophisticated, the requirement to perform dynamic analyses of these structures becomes more critical. Foster [46], Edge and Meyer [44], Borgman [20], Malhotra and Penzien [83,84], Nath and Harleman [92], Plate and Nath [104], Selna and Cho [114], Mansour and Millman [85], Berge and Penzien [12], Muga and Wilson [91], *inter alios*, have presented models for the dynamic response of permanent pile-supported structures to random forces. The random forces used in these studies were either a superposition of linear Fourier components with random phase angles which were uniformly distributed between $(-\pi, \pi)$ or a strictly periodic Stokian wave of finite amplitude. The purpose of this study is to provide a non-linear random time series realization of a surface gravity wave spectrum in an ocean of finite depth and to utilize this realization as a forcing function to a filter to obtain the kinematics required to predict pressure forces. The emphasis will be on the simulation of a random time series vice the determination of the invariant statistics of random realizations.

In Section 1, the most important results and conclusions obtained by others in related investigations toward obtaining second order perturbation corrections to the sea surface are briefly reviewed. In Section 2, the effect on the resulting sea surface profile of the linear superpositioning and the nonlinear interaction of two collinear waves is examined by means of a simple model. In Section 3, the application of the nonlinear sea surface simulation to obtain a random pressure force time series is briefly outlined.

1. Related Previous Studies

Tick has developed a method for generating a realization of a nonlinear sea surface for deep water [123] and for water of finite depth [125] by formally perturbing the energy spectrum. For a Gaussian initial estimate to the linear boundary value problem, the perturbed energy spectrum was shown to consist only of even powers of the perturbation parameter. The energy spectrum was then used as the measure of the nonlinearities. In order to graphically display the superposition of the linear energy spectrum with the quadratic energy spectrum, the ordinate values of the quadratic spectrum had to be greatly expanded near the origin (even in the cases of finite depth) in order that the measure of the quadratic perturbation of the energy spectrum could be observed.

In his initial study (cf. Kinsman [72]), Tick treated finite amplitude waves correct to second perturbation order

in deep water and he obtained a correction to the free surface displacements given by the following expression:

$$\begin{aligned} g \cdot {}_2\eta(x, t) &= -{}_2\Phi_t - \frac{1}{2}\{({}_1\Phi_x)^2 + ({}_1\Phi_z)^2\} + \frac{1}{g} {}_1\Phi_t \cdot {}_1\Phi_{tz}; \\ z &= 0, |x| < \infty, t > 0 \end{aligned} \quad (1.1)$$

where the alphabetical subscripts denote partial differentiation with respect to the independent variables indicated by the suffix and the numerical prefix denotes the perturbation order of the dependent variable. The last of these three terms represents the Maclaurin series expansion of the variation of the free surface about the still water level due to the presence of the wave. The second term in brackets represents the correction due to the local kinetic energy of the water particle motions. The first term represents the second order perturbation correction to the velocity potential. The second order perturbation correction to the velocity potential in deep water was given by Tikhonov in the following integral expression:

$$\begin{aligned} {}_2\Phi(x, z, t) &= 2i \int_{-\infty}^{\infty} G(\omega, \omega') \exp\{i(|\omega|\omega + |\omega'|\omega')\} \cdot \frac{z}{g} \cdot {}_1f(\omega') \cdot {}_1f(\omega) \cdot \\ &\quad \cdot \exp i\{\beta(\omega, x, t)\} \cdot \exp i\{\beta(\omega', x, t)\} d\omega d\omega' \end{aligned} \quad (1.2)$$

where the nonlinear interaction kernel, $G(\omega, \omega')$, is given by

$$G(\omega, \omega') = \frac{\omega(\omega\omega' - |\omega||\omega'|)}{(\omega + \omega')^2 - |(|\omega|\omega + |\omega'|\omega')|} \quad (1.3)$$

Kinsman [72] corrected the separation constant originally published by Tick [123] in order that the velocity potential satisfy exactly the equation of continuity. This correction has been incorporated in Eq. (1.2). The second order perturbation correction to the free surface computed from Eq. (1.1) by Tick was also expressed by an integral equation

$$_2\eta(x, t) = \frac{1}{g} \int_{-\infty}^{\infty} \int H(\omega, \omega') \cdot {}_1 f(x, \omega, t) \cdot {}_1 f'(x, \omega', t) d\omega d\omega' \quad (1.4)$$

where the nonlinear interaction kernel is given by

$$H(\omega, \omega') = 2(\omega + \omega') \cdot G(\omega, \omega') + (\omega)^2 - \frac{1}{2} |\omega\omega'| + \frac{1}{2} \omega\omega' \quad (1.5)$$

One of the most important results obtained by Tick was that the contribution to the perturbed energy spectrum at a given frequency by the second order perturbation correction to the sea surface was the result of the convolution of all first order perturbation energy densities whose sums and differences in frequencies contribute to the given frequency of the quadratic spectrum. The expression computed by Tick was

$${}_2 S(\omega) = \frac{1}{g^2} \int_{-\infty}^{\infty} K(\omega - \omega', \omega') \cdot {}_1 S(\omega - \omega') \cdot {}_1 S(\omega') d\omega' \quad (1.6)$$

This important result will be discussed in more detail in Chapter 2.

Tick [125] later extended his results to water of finite depth and presented the following nonlinear interaction kernel:

$$Q_h(\omega, \omega') = \frac{1}{2} \frac{|kk'| |kk'|}{\omega \omega'} + \frac{\omega \omega'}{2} - \frac{(\omega + \omega')^2}{2} + \\ + \frac{(\omega + \omega')^2 \left[\frac{|kk'| |kk'|}{\omega \omega'} + \frac{\omega \omega'}{2} + \frac{\omega(k')^4 + \omega'(k)^4}{2\omega \omega' (\omega + \omega')} - \frac{(\omega + \omega')^2}{2} \right]}{(|k|k+|k'|k') \tanh[d^2(|k|k+|k'|k')]] - (\omega + \omega')^2} \quad (1.7)$$

where $d^2 = (h/g)$ and the wave numbers $k = k(\omega)$ and $k' = k'(\omega)$ are solutions to the dispersion relation

$$\omega^2 = k^2 \tanh[d^2 k^2] \quad (1.8)$$

The sign of the second term given in Eq. (1.7) has been corrected from the typographical error in Reference [125]. Tick resolved the difficulties in obtaining an identity between the interaction kernels given by Eq. (1.5) and Eq. (1.7) as the water depth approaches infinity (i.e., $h \rightarrow \infty$) in terms of the discontinuities in hypersurfaces created by Dirac delta functions and by the nonuniqueness of perturbation expansions.

Tick [125] demonstrated a comparison between a linear realization computed from the Neumann-type spectrum [72] with a second perturbation order realization from the same spectrum for the case of an ocean of infinite depth. No realizations were available from the finite depth case due to the computational complexities involved. The Fast Fourier Transform (FFT) algorithm [37], which was not generally available at the date Tick published his work, has greatly facilitated the applications of quadratic sea simulations by reducing significantly the computational difficulties. No published comparisons of random quadratic sea simulations with measured wave data seem to be available.

In an extraordinary three-part series, Hasselmann [54, 55, 56] set forth a powerful theory for the nonlinear energy transfer in a spectrum of random waves. Later extensions [58, 59, 61] included the probabilistic structure of the initial conditions imposed through the nonlinear free surface boundary conditions as well as a general theory [60] for the wave-wave scattering processes in the oceanic wave guide. Recently [76, 120], portions of this powerful wave-wave scattering theory have been applied to measured data with excellent agreement. The incredible number of geophysical problems which are covered by this general theory offer many opportunities for comparison with measured data now becoming available.

In one of these works, Hasselmann [54] observed that the quadratic energy spectrum which was employed by Tick was not closed to the order of the perturbation parameter chosen. Hasselmann included in his development the mean lagged product of the initial Gaussian estimates with the solution to the third order perturbation correction to the sea surface realization. Therefore, in order to measure nonlinearities by a formal perturbation of the energy spectrum, the nonlinear contributions to the sea surface realizations must be computed from the boundary value problem correct to third order in the perturbation parameter if a perturbation of the energy spectrum is to be utilized as the measure of the nonlinearities. The bookkeeping problems of perturbation expansion orders are discussed by Hasselmann et al. [57] and equations which aid in this bookkeeping are given. Briefly, the problem is

if the energy spectrum (or, equivalently, the autocovariance function) is formally perturbed in a power series expansion in the following forms:

$$E(\omega) = \sum_n^{\infty} E_n(\omega) \quad (1.9a)$$

$$\gamma(\tau) = \sum_{nn}^{\infty} \sum_n^{\infty} n^n(t+\tau) \cdot \sum_m^{\infty} m^m n^*(t) \quad (1.9b)$$

the relationship between the energy perturbation orders and the time series perturbation orders must be complete and closed.

An intermediate result obtained by Hasselmann [54] in solving the problem of determining the rate of energy transfer between discrete components in random gravity wave trains in water of finite depth included a nonlinear interaction matrix which may also be used to construct nonlinear seas. In his power series expansion of the energy spectrum for the sea surface, Hasselmann included all perturbation orders omitted in the expansion used by Tuck.

These studies by Tuck and Hasselmann have introduced methods for simulating random nonlinear realizations of surface gravity waves. Other investigations related to nonlinear sea simulations have been directed toward describing the effects of nonlinearities on the statistics of the distributions of the realizations. In one of these statistical investigations, Longuet-Higgins [79] showed that the Gram-Chalier distribution more closely fits measured sea surface recordings and, moreover, the main distinction between the Gaussian and Gram-Chalier distributions are terms proportional to the measure of the skewness. Longuet-Higgins [79] also obtained the

important result for a discrete spectrum of waves first given by Tikhonov [123] for a continuous spectrum of waves that the quadratic energy distribution is the result of the summation of all discrete energy components whose sums and differences in phases contribute to the same spectral frequency.

Cartwright and Longuet-Higgins [32] have also demonstrated the effect of the bandwidth of a spectrum on the probability distribution of nonlinear seas with nonzero skewness. Therefore, from both the statistical (measured moments) and probabilistic (characteristic and probability density functions) results, the best measure of the nonlinearities and the non-Gaussian distribution of a sea simulation is the third statistical moment. Furthermore, it will be shown that the boundary value problem need only be solved to second perturbation order in order to measure the lowest order contribution to both the nonlinearities and non-Gaussian distribution.

The omission of certain perturbation orders in the power series expansion of the energy measure raises a closure problem similar to that encountered in turbulence (cf. Batchelor [4], Kampe de Feriet [70], or Lumley [81]). Attempts to resolve the closure problem as well as the irreversability paradox of the initial value problem resulted in a series of papers by Benney and Saffman [7], Hasselmann [61], Saffman [113], Benney [8], Benney and Newell [9,10,11], Newell [94], Ablowitz and Benney [1], Ablowitz [2], and Birkhoff, Bona and Kampe de Feriet [15] which eloquently describe the physics of these two problems in very sophisticated mathematical terms. Intermediate

results obtained in reaching their final objectives include nonlinear interaction matrices (for the discrete wave spectrum interactions) or nonlinear interaction kernels (for the continuous wave spectrum interactions) which may be used to construct nonlinear sea simulations. The sophisticated mathematics utilized in these papers contribute to the subordination of the practical applications of their intermediate results to the problem of simulating nonlinear seas.

The results obtained in this study circumvent the closure problem by appealing to the trivariate function as a measure of second order nonlinearities and circumvent the irreversibility paradox by appealing to stationarity and ergodicity.

Finally, Borgman [20] has developed a technique which is based on the statistical distributions of time series. The procedure involves the transformation of a time series which is normally distributed to a time series which is gamma distributed with zero mean by a set of polynomials. While this technique is extremely attractive for its computational efficiency, it is not based on the hydrodynamic equations of motion.

2. Linear Superposition and Nonlinear Wave-Wave Interactions

Whitham [130] has developed an extensive number of applications of the variational technique for the average Lagrangian which demonstrate the wave-wave interactions of nonlinear dispersive waves. The important effects of both amplitude and frequency dispersion are well covered. However, a simple

example of the separate effects of linear superposition and of nonlinear interaction for two dispersive wave components which is relatively free of mathematical complexities is instructive in distinguishing the relationships between the two effects.

Formulation of the complete boundary value problem for a continuous spectrum of dispersive surface gravity waves will be deferred until Chapter 2. However, the results of the formal solution in deep water may be summarized to provide a simple illustration of both the linear superposition and the nonlinear interaction of a pair of discrete wave components from a spectrum which are collinear and propagate in the positive \vec{x} direction. The resulting sea surface profile may be represented by

$$\eta(\vec{x}, t) = {}_1\zeta(\vec{x}, t) + {}_2\zeta(\vec{x}, t) \quad (2.1)$$

where ${}_1\zeta$ is the linear first order contribution and ${}_2\zeta$ is the nonlinear second order contribution. For a spectrum of two collinear wave components, the first order contribution, ${}_1\zeta$, represents the linear superposition of the two waves and the second order contribution, ${}_2\zeta$, represents the contribution of nonlinear products of the two waves. The linear superpositioning of the first order contributions will be examined briefly first.

2.a. Linear Superposition

Consider a simple line spectrum consisting of only two spectral components which are separated by a small frequency differential, $2\Delta\sigma$, and by a small wave number differential, $2\Delta\vec{k}$. Although adjacent spectral components usually differ in

the magnitude of their amplitudes (i.e., the spectrum is not flat), the two adjacent components will be considered to have the same amplitude equal to $H/2$, in order to simplify this illustration.

The deep water wave profile resulting from the linear superposition of these two waves is given by

$$_1\zeta = \eta_+ + \eta_- \quad (2.2)$$

where the two components are given by

$$\eta_+ = \frac{H}{2} \cos\{\sigma_+ t - \vec{k}_+ \cdot \vec{x} - \psi_+\} = \frac{H}{2} \cos \theta_+ \quad (2.3a)$$

$$\eta_- = \frac{H}{2} \cos\{\sigma_- t - \vec{k}_- \cdot \vec{x} - \psi_-\} = \frac{H}{2} \cos \theta_- \quad (2.3b)$$

where

$$\sigma_{\pm} = \sigma \pm \Delta\sigma \quad (2.4a)$$

$$\vec{k}_{\pm} = \vec{k} \pm \Delta\vec{k} \quad (2.4b)$$

$$\psi_{\pm} = \psi \pm \Delta\psi \quad (2.4c)$$

Substituting Eqs. (2.3a,b) into Eq. (2.2) and combining gives the following familiar profile:

$$_1\zeta = H \cos\{(\Delta\sigma)t - (\Delta\vec{k}) \cdot \vec{x} - \Delta\psi\} \cos\{\sigma t - \vec{k} \cdot \vec{x} - \psi\} \quad (2.5)$$

This resulting wave contains an amplitude which is modulated by the differences between the phases of the two components and which propagates at the group velocity, $\Delta\sigma/|\Delta\vec{k}|$. The profile of the resulting wave propagates at the wave speed, $\sigma/|\vec{k}|$.

The resulting wave is, of course, the well known beat profile which is the result of the superposition of two linear dispersive waves.

There are two time and space scale's involved in the beat profile given by Eq. (2.5). One is the scale of the envelope modulation which is spatially long and temporally slow compared to the scale of the profile. The relatively longer and slower scales are related to periodicities of $\Delta\vec{k}$ and $\Delta\sigma$, respectively, while the relatively shorter and faster scales of periodicities are related to \vec{k} and σ , respectively.

2.b. Nonlinear Interactions

The formal derivation of the second order contributions in Eq. (2.1) will be given in Chapter 2. However, for the purposes of this illustration, consider the following two linear velocity potentials for the deep water wave components given by Eqs. (2.3a,b):

$$\phi_+ = \frac{Hg}{2\sigma_+} \exp\{\kappa_+ z\} \sin\{\sigma_+ t - \vec{k}_+ \cdot \vec{x} - \psi_+\} = \frac{Hg}{2\sigma_+} \exp\{\kappa_+ z\} \sin\theta_+ \quad (2.6a)$$

$$\phi_- = \frac{Hg}{2\sigma_-} \exp\{\kappa_- z\} \sin\{\sigma_- t - \vec{k}_- \cdot \vec{x} - \psi_-\} = \frac{Hg}{2\sigma_-} \exp\{\kappa_- z\} \sin\theta_- \quad (2.6b)$$

with the linear dispersion equation for deep water given by

$$(\sigma_{\pm})^2 = gk_{\pm} \quad (2.7)$$

Equation (1.1) indicates that the second order contribution to the wave profile is a function of the temporal derivative of the second order velocity potential. Using a discrete form of the second order velocity potential from

Chapter 2 and substituting the appropriate derivatives of Eqs. (2.6a,b) into Eq. (1.1) with the sign of the first term changed from a minus to a plus results in the following second order contributions:

$$\begin{aligned} 2\zeta = & \frac{H^2}{8} k_+ \cdot \cos 2\theta_+ + \frac{H^2}{8} k_- \cdot \cos 2\theta_- + \frac{H^2}{4} k \cos 2\{\sigma t - \vec{k} \cdot \vec{x} - \psi\} \\ & + \frac{H^2}{8g} (\sigma_+ - \sigma_-)^2 \left[\frac{4\sigma_+ \cdot \sigma_-}{(\sigma_+ - \sigma_-)^2 - g|k_+ - k_-|} + 1 \right] \cos 2\{(\Delta\sigma)t - (\Delta\vec{k}) \cdot \vec{x} - \Delta\psi\} \end{aligned} \quad (2.8)$$

The first two terms in Eq. (2.8) represent the nondispersive Stokian waves resulting from the self interactions of the two spectral components given in Eqs. (2.3a,b). These two Stokian waves contribute to the skewness of the spectral components by adding both to their troughs and crests. The third term in Eq. (2.8), which represents the result of the cross product of the interactions between the two spectral components, propagates at the profile phase speed for the linear wave given by Eq. (2.5) but with twice the phase. This wave will contribute to the skewness of the resulting linear profile. The final term in Eq. (2.8) represents the result of the cross product of the interactions between the two spectral components which propagates at the envelope phase speed, $\Delta\sigma/|\Delta\vec{k}|$, but with twice the phase. The contribution which this wave makes to the envelope depends on the sign of the term in the bracket. For $\sigma_+ > \sigma_-$, the expression becomes the following:

$$\frac{H^2}{8g} \sigma_+^2 \cdot [1 - (\sigma_-/\sigma_+)^2] \cos 2\{(\Delta\sigma)t - (\Delta\vec{k}) \cdot \vec{x} - \Delta\psi - \frac{\pi}{2}\} \quad (2.9)$$

This wave is 180° out of phase with respect to the envelope phase. Its maxima occur under the nodes of the envelope and its minima occur under the antinodes of the envelope. This wave also has a nonzero value when averaged over either the faster temporal or shorter spatial scales of the resultant profile phase given by Eq. (2.5). Longuet-Higgins and Stewart [77] discuss numerous effects which result from this wave component.

It can be shown that the right side of the boundary condition equation which determines the second order velocity potential in deep water reduces to the temporal derivative of twice the kinetic energy. The second order contribution to the resulting wave profile given in Eq. (2.8) above may be seen from Eq. (1.1) to be proportional to the temporal derivative of this second order velocity potential and to the kinetic energy. Since these two equations demonstrate that the kinetic energy plays such an important role in the second order contributions, it is of value to examine this term in some detail.

For the case of deep water waves, the right side of the combined free surface boundary condition reduces to the temporal derivative of twice the kinetic energy which may be expressed by

$$z^{\Phi}_{tt} + g z^{\Phi}_z = \frac{\partial}{\partial t} |\vec{\nabla}\phi|^2 ; \quad z=0, \quad |\vec{x}|<\infty, \quad t \geq 0 \quad (2.10)$$

Substituting the appropriate spatial derivatives of Eqs. (2.6a,b) into the right side yields

$$\begin{aligned} \frac{\partial}{\partial t} |\vec{\nabla}\Phi|^2 &= \frac{\partial}{\partial t} \left(\left[\frac{\partial\Phi_+}{\partial \vec{x}} \right]^2 + \left[\frac{\partial\Phi_+}{\partial z} \right]^2 + \left[\frac{\partial\Phi_-}{\partial \vec{x}} \right]^2 + \left[\frac{\partial\Phi_-}{\partial z} \right]^2 \right) + \\ &+ 2 \frac{\partial}{\partial t} \left(\frac{\partial\Phi_+}{\partial \vec{x}} \cdot \frac{\partial\Phi_-}{\partial \vec{x}} + \frac{\partial\Phi_+}{\partial z} \cdot \frac{\partial\Phi_-}{\partial z} \right); \quad z=0, \quad |\vec{x}|<\infty, \quad t \geq 0 \end{aligned} \quad (2.11)$$

It may be seen by inspection of Eqs. (2.6a,b) that the vertical and horizontal velocity components are 90° out-of-phase and, consequently, the sum of their squares evaluated at $z=0$ is a constant which is independent of time. These represent Stokian self-interactions and the temporal derivative of the first term in brackets in Eq. (2.11) vanishes in deep water.

Substituting the appropriate spatial derivatives of Eqs. (2.6a,b) into the nonvanishing temporal derivative in Eq. (2.11) yields

$$\frac{\partial |\vec{\nabla}\Phi|^2}{\partial t} = - \frac{H^2 g^2}{4\sigma_+ \sigma_-} \left(\vec{k}_+ \vec{k}_- [(\Delta\sigma) \sin\{\theta_+ - \theta_-\} + \sigma \sin\{\theta_+ + \theta_-\}] + \vec{k}_+ \vec{k}_- [(\Delta\sigma) \sin\{\theta_+ - \theta_-\} - \sigma \sin\{\theta_+ + \theta_-\}] \right) \quad (2.12)$$

For a collinear spectrum, it is easily seen that only the differences in phases result in nonvanishing contributions. Moreover, for Stokian second order waves (i.e., $\Delta\sigma = \Delta k \equiv 0$), the right side vanishes and the linear velocity potential given by the sum of Eqs. (2.6a,b) is exact to second order.

For the interaction of a directional spectrum of deep water waves, the contributions from the horizontal velocity fields are decreased by a multiplicative constant proportional to $\cos\{\alpha_{+-}\}$ where α_{+-} is the azimuthal difference between the directions of propagation of the two wave components given by Eqs. (2.3a,b). The multiplicative constants in Eq. (2.12) no

longer may be factored and the contributions from the sums of the phases of the interacting wave components no longer cancel. Consequently, a finite contribution to the second order velocity potential from both the sums and differences of the phases of the horizontal and vertical velocity fields is obtained.

The important differences between strictly periodic Stokian interactions, collinear spectral interactions, and directional spectral interactions are demonstrated simply for the deep water case. For the case of finite depth, additional algebraic factors are encountered which detract from its usefulness as a simple illustrative example.

3. Simulating Wave Forces by the Digital Linear Filter Technique

One of the practical applications for the simulation of a random sea surface realization is to obtain a random force input for the dynamic analyses of permanent pile-supported structures. Reid [106] has developed a method for the linear filtering of a sea surface realization in order to obtain the kinematics required to compute pressure forces by the Morison equation. Wheeler [129] used this technique to compute pressure force coefficients from measured hurricane realizations and obtained very low errors between the measured and predicted peak pressure forces at varying elevations along an instrumented platform piling. Another application [67] of

this technique using hurricane realizations yielded mean square errors for pressure forces computed over the crest portion of the realizations which compared favorably with mean square errors from pressure forces computed using the Dean Stream Function [39]. Since these relatively successful applications of the digital linear filter technique to analysis involved measured sea surface realizations with finite skewness, the extension of linear digital filtering to design should involve simulated nonlinear realizations with nonzero skewness.

The theory for nonlinear sea simulations will be developed in Chapter 2. Selected realizations will be filtered in Chapter 3 to obtain the kinematics required to compute pressure forces. Pressure forces computed from nonlinear realizations by the linear digital filter will be compared with measured pressure forces recorded from hurricane generated waves.

CHAPTER 2

THEORY OF RANDOM NONLINEAR WAVE-WAVE INTERACTIONS

Section 1 of this chapter briefly outlines the probability assumptions to be employed in formulating the random sea problem. Section 2 introduces the notations to be used in describing random functions and gives, without proofs, some of the mathematical transforms to be used in developing the theory for random surface gravity waves correct to second order. Section 3 defines the third order statistical moment which will be utilized as a measure of the nonlinearities of the random sea simulation and shows that this statistical measure is closed at second order in the perturbation parameter. Section 4 formulates the random boundary value problem and solves for the first and second order random measures and spectral response functions required to simulate nonlinear random sea realizations. Section 5 returns to the nonlinear statistical measure of the second order correction to the sea surface realization which was developed in Section 3 and discusses its Fourier transform. Section 6 computes the second order spectral density of the sea surface realization and shows that it is a convolution of all first order spectral densities.

1. Random Differential Equations

Many physical processes demonstrate random variations which cannot be modeled by physical laws that may be solved by deterministic mathematics. Wiener [133] gives several examples with applications. These random variations may enter into the mathematical equations which are used to approximate the random physical process either through (1) the dependent variables or (2) the coefficients in the differential equations or (3) through both methods. In addition, the random dependent variable may be a random function of still another random function through a filtering process (cf. Soong [116], Jazwinski [68], or Sveshnikov [119]).

In any event, the description of a physical process as "random" requires an estimate of the probabilistic structure of the random function. When these random functions are determined by differential equations, there are at least four convergence questions which must be satisfied for each single convergence question in the deterministic differential equation (cf. Soong [116], Jazwinski [68], or Sveshnikov [119]).

One of the most well known probabilistic structures is the Gaussian density and a Gaussian probabilistic field is frequently assumed in many hydrodynamic problems. Chorin [34] describes many of the implications of assuming a Gaussian field for random flow problems in hydrodynamics. Rosenblatt [111] and Kampe de Feriet [71] address specifically the probabilistic questions posed by the Gaussian field assumption

for the random linear sea problem. The probabilistic structure of many physical problems are frequently assumed to be known and the assumption of a Gaussian field for the random linear sea will be used herein. A brief discussion of the probabilistic assumptions used is unavoidable in order that the limitations and interpretations of the probability structure of the applications of the results to be derived may be fully understood.

The solution to the random sea problem is a random function which is determined by a partial differential equation (*viz.*, the Bernoulli equation) in which one of the dependent variables is the velocity potential which is also a random function. The random velocity potential is determined from a boundary value problem in which the coefficients of the governing field equation and of the boundary conditions are deterministic. The random velocity potential is a random function of a random variable called the phase angle. The probability density function of the random phase angle is assumed to be independently and identically uniformly distributed between $\{-\pi, \pi\}$. Papoulis [96,97] demonstrates that a sum of random functions which depends on an identically uniformly distributed random variable tends very rapidly toward a Gaussian distribution even for cases when the sum includes relatively few random variables. The rigorous proof of the tendency toward a Gaussian distribution by random fields as the number of the random variables increases without limit may be found in Rosenblatt [112] by means of the Central Limit Theorem.

The three fundamental convergence theorems required in deterministic calculus involve continuity, differentiation and integration. In random differential calculus, each of these three fundamental theorems must be shown to converge (1) in probability, (2) in mean square, (3) in distribution, and (4) in "almost sure" probability (cf. Soong [116]). Mean square calculus will be used to determine the convergence of functions and mathematical operators. The linear solution to the random sea problem will be assumed to be second order stationary and homogeneous in the statistical moments. This assumption of stationarity and homogeneity renders the probability distribution independent of time and space, respectively (cf. Yaglom [135]). The assumption that a random process is second order stationary or homogeneous has been widely studied and exploited in terms of the correlation theory (cf. Jenkins and Watts [69]). The tendency toward a Gaussian distribution of a sum of random functions which are identically and uniformly distributed between $\{-\pi, \pi\}$ results in the probability structure of the random linear sea process being completely described by its mean and variance. The complexities associated with demonstrating "almost sure" probability are discussed by Bartlett [3] and will not be postulated for the random sea problem. The determination of the evolution of the probability density function for the random nonlinear sea will also not be attempted (cf. Jazwinski [68]).

The complete formulation of the covariance equations for the random linear sea problem using correlation theory may be

found in Snyder [120]. The distinctions between and simplifications of the solutions to the linear sea problem for the probability density functions using probability theory versus the covariance functions using correlation theory are demonstrated by comparing the papers by Rosenblatt [111] and Kampe de Feriet [71] with the paper by Snyder [120].

2. Introduction to Random Functions

Kinsman [72; cf. Chs. 7 and 8] develops a general expression for the three-dimensional energy spectrum for a random sea surface realization. His development involves the three concepts of (1) Fourier analysis, (2) stochastic processes and probability, and (3) the hydrodynamics of the random sea. In the general derivation (Kinsman [72], Ch. 7), each of the three concepts are developed separately in order that the effects of modifications of a single concept may be examined only in terms of the one concept which it modifies. The general model is then explicitly defined in terms of both a deterministic and a stochastic model in which the interdependencies between the three concepts are examined (Kinsman [72], Ch. 8).

This procedure utilized by Kinsman [72] to develop a model for the energy spectrum of a random function will be followed in obtaining a solution for the second order contribution to a random sea surface realization. However, the notational conventions used to describe random functions differ in

some respects from reference to reference. In order to avoid possible confusion, as well as for ease of reference, the mathematical expressions and definitions to be used in developing the second order theory of a random nonlinear sea are given in this section.

The general definitions for random functions and for the correlation theory functions with both time and space arguments are given by Kinsman [72; Chs. 7 and 8] and by Phillips [100; Ch. 4]. Definitions for functions with only temporal arguments are given by Sveshnikov [119] or Yaglom [135]. The solution developed in Section 4 of this chapter is initially a solution to a spatial boundary value problem. Therefore, the definitions given below are for functions having only spatial arguments.

A random function which is a continuous function of time or space is called a random process. A random function which is a discrete function of time or space is called a random sequence (cf. Sveshnikov [119], p. 11). Any random process may be represented by the following Fourier-Stieltjes integral:

$$\zeta(\vec{x}) = \int_{-\infty}^{\infty} \exp i\{\vec{k} \cdot \vec{x}\} \cdot d\xi(\vec{k}) \quad (2.1)$$

where $\xi(\vec{k})$ is a random measure with orthogonal increments. For the process represented by Eq. (2.1) to be a real function, the following complex conjugate relationship must be satisfied:

$$d\xi(-\vec{k}) = d\xi^*(\vec{k}) \quad (2.2)$$

A good discussion of the distinctions between Fourier-Stieltjes integrals, Stieltjes integrals, and Fourier integrals may be found in Yaglom [135; Ch. 2, Sec. 9]. In Eq. (2.1) and in those which follow, the parameter of the argument is space but a representation for an argument in which the parameter is time may be similarly defined. The autocovariance function for a process with random measure is given by

$$\gamma_{\zeta\zeta}(\vec{x}, \vec{r}) = E\{\zeta(\vec{x}) \cdot \zeta(\vec{x} + \vec{r})\} \quad (2.3)$$

For a process which is spatially homogeneous (or temporally stationary), the autocovariance function depends only on the spatial lag \vec{r} (or temporal lag τ) and has spectral representation given by Khinchin's Theorem (cf. Sveshnikov [119], Ch. II, Sec. 10, or Yaglom [135], Ch. 2, Sec. 10):

$$\gamma_{\zeta\zeta}(\vec{r}) = \int_{-\infty}^{\infty} \exp i\{\vec{k} \cdot \vec{r}\} ds(\vec{k}) \quad (2.4)$$

where the spectral distribution function, $s(\vec{k})$, is related to the random measure, $\xi(\vec{k})$, for a homogeneous process by

$$E\{d\xi(\vec{k}) d\xi(\vec{k}')\} = s(\vec{k}') \cdot \delta(\vec{k}' + \vec{k}) d\vec{k}' d\vec{k} \quad (2.5)$$

where $\delta(\cdot)$ is the Dirac delta distribution (Friedman [49]). This distribution may be defined in the space domain by

$$(2\pi)^2 \delta(\pm \vec{x}) = \int_{-\infty}^{\infty} \exp i\{\pm \vec{k} \cdot \vec{x}\} d\vec{k} \quad (2.6)$$

and in the wave number domain by

$$(2\pi)^2 \delta(\pm \vec{k}) = \int_{-\infty}^{\infty} \exp i\{\mp \vec{k} \cdot \vec{x}\} d\vec{x} \quad (2.7)$$

Equation (2.6) implies that a constant spectral distribution function is given by a Dirac delta distribution in space, and Eq. (2.7) implies that a constant function in the spatial domain has a spectral distribution function given by the Dirac delta distribution. This interpretation of Eq. (2.6) and Eq. (2.7) follows from the definition of Fourier transform pairs and demonstrates one of the relationships between the concept of stochastic processes and the concept of Fourier analysis.

The Fourier transform pair for a real spatial function with a complex spectral density function will be denoted by

$$\zeta(\pm \vec{x}) = \int_{-\infty}^{\infty} F(\vec{k}) \exp i\{\pm \vec{k} \cdot \vec{x}\} d\vec{k} \quad (2.8a)$$

$$F(\pm \vec{k}) = \frac{1}{(2\pi)^2} \int_{-\infty}^{\infty} \zeta(\vec{x}) \exp i\{\pm \vec{k} \cdot \vec{x}\} d\vec{x} \quad (2.8b)$$

In place of the Wiener-Khinchin transform pair [5,26,88,131], the Fourier transform pair for the autocovariance function and the spectral density function for a homogeneous process will be given by the following:

$$\gamma(\vec{r}) = \int_{-\infty}^{\infty} S(\vec{k}) \exp i\{\vec{k} \cdot \vec{r}\} d\vec{k} \quad (2.9a)$$

$$S(\vec{k}) = \frac{1}{(2\pi)^2} \int_{-\infty}^{\infty} \gamma(\vec{r}) \exp i\{-\vec{k} \cdot \vec{r}\} d\vec{r} \quad (2.9b)$$

The norming constant required for the inversion of a Fourier transform pair will always be associated with the transform which defines the spectral density function. The Dirac delta distributions defined by Eqs. (2.6) and (2.7) were multiplied by 2π in order that their Fourier transform would be proportional to unity. The improper integral given in Eq. (2.4) is

often associated with Bochner (cf. Wilks [134]) or, if the spectral distribution function is confined to an interval $\{-\pi, \pi\}$, with Herglotz (cf. Wilks [134]).

Comparing the stochastic Fourier-Stieltjes integral representation of a random function given by Eq. (2.1) with the Fourier integral representation of any function (i.e., both deterministic and nondeterministic functions) which satisfies the requirements for the existence of a Fourier transform pair (cf. Titchmarsh [126]), the relationship between the random measure, $d\xi(\vec{k})$, given by Eq. (2.1), and the Fourier spectrum, $F(\vec{k})$, given by Eq. (2.8a), is seen to be

$$F(\vec{k}) = \frac{d\xi(\vec{k})}{d\vec{k}} \quad (2.10)$$

i.e., the random measure of the process must have a density. Similarly, comparing the spectral representation of a homogeneous process, $ds(\vec{k})$, given by Khinchin's Theorem in Eq. (2.4) with the Fourier transform of the autocovariance function, $S_{\zeta\zeta}(\vec{k})$, given by Eq. (2.9a), the relationship again implies that the distribution function has density

$$S_{\zeta\zeta}(\vec{k}) = \frac{ds(\vec{k})}{d\vec{k}} \quad (2.11)$$

The major distinction between a random function represented by a Fourier-Stieltjes integral and a random function represented by a Fourier integral is the existence of a derivative of the distribution function.

In applications to random surface gravity wave problems, the restriction of the *a priori* assumption that the process has a density function is frequently unimportant. Kinsman [72; Ch. 8.3] discusses the mean square integrability requirement between stochastic and Fourier integrals in terms of the scales of the process.

The shifting property of the Dirac delta distribution (cf. Papoulis [96]) plays an important role in the filtering problem which is discussed in Chapter 3. This shifting property is defined in the space domain by

$$(2\pi)^2 \delta(\vec{x} \pm \vec{r}) = \int_{-\infty}^{\infty} \exp i\{\vec{k} \cdot (\vec{x} \pm \vec{r})\} d\vec{k} \quad (2.12)$$

and in the wave number domain by

$$\delta(\vec{k} \pm \vec{k}_0) = \frac{1}{(2\pi)^2} \int_{-\infty}^{\infty} \exp i\{-\vec{x} \cdot (\vec{k} \pm \vec{k}_0)\} d\vec{x} \quad (2.13)$$

The autocovariance function defined above is one of the statistical measures which will be required to compare and to characterize a random process. These statistical measures are defined by an ensemble averaging operator denoted by the expectation symbol, E , and defined by

$$E\{z^n\} = \int_{-\infty}^{\infty} \zeta^n p(\zeta) d\zeta \quad (2.14)$$

where $p(\zeta)$ is the probability density of the random variable z . The variance, σ_N^2 , is the second order statistical moment which measures the dispersion about the mean and is computed from

$$\sigma_N^2 = E\{(Z - E\{Z\})^2\} = E\{Z^2\} - E^2\{Z\} \quad (2.15)$$

The standard deviation is the positive square root of the variance as defined by

$$\text{STD DEV} = \sqrt{\sigma_N^2} \quad (2.16)$$

The autocovariance function given by Eq. (2.3) for a random process with a zero mean evaluated for zero spatial lag \vec{r} is equivalent to the variance.

The trivariance function is a third order statistical moment defined by the expectation operator as

$$\gamma_{\zeta\zeta\zeta}(\vec{x}, \vec{r}_1, \vec{r}_2) = E\{\zeta(\vec{x}) \cdot \zeta(\vec{x} + \vec{r}_1) \cdot \zeta(\vec{x} + \vec{r}_2)\} \quad (2.17)$$

The skewness is a measure of the asymmetry of the random sea surface about the mean normalized by the cube of the standard deviation, i.e.,

$$SK = \frac{E\{(Z - E\{Z\})^3\}}{\sigma_N^{3/2}} \quad (2.18)$$

The skewness measure may be evaluated from the trivariance function for a random process with zero mean for zero spatial lags \vec{r}_1, \vec{r}_2 .

Although higher order polyspectra measures may be defined (cf. Brillinger and Rosenblatt [29,30]), only the kurtosis measure will be evaluated herein. The kurtosis is the fourth statistical moment about the mean normalized by the square of the variance and is referenced to an equivalent normal random process with the same mean and variance by reducing the

quotient by 3; i.e.,

$$K = \frac{E\{(Z - E\{Z\})^4\}}{\sigma_N^4} - 3 \quad (2.19)$$

3. Trivariance Function

The statistical moment which gives the best measure of the second order perturbation contributions to the random non-linear sea process through a measure of the asymmetry of the random realization about the mean is the third statistical moment or skewness. Formally, the assumptions of stationarity and homogeneity results in making the functions from correlation theory (i.e., covariance, trivariance, etc.) dependent only on the differences in the temporal and spatial parameters of its argument. Although the assumptions of stationarity and homogeneity are used, the explicit dependence of these correlation functions on the temporal and spatial parameters t and \vec{x} will be retained in order that the relationship between random measures and the spectral distribution function given by Eq. (2.5) may be employed. This definition for the spectral distribution function involves the Dirac delta distribution as a result of the assumptions of stationarity and homogeneity. The Dirac delta distribution greatly facilitates the derivation of certain results obtained in later sections.

The trivariance function for both time and space parameters involves two lags and may be represented by

$$\gamma_{nnn}(\tau_1, \tau_2; \vec{r}_1, \vec{r}_2) = E\{\eta(t, \vec{x}) \cdot \eta(t+\tau_1; \vec{x}+\vec{r}_1) \cdot \eta(t+\tau_2; \vec{x}+\vec{r}_2)\} \quad (3.1)$$

If the random sea realization, $n(t, \vec{x})$, is assumed to be composed of a linear Gaussian estimate plus a nonlinear, non-Gaussian second order perturbation component, the random process may be expanded in a power series given by

$$n(t, \vec{x}) = {}_1 n(t, \vec{x}) + {}_2 n(t, \vec{x}) \quad (3.2)$$

where the order of the perturbation power series parameter has been implicitly absorbed into the random sea function and the order of the perturbation parameter is indicated by the preceding numerical prefix. Substituting Eq. (3.2) into Eq. (3.1) and using the linearity of the expectation operator, E , yields the following:

$$\begin{aligned} r(\tau_1, \tau_2; \vec{r}_1, \vec{r}_2) &= E\{{}_1 n(t, \vec{x}) \cdot {}_1 n(t+\tau_1; \vec{x}+\vec{r}_1) \cdot {}_1 n(t+\tau_2; \vec{x}+\vec{r}_2)\} + \\ &\quad + E\{{}_1 n(t, \vec{x}) \cdot {}_1 n(t+\tau_1; \vec{x}+\vec{r}_1) \cdot {}_2 n(t+\tau_2; \vec{x}+\vec{r}_2)\} + \\ &\quad + E\{{}_1 n(t, \vec{x}) \cdot {}_2 n(t+\tau_1; \vec{x}+\vec{r}_1) \cdot {}_1 n(t+\tau_2; \vec{x}+\vec{r}_2)\} + \\ &\quad + E\{{}_2 n(t, \vec{x}) \cdot {}_1 n(t+\tau_1; \vec{x}+\vec{r}_1) \cdot {}_1 n(t+\tau_2; \vec{x}+\vec{r}_2)\} + \\ &\quad + E\{O({}_5 n)\} \end{aligned} \quad (3.3)$$

where $E\{O({}_5 n)\}$ means of order five in the perturbation parameter.

Assuming that the random measure of the linear Gaussian estimate is uniformly distributed between $\{-\pi, \pi\}$, the Fourier-Stieltjes integral for the linear estimate may be replaced by the density of the random measure to obtain the following:

$$\begin{aligned} {}_1\eta(t, \vec{x}) &= \iint_{-\infty}^{\infty} F[\vec{k}] \exp i\{\sigma t - \vec{k} \cdot \vec{x}\} d\sigma d\vec{k} \\ &= \iint_{-\infty}^{\infty} |F[\vec{k}]| \cdot \exp i\{\sigma t - \vec{k} \cdot \vec{x}\} \cdot \exp i\{-\psi(\vec{k})\} d\sigma d\vec{k} \end{aligned} \quad (3.4)$$

where $\psi(\vec{k})$ is an independent random phase angle uniformly distributed between $\{-\pi, \pi\}$. Papoulis [96, 97] demonstrates that a random function with this distribution tends rapidly toward a Gaussian random function. The first expectation operator in Eq. (3.3) is, therefore, a third order statistical moment of a Gaussian random variable and is of third order in the perturbation parameter. Appendix A demonstrates that differentiating the moment generating function for a Gaussian random variable three times yields a zero product for this term. The vanishing of this term for a Gaussian random function may also be seen by substituting Eq. (3.4) into the first term of Eq. (3.3) with the following results:

$$\begin{aligned} E\{{}_1\eta(t, \vec{x}) \cdot {}_1\eta(t+\tau_1; \vec{x}+\vec{r}_1) \cdot {}_1\eta(t+\tau_2; \vec{x}+\vec{r}_2)\} &= \\ \iint_{-\infty}^{\infty} \iint_{-\infty}^{\infty} \iint_{-\infty}^{\infty} &|{}_1F(\vec{k}_1)| \cdot |{}_2F(\vec{k}_2)| \cdot |{}_3F(\vec{k}_3)| \cdot \\ \cdot \exp i\{(\sigma_1 + \sigma_2 + \sigma_3)t - (\vec{k}_1 + \vec{k}_2 + \vec{k}_3) \cdot \vec{x}\} \cdot \\ \cdot \exp i\{\sigma_2 \tau_1 - \vec{k}_2 \cdot \vec{r}_1 + \sigma_3 \tau_2 - \vec{k}_3 \cdot \vec{r}_2\} \cdot \\ \cdot E\{\exp i\{-\psi_1(\vec{k}_1) - \psi_2(\vec{k}_2) - \psi_3(\vec{k}_3)\}\} d\vec{k}_1 d\vec{k}_2 d\vec{k}_3 \end{aligned} \quad (3.5)$$

Since the random phase angles, $\psi(\vec{k})$, are independent, the expectation operator may be decomposed into the product of three expectations, i.e.,

$$\begin{aligned} E\{\exp i\{-\psi_1(\vec{k}_1) - \psi_2(\vec{k}_2) - \psi_3(\vec{k}_3)\}\} = \\ E\{\exp i\{-\psi_1(\vec{k}_1)\}\} \cdot E\{\exp i\{-\psi_2(\vec{k}_2)\}\} \cdot E\{\exp i\{-\psi_3(\vec{k}_3)\}\} \end{aligned} \quad (3.6)$$

each of which has zero expectation and is, therefore, equivalent to the probabilistic results derived in Appendix A. Other examples of uniformly distributed random variables are given by Borgman [24].

These results demonstrate an important method of measuring a random process which is Gaussian only in its first order estimate. The lowest order nonvanishing statistical measure of the trivariance function given by Eq. (3.3) for a random process with a Gaussian linear estimate is of fourth order in the perturbation parameter and is due solely to existence of the second order nonlinear correction to the linear Gaussian estimate. Moreover, this lowest order nonvanishing measure is closed at second order in the perturbation parameter as no other higher perturbation orders may form third order statistical moments which are of fourth order in the perturbation parameter. In order to interpret further the effects of the second order correction on the trivariance function, an explicit form of this correction is required and will be computed in the following section.

4. Nonlinear Wave-Wave Interactions Correct to Second Perturbation Order

An excellent formulation of the boundary value problem for surface gravity waves is given by Wehausen [127; pp. 447-455] and this formulation is equally valid for random surface gravity waves. As noted in Section 1, the convergence of random functions, derivatives and integrals used in the random boundary value problem will be in mean square. In addition, Fourier-Stieltjes integrals which require no *a priori* assumption regarding the existence of a density function will be utilized. (cf. Bharuchua-Reid [13]).

The fluid is assumed to be inviscid and incompressible. The fluid motion is assumed to be irrotational and three-dimensional. The x, y coordinate axes lie in a horizontal plane at the mean sea level, $z=0$, with the z axis positive upwards. A random velocity potential, Φ , exists such that

$$\vec{u}(x, y, z, t) = -\vec{\nabla}\Phi \quad (4.1)$$

For notational compactness, the horizontal x, y plane will be denoted by

$$\vec{x} = x\vec{e}_x + y\vec{e}_y \quad (4.2)$$

The governing partial differential field equation for the random velocity potential, Φ , is the equation of continuity for an irrotational fluid flow;

$$\Delta\Phi = \nabla^2\Phi = 0 ; \quad |\vec{x}| < \infty, -h \leq z \leq \eta(\vec{x}, t), t \geq 0 \quad (4.3)$$

where the three-dimensional gradient operator, $\vec{\nabla}(\cdot)$, is given by

$$\vec{\nabla}(\cdot) = \frac{\partial(\cdot)}{\partial x} \hat{e}_x + \frac{\partial(\cdot)}{\partial y} \hat{e}_y + \frac{\partial(\cdot)}{\partial z} \hat{e}_z \quad (4.4)$$

and \hat{e}_i are the orthogonal unit vectors in the three-dimensional cartesian coordinate system. The finite depth fluid domain is assumed to be unbounded in the horizontal dimensions so that the boundary conditions required at the horizontal boundaries located at infinity are those which preclude partial standing waves; and the boundary conditions required to quantify the unknown coefficients or eigenvalues are prescribed at the free surface and horizontal bottom boundaries. The fluid is assumed to occupy a finite depth, h , in the lower half plane and to satisfy the following no flow bottom boundary condition (BBC) across the horizontal impermeable bottom:

$$\text{BBC: } \Phi_z = 0 ; \quad z = -h, |\vec{x}| < \infty, t \geq 0 \quad (4.5)$$

The fluid surface, $\eta(t, \vec{x})$, is unconstrained and a kinematic free surface boundary condition (KFSBC) is required to prescribe mathematically the continuity of fluid motion at the interface and to ensure physically that no fluid particles are convected across this interface; i.e.,

$$\text{KFSBC: } n_t - 2\vec{\nabla}\Phi \cdot \vec{\nabla}\eta + \Phi_z = 0 ; \quad z = \eta(\vec{x}, t), |\vec{x}| < \infty, t \geq 0 \quad (4.6)$$

where the two-dimensional horizontal gradient operator, ${}_2\vec{\nabla}(\cdot)$, is given by

$$_2\vec{\nabla}(\cdot) = \frac{\partial(\cdot)}{\partial x} \vec{e}_x + \frac{\partial(\cdot)}{\partial y} \vec{e}_y \quad (4.7)$$

An additional dynamic free surface boundary constraint is required to ensure that all stresses acting along the free surface are continuous. In the absence of surface tension and for an atmospheric pressure assumed to be zero, the dynamic free surface boundary condition (DFSBC) may be obtained via the Bernoulli equation, i.e.,

$$-\Phi_t + gn + \frac{1}{2}|\vec{\nabla}\Phi|^2 = Q(t); \quad z = \eta(\vec{x}, t), |\vec{x}| < \infty, t \geq 0 \quad (4.8)$$

The total derivative of the Bernoulli equation (cf. Phillips [100], p. 23) combined with the KFSBC eliminates the unknown scalar free surface elevation, $\eta(\vec{x}, t)$, from the DFSBC boundary condition to yield the following combined free surface boundary condition (CFSBC):

$$\left(\frac{\partial}{\partial t} - \vec{\nabla}\Phi \cdot \vec{\nabla} \right) \left(\Phi_t - gn - \frac{1}{2}|\vec{\nabla}\Phi|^2 + Q(t) \right) = 0; \quad z = \eta(\vec{x}, t), |\vec{x}| < \infty, t \geq 0 \quad (4.9)$$

which may be expanded to the following form:

$$\Phi_{tt} + g\Phi_z + Q_t - \left(\frac{\partial}{\partial t} - \frac{\vec{\nabla}\Phi}{2} \cdot \vec{\nabla} \right) |\vec{\nabla}\Phi|^2 = 0; \quad z = \eta(\vec{x}, t), |\vec{x}| < \infty, t \geq 0 \quad (4.10)$$

In order to avoid evaluating the CFSBC at the unknown free surface elevation, $\eta(\vec{x}, t)$, and in order to utilize a separable coordinate system to solve the governing field equation [Eq. (4.3)], the CFSBC is expanded in a Maclaurin series about the still water level, $z=0$, i.e.,

$$\sum_{v=0}^{\infty} n^v \frac{\partial^v}{\partial z^v} \left(\Phi_{tt} + g\Phi_z + Q_t - \left[\frac{\partial}{\partial t} - \frac{\vec{\nabla}\Phi}{2} \cdot \vec{\nabla} \right] |\vec{\nabla}\Phi|^2 \right) = 0; \quad z = 0, |\vec{x}| < \infty, t \geq 0 \quad (4.11)$$

In order to obtain approximate solutions to Eq. (4.3) subject to the nonlinear CFSBC, the nonlinearities are assumed to impose small perturbations on an initial linear approximation. The measure of the perturbation is assumed to be proportional to the wave slope and will be used as the measure of the perturbation ordering parameter. However, it is not *a priori* clear that the ordering of the perturbations by a parameter is valid for either a continuous or discrete spectrum of random surface gravity waves. Rellich [108] has devoted considerable research into providing mathematical rigor to problems of perturbing spectra in Hilbert space and has established a sufficient set of proofs to ensure the validity of the perturbation concept. Friedrichs [50] continued the work initiated by Rellich and contributed further to the completeness of the proofs. The proofs which are required to establish the existence of a perturbation ordering parameter for a continuous spectrum in Hilbert space are too complex to be covered here. The material given by Rellich [108] and Friedrichs [50] and summarized by Dunford and Schwartz [43] establish the validity of a perturbation ordering parameter for a continuous spectrum and will be assumed without proof in the following development.

The random velocity potential, random sea surface realization, and the Bernoulli constant are assumed to be expandable in the following power series with the perturbation

ordering parameter implicitly absorbed into the functional notation:

$$\Phi(\vec{x}, z, t) = \sum_{v=1}^{\infty} v \Phi_v(\vec{x}, z, t) \quad (4.12a)$$

$$\eta(\vec{x}, t) = \sum_{v=1}^{\infty} v \eta_v(\vec{x}, t) \quad (4.12b)$$

$$Q(t) = \sum_{v=1}^{\infty} v Q_v(t) \quad (4.12c)$$

Substituting Eqs. (4.12a,b,c) into the equations of the boundary value problem and equating equal orders of v , the following set of linear boundary value problems is obtained:

$$v = 1: \quad \nabla_1^2 \Phi = 0; \quad -h \leq z \leq 0, |\vec{x}| < \infty \quad (4.13a)$$

$$1^\Phi_z = 0; \quad z = -h, |\vec{x}| < \infty \quad (4.13b)$$

$$1^\Phi_{tt} + g_1^\Phi z + 1^Q_t = 0; \quad z = 0, |\vec{x}| < \infty, t \geq 0 \quad (4.13c)$$

$$1^\eta = \frac{1}{g} \{ 1^\Phi_t + 1^Q \}; \quad z = 0, |\vec{x}| < \infty, t \geq 0 \quad (4.13d)$$

$$v = 2: \quad \nabla_2^2 \Phi = 0; \quad -h \leq z \leq 0, |\vec{x}| < \infty \quad (4.14a)$$

$$2^\Phi_z = 0; \quad z = -h, |\vec{x}| < \infty \quad (4.14b)$$

$$2^\Phi_{tt} + g_2^\Phi z + 2^Q_t = \frac{\partial}{\partial t} |\vec{\nabla}_1 \Phi|^2 - 1^\eta \cdot \frac{\partial}{\partial z} \{ 1^\Phi_{tt} + g_1^\Phi z \}; \\ z = 0, |\vec{x}| < \infty, t \geq 0 \quad (4.14c)$$

$$2^\eta = \frac{1}{g} \{ 2^\Phi_t - \frac{|\vec{\nabla}_1 \Phi|^2}{2} + \frac{1^\eta}{g} 1^\Phi_t z + 2^Q \};$$

$$z = 0, |\vec{x}| < \infty, t \geq 0 \quad (4.14d)$$

A solution which satisfies exactly Eqs. (4.13a,b) is given by the following Fourier-Stieltjes integral:

$$1^{\Phi}(\vec{x}, z, t) = -i \int_{-\infty}^{\infty} g \cdot \frac{\cosh\{|\vec{k}|(h+z)\}}{\cosh\{|\vec{k}|h\}} \cdot \exp i\{-\vec{k} \cdot \vec{x}\} d_1 A[\vec{k}, t] \quad (4.15)$$

where $d_1 A[\vec{k}, t]$ is the random measure of the velocity potential. Equation (4.15) requires no *a priori* assumption regarding either the existence of a density function or the temporal dependence of the random velocity potential.

Absorbing the temporal derivative of the Bernoulli constant in Eq. (4.13c) into the random measure, $d_1 A[\vec{k}, t]$, by requiring that the random process maintain a zero mean, yields the following initial value problem for the time dependence of the random measure:

$$-i \int_{-\infty}^{\infty} g \cdot \exp i\{-\vec{k} \cdot \vec{x}\} \cdot [\frac{\partial^2}{\partial t^2} + g |\vec{k}| \tanh\{|\vec{k}|h\}] d_1 A[\vec{k}, t] = 0 \quad (4.16)$$

The deterministic Green's function which satisfies this initial value problem was first derived by Finkelstein [45]. Friedman and Shinbrot [47,48] have extended his results to generalized normal domains and have discussed the deterministic solutions in exhaustive detail. The solutions to the random initial value problem, however, are less perspicuous and involve an irreversibility paradox with regard to the statistics of the initial conditions. In order to avoid the complications attendant with these initial value statistics, the random process will be assumed to be both stationary and ergodic. These assumptions render the solution statistically

independent of any initial conditions. A discussion of the effect of these assumptions on the stochastic integral given by Eq. (4.15) may be found in Kinsman [72; Ch. 8].

Equation (4.16) may be solved by the application of the spectral theory of random operators (cf. Dunford and Schwartz [43] or Friedman [49]). The integrand in Eq. (4.16) may be written in spectral operator notation by

$$L[\vec{k}, t] \cdot \{d_1 A\} = 0 \quad (4.17)$$

where the linear spectral operator, L , is given by

$$L[\vec{k}, t] = \frac{\partial^2}{\partial t^2} + g|\vec{k}| \tanh\{| \vec{k} | h\} \quad (4.18)$$

Equation (4.17) is satisfied either by the trivial solution

$$d_1 A[\vec{k}, t] \equiv 0 \quad \forall \vec{k}, t \quad (4.19)$$

or by the zeroes of the spectral operator

$$L[\vec{k}, t] = 0 \quad (4.20)$$

Equation (4.17) requires that the spectrum of the random measure, $d_1 A[\vec{k}, t]$, vanish identically everywhere except along the hypersurface given by the zeroes of the spectral operator. An integral which satisfies Eq. (4.17) may be represented by the following:

$$d_1 A[\vec{k}, t] = \int_{-\infty}^{\infty} \exp i\{\sigma t\} d_1^2 A[\vec{k}, \sigma] \quad (4.21)$$

where the eigenvalues, \vec{k} , are determined by the zeroes of the spectral operator, L ; viz.,

$$\sigma^2 = g|\vec{k}| \tanh\{|\vec{k}|h\} \quad (4.22)$$

Equation (4.22) establishes a relationship between the stochastic integral given by Eq. (4.15) and the hydrodynamics of the boundary value problem. The hydrodynamic boundary condition requires that the spectral representation of the random measure vanish everywhere in the \vec{k}, σ space except along the curve given by Eq. (4.22). This restriction on the spectrum of $d_{1A}[\vec{k}, \sigma]$ may be given by the following Dirac delta distribution (cf. Kinsman [72], Ch. 7.3).

$$d_{1A}[\vec{k}(\sigma)] = d_{1A}[\vec{k}, \sigma'] \delta(\sigma' - \sigma) \quad (4.23)$$

Alternate methods for computing the eigenvalues given by Eq. (4.22) and the spectrum of the random measure given by Eq. (4.23) for general random differential equations are given by Boyce [26]. Methods which are specifically applicable to random waves in a dispersive media are given by Frisch [51]. For the random surface gravity wave problem formulated above the fluid media is assumed to be nonrandom and the eigenvalues computed by Eq. (4.22) are deterministic. Additional methods for applying the CFSBC given by Eqs. (4.13c) and (4.14c) are given by Phillips [100] who has pointed out the similarity of the CFSBC to the equation of an undamped harmonic oscillator.

Substituting Eq. (4.21) into the general solution given by Eq. (4.15) and using Eq. (4.23) gives the following random velocity potential:

$$l^{\Phi}(\vec{x}, z, t) = -i \int_{-\infty}^{\infty} g \cdot \frac{\cosh\{|\vec{k}|(h+z)\}}{\cosh\{|\vec{k}|h\}} \cdot \exp i\{\sigma t - \vec{k} \cdot \vec{x}\} d_1 A[\vec{k}(\sigma)] \quad (4.24)$$

where the reality of the random velocity potential requires the following complex conjugate relationship:

$$d_1 A[-\vec{k}(\sigma)] = d_1 A^*[\vec{k}(\sigma)] \quad (4.25)$$

The random sea surface realization is determined from Eq. (4.13d), i.e.,

$$l^n(\vec{x}, t) = \int_{-\infty}^{\infty} \sigma \cdot \exp i\{\sigma t - \vec{k} \cdot \vec{x}\} d_1 A[\vec{k}(\sigma)] \quad (4.26)$$

The spectral representation of the random measure of the random velocity potential may be redefined in terms of the spectral representation of the random sea surface elevation by the following:

$$d_1 F[\vec{k}(\sigma)] = \sigma \cdot d_1 A[\vec{k}(\sigma)] \quad (4.27)$$

In terms of the spectral representation of the random sea surface measure, $d_1 F[\vec{k}(\sigma)]$, the random velocity potential and random sea surface realization become the following:

$$l^{\Phi}(\vec{x}, z, t) = -i \int_{-\infty}^{\infty} \frac{g}{\sigma} \cdot \frac{\cosh\{|\vec{k}|(h+z)\}}{\cosh\{|\vec{k}|h\}} \cdot \exp i\{\sigma t - \vec{k} \cdot \vec{x}\} d_1 F[\vec{k}(\sigma)] \quad (4.28a)$$

$$l^n(\vec{x}, t) = \int_{-\infty}^{\infty} \exp i\{\sigma t - \vec{k} \cdot \vec{x}\} d_1 F[\vec{k}(\sigma)] \quad (4.28b)$$

The functional form of the solution to the second set of equations which are correct to second order in the perturbation parameter and which are given by Eqs. (4.14a,b,c,d) is assumed to be similar to the first order solution given by

Eq. (4.28a). Denoting the frequency, ω , and the separation constant, $\kappa(\omega)$, in a general form which are to be evaluated through the boundary conditions, a solution which satisfies exactly Eqs. (4.14a,b) is given by the following random integral:

$${}_2\Phi(\vec{x}, z, t) = -i \int_{-\infty}^{\infty} \frac{\cosh\{|\vec{\kappa}|(h+z)\}}{\cosh\{|\vec{\kappa}|h\}} \cdot \exp i\{\omega t - \vec{\kappa} \cdot \vec{x}\} \cdot d_2 B[\vec{\kappa}(\omega)] \quad (4.29)$$

As noted previously, Eq. (4.14c) is equivalent to the equation for a forced, undamped harmonic oscillator. This equation has been studied extensively in the theory of spectral operators and may be written in the following spectral operator form:

$$\begin{aligned} -i \int_{-\infty}^{\infty} \exp i\{\omega t - \vec{\kappa} \cdot \vec{x}\} \cdot L[\omega, \vec{\kappa}(\omega)] \cdot d_2 B[\vec{\kappa}(\omega)] &= \\ = \int_{-\infty}^{\infty} \exp i\{(\sigma_1 + \sigma_2)t - (\vec{k}_1 + \vec{k}_2) \cdot \vec{x}\} \cdot N[\sigma_1, \sigma_2; \vec{k}_1(\sigma_1) \vec{k}_2(\sigma_2)] \cdot \\ \cdot d_1 F[\vec{k}_1(\sigma_1)] d_2 F[\vec{k}_2(\sigma_2)] \end{aligned} \quad (4.30)$$

where $L[\omega, \vec{\kappa}(\omega)]$ is a linear spectral operator and $N[\sigma_1, \sigma_2; \vec{k}_1(\sigma_1) \vec{k}_2(\sigma_2)]$ is the spectral operator for the non-linear derivatives given by the right side of Eq. (4.14c). The general functional form of the separation constant, $\kappa(\omega)$, and frequency, ω , may now be quantified by requiring equivalence of the temporal and spatial functions in Eq. (4.30). This equivalence requires a change of variables in the integral for the second order random velocity potential. Hildebrand [64] or Sokolnikoff and Redheffer [115] give the

requirements for the application of the following change of variables equation:

$$\int_R \xi(x, y) dx dy = \int_R \xi\{f(u, v), g(u, v)\} |J(\frac{x, y}{u, v})| du dv \quad (4.31)$$

where $|J(\cdot)|$ is the absolute value of the Jacobian of the change of variables and R, R are the regions of integration.

Introduce the following change of variables in Eq. (4.30):

$$\omega = \sigma_1 + \sigma_2 \quad (4.32a)$$

$$\vec{k} = \vec{k}_1(\sigma_1) + \vec{k}_2(\sigma_2) \quad (4.32b)$$

which have the following nonvanishing Jacobian:

$$J\left(\frac{\vec{k}, \omega}{\vec{k}_1(\sigma_1), \vec{k}_2(\sigma_2)}\right) = \begin{vmatrix} \frac{\partial \vec{k}}{\partial \vec{k}_1} & \frac{\partial \vec{k}}{\partial \vec{k}_2} \\ \frac{\partial \omega}{\partial \sigma_1} \cdot \frac{d\sigma_1}{d\vec{k}_1} & \frac{\partial \omega}{\partial \sigma_2} \cdot \frac{d\sigma_2}{d\vec{k}_2} \end{vmatrix} = C_{g_2} - C_{g_1} \quad (4.33)$$

where C_{g_i} is the group velocity of the i^{th} component. The CFSBC now becomes

$$\begin{aligned} -i \int_{-\infty}^{\infty} \exp i\{(\sigma_1 + \sigma_2)t - (\vec{k}_1 + \vec{k}_2) \cdot \vec{x}\} \cdot \left| J\left(\frac{\vec{k}, \omega}{\vec{k}_1(\sigma_1), \vec{k}_2(\sigma_2)}\right) \right| \cdot \\ \cdot L[\sigma_1, \sigma_2; \vec{k}_1, \vec{k}_2] \cdot d_2 B[\vec{k}_1(\sigma_1), \vec{k}_2(\sigma_2)] = \\ = \int_{-\infty}^{\infty} \exp i\{(\sigma_1 + \sigma_2)t - (\vec{k}_1 + \vec{k}_2) \cdot \vec{x}\} \cdot \\ \cdot n[\sigma_1, \sigma_2; \vec{k}_1, \vec{k}_2] d_1 F[\vec{k}_1(\sigma_1)] d_2 F[\vec{k}_2(\sigma_2)] \end{aligned} \quad (4.34)$$

which may be solved for the spectral representation of the random velocity potential correct to second order to give the following:

$$d_{2B}[\vec{k}_1(\sigma_1), \vec{k}_2(\sigma_2)] = \frac{N[\sigma_1, \sigma_2; \vec{k}_1, \vec{k}_2] d_{1F}[\vec{k}_1(\sigma_1)] d_{2F}[\vec{k}_2(\sigma_2)]}{|J\{\frac{\vec{k}, \omega}{\vec{k}_1(\sigma_1), \vec{k}_2(\sigma_2)}\}| \cdot L[\sigma_1, \sigma_2; \vec{k}_1(\sigma_1), \vec{k}_2(\sigma_2)]} \quad (4.35)$$

provided that neither the Jacobian, $|J(\cdot)|$, nor the linear spectral operator, $L[\cdot]$, are singular. The diagonal terms of the Jacobian are Stokian nondispersive waves and the Jacobian, therefore, may be seen from Eq. (4.33) to be nonsingular.

Phillips [101] and Hasselmann [54] have demonstrated by separate proofs that the linear dispersion equation given by Eq. (4.22) is convex toward the \vec{k} axis in the σ, \vec{k} plane and, therefore, no zeroes may occur in $L[\cdot]$. Dunford and Schwartz [43], Friedman [49], and Sveshnikov [119] give polynomial expansions for the ratio of spectral operators equivalent to those given in Eq. (4.35) whenever zeroes occur in the spectral operator $L[\cdot]$. In addition, since Eq. (4.30) is an inhomogeneous boundary condition resulting from the perturbation expansions, the homogeneous solutions to Eq. (4.30) are identical to those given by Eq. (4.17). Therefore, since the spectral operator in Eq. (4.35) is nonsingular and since the homogeneous solutions which correspond to the zeroes in $L[\cdot]$ are identical to the linear solution and limited by the Dirac delta distribution given in Eq. (4.23), no "free wave" solutions may exist at second order.

Substituting the appropriate derivatives into the two spectral operators in Eq. (4.35) yields the following spectral response function for the random second order velocity potential:

$$\begin{aligned} \frac{n[\sigma_1, \sigma_2; \vec{k}_1, \vec{k}_2]}{z[\sigma_1, \sigma_2; \vec{k}_1, \vec{k}_2]} &= \\ &= \left\{ \frac{2(\sigma_1 + \sigma_2) \cdot [g^2 \vec{k}_1 \cdot \vec{k}_2 - \sigma_1^2 \sigma_2^2] - \sigma_1 \sigma_2 (\sigma_1^3 + \sigma_2^3) + g^2 [\vec{k}_1^2 \sigma_2^2 + \vec{k}_2^2 \sigma_1^2]}{2\sigma_1 \sigma_2 \{(\sigma_1 + \sigma_2)^2 - g |\vec{k}_1 + \vec{k}_2| \cdot \tanh[|\vec{k}_1 + \vec{k}_2| h]\}} \right\} \end{aligned} \quad (4.36)$$

Making the change of variables given by Eqs. (4.32a,b) with the Jacobian given by Eq. (4.33) results in the following equation for the random second order velocity potential:

$$\begin{aligned} z^\Phi(\vec{x}, z, t) &= -i \iint_{-\infty}^{\infty} \frac{\cosh\{|\vec{k}_1 + \vec{k}_2|(h+z)\}}{\cosh\{|\vec{k}_1 + \vec{k}_2|h\}} \cdot \\ &\quad \cdot \exp i\{(\sigma_1 + \sigma_2)t - (\vec{k}_1 + \vec{k}_2) \cdot \vec{x}\} \cdot \\ &\quad \cdot \left| J\left(\frac{\vec{k}, \omega}{\vec{k}_1(\sigma_1), \vec{k}_2(\sigma_2)} \right) \right| d_2 B[\vec{k}_1(\sigma_1), \vec{k}_2(\sigma_2)] \end{aligned} \quad (4.37)$$

Substitution for the random spectral representation, $d_2 B[\vec{k}_1(\sigma_1), \vec{k}_2(\sigma_2)]$, given by Eq. (4.35) and for the spectral response function given by Eq. (4.36) yields the following expression for the random second order velocity potential:

$$\begin{aligned} z^\Phi(\vec{x}, z, t) &= -i \iint_{-\infty}^{\infty} \frac{\cosh\{|\vec{k}_1 + \vec{k}_2|(h+z)\}}{\cosh\{|\vec{k}_1 + \vec{k}_2|h\}} \cdot \\ &\quad \cdot \exp i\{(\sigma_1 + \sigma_2)t - (\vec{k}_1 + \vec{k}_2) \cdot \vec{x}\} \cdot D[\sigma_1, \sigma_2; \vec{k}_1(\sigma_1), \vec{k}_2(\sigma_2)] \cdot \\ &\quad \cdot d_1 F[\vec{k}_1(\sigma_1)] \cdot d_2 F[\vec{k}_2(\sigma_2)] \end{aligned} \quad (4.38)$$

where the nonlinear interaction kernel, $D[\sigma_1, \sigma_2; \vec{k}_1(\sigma_1), \vec{k}_2(\sigma_2)]$, is equivalent to the spectral response function given by Eq. (4.36).

The second order correction for the random sea surface realization may now be evaluated by substituting into Eq. (4.14d) the proper derivatives of Eqs. (4.28a,b) and Eq. (4.38). Evaluating, as before, the second order Bernoulli constant, σ_2^Q , in order to maintain a zero mean second order random process yields the following expression for the second order random sea realization:

$$\sigma_2^n(\vec{x}, t) = \frac{1}{2g} \int_{-\infty}^{\infty} \exp i\{(\sigma_1 + \sigma_2)t - (\vec{k}_1 + \vec{k}_2) \cdot \vec{x}\} \cdot H[\sigma_1, \sigma_2; \vec{k}_1, \vec{k}_2] \cdot d_1 F[\vec{k}_1(\sigma_1)] \cdot d_2 F[\vec{k}_2(\sigma_2)] \quad (4.39)$$

where the nonlinear interaction kernel, $H[\sigma_1, \sigma_2; \vec{k}_1, \vec{k}_2]$, is the spectral response function determined by the derivatives of the right side of Eq. (4.14d) and is given by

$$H[\sigma_1, \sigma_2; \vec{k}_1(\sigma_1), \vec{k}_2(\sigma_2)] = 2(\sigma_1 + \sigma_2) \cdot D[\sigma_1, \sigma_2; \vec{k}_1(\sigma_1), \vec{k}_2(\sigma_2)] - \frac{g^2 \vec{k}_1 \cdot \vec{k}_2}{\sigma_1 \sigma_2} + \sigma_1 \sigma_2 + \sigma_1^2 + \sigma_2^2 \quad (4.40)$$

Note that the second order random sea realization given by Eq. (4.39) is inversely proportional to the gravitational constant, g.

The nonlinear interaction kernel given by Eq. (4.40) is expressed in a symmetric form. Different forms may be obtained when the appropriate derivatives are substituted into the inhomogeneous forcing term on the right side of Eq. (4.14d). Wiener [132] has pointed out that any kernel operating on the product of identical random functions having

symmetric domains of integrations may be rendered symmetric by reversing the arguments in the kernel, adding the two kernels and dividing by two. This procedure has been used to obtain the symmetric kernels used in Eqs. (4.36) and (4.40).

The equation for the nonlinear sea surface realization correct to second order is obtained by adding Eqs. (4.28b) and (4.39), i.e.,

$$\begin{aligned} n(\vec{x}, t) = & \mathbf{1}n(\vec{x}, t) + \mathbf{2}n(\vec{x}, t) = \int_{-\infty}^{\infty} \exp i\{\sigma t - \vec{k} \cdot \vec{x}\} \cdot dF[\vec{k}(\sigma)] + \\ & + \frac{1}{2g} \int_{-\infty}^{\infty} \int_{-\infty}^{\infty} H\{\sigma_1, \sigma_2; \vec{k}_1(\sigma_1), \vec{k}_2(\sigma_2)\} \cdot \\ & \cdot \exp i\{(\sigma_1 + \sigma_2)t - (\vec{k}_1 + \vec{k}_2) \cdot \vec{x}\} \cdot d_1 F[\vec{k}_1(\sigma_1)] \cdot d_2 F[\vec{k}_2(\sigma_2)] \end{aligned} \quad (4.41)$$

Upon making the following change of variables in the integral for the second order random sea,

$$\sigma = \sigma_1 + \sigma_2 \quad (4.42)$$

the expression for the random sea realization becomes

$$\begin{aligned} n(\vec{x}, t) = & \int_{-\infty}^{\infty} \{\exp i\{-\vec{k}(\sigma) \cdot \vec{x}\} \cdot dF[\vec{k}(\sigma)] + \\ & + \frac{1}{2g} \int_{-\infty}^{\infty} H\{\sigma, \sigma - \sigma_1; \vec{k}_1(\sigma_1), \vec{k}_2(\sigma - \sigma_1)\} \cdot \\ & \cdot \exp i\{-[\vec{k}_1(\sigma_1) + \vec{k}_2(\sigma - \sigma_1)] \cdot \vec{x}\} \cdot d_1 F[\vec{k}_1(\sigma_1)] \cdot d_2 F[\vec{k}_2(\sigma - \sigma_1)]\} \cdot \\ & \cdot \exp i\{\sigma t\} \end{aligned} \quad (4.43)$$

Comparing Eq. (4.43) with Eq. (2.1), the random nonlinear sea surface correct to second order is seen to be

$$\eta(\vec{x}, t) = \int_{-\infty}^{\infty} \exp i\{\sigma t\} \cdot dx[\vec{k}(\sigma), \vec{x}] \quad (4.44)$$

where

$$dx[\vec{k}(\sigma), \vec{x}] = \exp i\{-\vec{k} \cdot \vec{x}\} \cdot d_F[\vec{k}(\sigma)] \\ + \frac{1}{2g} \int_{-\infty}^{\infty} H[\sigma_1, \sigma - \sigma_1; \vec{k}_1(\sigma_1), \vec{k}_2(\sigma - \sigma_1)] \cdot \\ \cdot \exp i\{-[\vec{k}_1 + \vec{k}_2] \cdot \vec{x}\} \cdot d_1 F[\vec{k}_1(\sigma_1)] \cdot d_2 F[\vec{k}_2(\sigma - \sigma_1)] \quad (4.45)$$

The important point to note about this final expression for the random sea surface realization is that for a fixed set of horizontal spatial coordinates, the quadratic contributions occur at the same frequencies as those of the linear Gaussian realization. This is a key point in the application of the fast Fourier transform and the resulting simplification of the computation of nonlinear random realizations. Note also that the second order contributions to the random measure, $dx[\vec{k}(\sigma), \vec{x}]$, which are given by the integral term in Eq. (4.44), are a function of the sums and differences in wave numbers, $\vec{k}(\sigma)$. Consequently, all of the second order contributions which result from this convolution integral are not phase locked or nondispersive with respect to the linear Gaussian estimate at that same frequency. The simple example for deep water waves given in Section 2 of Chapter 1 illustrated the manner in which these second order contributions are nondispersive with respect to the linear Gaussian spectrum and the resulting linear profile.

5. The Bispectrum

The bispectrum is the Fourier transform of the trivariate function and represents the spectral density of the contributions to the mean cube of the random sea realization, $\eta(\vec{x}, t)$, by a product of three Fourier densities whose resultant frequency equals zero (cf. Hasselmann et al. [57]). This Fourier transform pair was shown in Section 3 to yield a measure of the second order contributions to the random sea realization which is closed to the second order in perturbation parameter. Since much useful information regarding stationary, homogeneous random processes may be obtained from this transform pair, a brief discussion of the bispectrum is developed in this section.

The lowest order nonvanishing third order statistical moment for a linear Gaussian estimate was computed in Eq. (3.3) and may now be decomposed explicitly into first and second order perturbation contributions using the results of Section 4:

$$\begin{aligned}
 & \gamma(\tau_1, \tau_2; \vec{r}_1, \vec{r}_2) = \\
 & = \int_{-\infty}^{\infty} \int_{-\infty}^{\infty} \left[H[\sigma_3, \sigma_4; \vec{k}_3, \vec{k}_4] \cdot \exp i\{\sigma_2 \tau_1 + (\sigma_3 + \sigma_4) \tau_2 - \vec{k}_2 \cdot \vec{r}_1 - (\vec{k}_3 + \vec{k}_4) \cdot \vec{r}_2\} \right. \\
 & \quad \left. + H[\sigma_2, \sigma_3; \vec{k}_2, \vec{k}_3] \cdot \exp i\{(\sigma_2 + \sigma_3) \tau_1 + \sigma_4 \tau_2 - (\vec{k}_2 + \vec{k}_3) \cdot \vec{r}_1 - \vec{k}_4 \cdot \vec{r}_2\} + \right. \\
 & \quad \left. + H[\sigma_1, \sigma_2; \vec{k}_1, \vec{k}_2] \cdot \exp i\{\sigma_3 \tau_1 + \sigma_4 \tau_2 - \vec{k}_3 \cdot \vec{r}_1 - \vec{k}_4 \cdot \vec{r}_2\} \right] \\
 & \quad \cdot \exp i\{(\sigma_1 + \sigma_2 + \sigma_3 + \sigma_4) t - (\vec{k}_1 + \vec{k}_2 + \vec{k}_3 + \vec{k}_4) \cdot \vec{x}\} \cdot \\
 & \quad \cdot E\{d_1 F[\vec{k}_1(\sigma_1)] \cdot d_2 F[\vec{k}_2(\sigma_2)] \cdot d_3 F[\vec{k}_3(\sigma_3)] \cdot d_4 F[\vec{k}_4(\sigma_4)]\} \\
 & \quad + O\{\zeta\}
 \end{aligned} \tag{5.1}$$

This is a fourth order moment of the Gaussian random measure, $d\Gamma[\vec{k}(\sigma)]$, which may be factored as shown in Appendix A into the sum of three product pairs of all possible permutations of the four Gaussian variates. If the process is assumed to be spatially homogeneous, the spectral distribution function may be expressed by Eq. (2.5) in which the arguments of the Dirac delta distributions are all possible permutations of wave numbers which result from the products of the decomposition of a fourth order Gaussian random measure. The frequency dependence of the wave number given by the linear dispersion equation in Eq. (4.22) also results in a temporally stationary process when the integrations over the Dirac delta distributions are performed. This fact has already been used to eliminate the frequency dependence from the random spectral measure in Section 4. It can be shown, finally, that the term of lowest order in the perturbation parameter which is nonvanishing in the trivariate function for homogeneous, stationary random surface gravity waves reduces to:

$$\gamma(\tau_1, \tau_2; \vec{r}_1, \vec{r}_2) = \iint_{-\infty}^{\infty} s[\vec{k}_1(\sigma_1)] \cdot s[\vec{k}_2(\sigma_2)] \cdot \bar{H}[\sigma_1, \sigma_2, \tau_1, \tau_2; \vec{k}_1, \vec{k}_2, \vec{r}_1, \vec{r}_2] d\vec{k}_1 d\vec{k}_2 \quad (5.2)$$

where the nonlinear interaction kernel $\bar{H}[\sigma_1, \sigma_2, \tau_1, \tau_2; \vec{k}_1, \vec{k}_2, \vec{r}_1, \vec{r}_2]$ includes nine permutations of the previously derived nonlinear interaction kernel, $H[\sigma_1, \sigma_2; \vec{k}_1, \vec{k}_2]$, and the complex unit vectors of the time and space lags, τ and \vec{r} .

Formally, the double Fourier transform of the trivariate function is the bispectrum and may be expressed by

$$\begin{aligned} B[\vec{k}_1(\sigma_1), \vec{k}_2(\sigma_2)] = & \frac{1}{(2\pi)^6} \iiint_{-\infty}^{\infty} \gamma[\tau_1, \tau_2; \vec{r}_1, \vec{r}_2] \\ & \exp i\{-\omega_1\tau_1 - \omega_2\tau_2 + \vec{k}_1 \cdot \vec{r}_1 + \vec{k}_2 \cdot \vec{r}_2\} d\vec{r}_1 d\vec{r}_2 d\tau_1 d\tau_2 \end{aligned} \quad (5.3)$$

Hasselmann et al. [57] have given the symmetry properties of the Fourier transform pair for the trivariate function and bispectrum and have investigated the bispectrum of pressure records from surface gravity waves to determine the directional spread of the wave spectra. Brillinger and Rosenblatt [29,30] give smoothing functions and other useful relations for these general higher order polyspectra.

MacDonald [82], Hinch and Clay [66], and Haubrich [63] derive useful expressions for determining bispectral estimates via the Fast Fourier Transform algorithm. Although much useful information about the random sea process appears to be discernible from bispectral estimates, only the coarse measure of the trivariate function for time and space lags which are identically zero (*viz.*, the skewness) will be employed in this study.

Attempts to obtain a convolution relationship from Eq. (5.2) for the bispectral estimates given in Eq. (5.3) which would be similar to those given by Tick [123] for the second order spectra did not prove successful.

6. Second Perturbation Order Spectra

Although the autocovariance function for random sea surface realizations is not closed at the second perturbation order, it is of interest to compute the spectral contribution which results from the second perturbation order correction to the random linear sea realization.

The autocovariance function for homogeneous, stationary random sea correct to second perturbation order is given by

$$\begin{aligned}
 \gamma(\tau, \vec{r}) &= E\{[{}_1n(t, \vec{x}) + {}_2n(t, \vec{x})] \cdot [{}_1n(t+\tau; \vec{x}+\vec{r}) + {}_2n(t+\tau; \vec{x}+\vec{r})]\} \\
 &= E\{{}_1n(t; \vec{x}) {}_1n(t+\tau; \vec{x}+\vec{r})\} + \\
 &\quad + E\{{}_1n(t; \vec{x}) \cdot {}_2n(t+\tau; \vec{x}+\vec{r}) + {}_2n(t; \vec{x}) \cdot {}_1n(t+\tau; \vec{x}+\vec{r})\} + \\
 &\quad + E\{{}_2n(t; \vec{x}) \cdot {}_2n(t+\tau; \vec{x}+\vec{r})\} \\
 &= \int_{-\infty}^{\infty} \int_{-\infty}^{\infty} \exp i\{(\sigma_1 + \sigma_2)t - (\vec{k}_1 + \vec{k}_2) \cdot \vec{x}\} \cdot \exp i\{\sigma_2 \tau - \vec{k}_2 \cdot \vec{r}\} \cdot \\
 &\quad \cdot E\{d_{1F}[\vec{k}_1, \sigma_1] \cdot d_{2F}[\vec{k}_2, \sigma_2]\} + \\
 &\quad + \int_{-\infty}^{\infty} \int_{-\infty}^{\infty} \int_{-\infty}^{\infty} \int_{-\infty}^{\infty} \exp i\{(\sigma_1 + \sigma_2 + \sigma_3 + \sigma_4)t - (\vec{k}_1 + \vec{k}_2 + \vec{k}_3 + \vec{k}_4) \cdot \vec{x}\} \cdot \\
 &\quad \cdot \exp i\{(\sigma_3 + \sigma_4)\tau - (\vec{k}_3 + \vec{k}_4) \cdot \vec{r}\} \cdot \\
 &\quad \cdot H[\sigma_1, \sigma_2; \vec{k}_1, \vec{k}_2] \cdot H[\sigma_3, \sigma_4; \vec{k}_3, \vec{k}_4] \cdot \\
 &\quad \cdot E\{d_{1F}[\vec{k}_1, \sigma_1] \cdot d_{2F}[\vec{k}_2, \sigma_2] \cdot d_{3F}[\vec{k}_3, \sigma_3] \cdot d_{4F}[\vec{k}_4, \sigma_4]\} \quad (6.1)
 \end{aligned}$$

since the expectation of the product of the first and second order contributions is a third order Gaussian moment of independent random variables and identically equal to zero.

Using the identity between a random measure and the spectral distribution given by Eq. (2.5) and the decomposition of a Gaussian fourth order moment given in Appendix A, the following spectral representation of the autocovariance function for a random sea correct to second order is obtained.

$$\begin{aligned}
 \gamma(\tau, \vec{r}) = & \int_{-\infty}^{\infty} \exp i\{(\sigma_1 + \sigma_2)t - (\vec{k}_1 + \vec{k}_2) \cdot \vec{x}\} \cdot \exp i\{\sigma_2 \tau - \vec{k}_2 \cdot \vec{x}\} \cdot \\
 & \cdot s[\vec{k}_2, \sigma_2] \cdot \delta(\vec{k}_2 + \vec{k}_1) \cdot \delta(\sigma_2 + \sigma_1) \cdot d\vec{k}_2 d\vec{k}_1 d\sigma_2 d\sigma_1 + \\
 & + \int_{-\infty}^{\infty} \int_{-\infty}^{\infty} \int_{-\infty}^{\infty} \int_{-\infty}^{\infty} \exp i\{(\sigma_1 + \sigma_2 + \sigma_3 + \sigma_4)t - (\vec{k}_1 + \vec{k}_2 + \vec{k}_3 + \vec{k}_4) \cdot \vec{x}\} \cdot \\
 & \cdot \exp i\{(\sigma_3 + \sigma_4)\tau - (\vec{k}_3 + \vec{k}_4) \cdot \vec{r}\} \cdot \\
 & \cdot \{H[\sigma_1, \sigma_2; \vec{k}_1(\sigma_1), \vec{k}_2(\sigma_2)] \cdot H[\sigma_3, \sigma_4; \vec{k}_3(\sigma_3), \vec{k}_4(\sigma_4)] \cdot \\
 & \cdot \{s[\vec{k}_2, \sigma_2] \cdot \delta(\vec{k}_2 + \vec{k}_1) \cdot \delta(\sigma_2 + \sigma_1) \cdot s[\vec{k}_4, \sigma_4] \cdot \delta(\vec{k}_4 + \vec{k}_3) \cdot \delta(\sigma_4 + \sigma_3) + \\
 & + s[\vec{k}_3, \sigma_3] \cdot \delta(\vec{k}_3 + \vec{k}_1) \cdot \delta(\sigma_3 + \sigma_1) \cdot s[\vec{k}_4, \sigma_2] \cdot \delta(\vec{k}_4 + \vec{k}_2) \delta(\sigma_4 + \sigma_2) + \\
 & + s[\vec{k}_4, \sigma_4] \cdot \delta(\vec{k}_4 + \vec{k}_1) \cdot \delta(\sigma_4 + \sigma_1) \cdot s[\vec{k}_3, \sigma_3] \cdot \delta(\vec{k}_3 + \vec{k}_2) \cdot \\
 & \cdot \delta(\sigma_3 + \sigma_2)\} \} d\vec{k}_1 d\vec{k}_2 d\vec{k}_3 d\vec{k}_4 d\sigma_1 d\sigma_2 d\sigma_3 d\sigma_4 \quad (6.2)
 \end{aligned}$$

Integrating and employing the shifting property of the Dirac delta distribution, the following expression for the autocovariance is obtained:

$$\begin{aligned}
 \gamma(\tau, \vec{r}) = & \int_{-\infty}^{\infty} \exp i\{-\sigma_1 \tau + \vec{k} \cdot \vec{r}\} \cdot s[-\vec{k}_1, -\sigma_1] d\vec{k}_1 d\sigma_1 + \\
 & + \int_{-\infty}^{\infty} \int_{-\infty}^{\infty} \exp i\{-(\sigma_1 + \sigma_2)\tau + (\vec{k}_1 + \vec{k}_2) \cdot \vec{r}\} \cdot s[-\vec{k}_1, -\sigma_1] \cdot s[-\vec{k}_2, -\sigma_2]
 \end{aligned}$$

(continued)

$$\cdot \left[\begin{array}{l} {}^H[\sigma_1, -\sigma_1; \vec{k}_1, -\vec{k}_1] \cdot {}^H[\sigma_2, \sigma_2; \vec{k}_2, -\vec{k}_2] + {}^H[\sigma_1, \sigma_2; \vec{k}_1, \vec{k}_2] \cdot \\ \cdot {}^H[-\sigma_1, -\sigma_2; -\vec{k}_1, -\vec{k}_2] \cdot \exp i\{-(\sigma_1 + \sigma_2)\tau + (\vec{k}_1 + \vec{k}_2) \cdot \vec{r}\} + \\ + {}^H[\sigma_1, \sigma_2; \vec{k}_1, \vec{k}_2] \cdot {}^H[-\sigma_2, -\sigma_1; -\vec{k}_2, -\vec{k}_1] \cdot \\ \cdot \exp i\{-(\sigma_2 + \sigma_1)\tau + (\vec{k}_2 + \vec{k}_1) \cdot \vec{r}\} \end{array} \right] \cdot d\vec{k}_1 d\vec{k}_2 d\sigma_1 d\sigma_2 \quad (6.3)$$

The symmetric properties of both the spectral distribution function, $s[\vec{k}, \sigma]$, and the nonlinear interaction kernel, ${}^H[\sigma_1, \sigma_2; \vec{k}_1, \vec{k}_2]$, reduces Eq. (6.3) to the following:

$$\begin{aligned} \gamma(\tau, \vec{r}) = & \int_{-\infty}^{\infty} \exp i\{-\sigma\tau + \vec{k} \cdot \vec{r}\} \cdot s[\vec{k}, \sigma] d\vec{k} d\sigma + \int_{-\infty}^{\infty} \int_{-\infty}^{\infty} s[\vec{k}_1, \sigma_1] \cdot \\ & \cdot s[\vec{k}_2, \sigma_2] \cdot {}^H[\sigma_1, -\sigma_1; \vec{k}_1, -\vec{k}_1] \cdot {}^H[\sigma_2, -\sigma_2; \vec{k}_2, -\vec{k}_2] d\vec{k}_1 d\vec{k}_2 d\sigma_1 d\sigma_2 + \\ & + 2 \int_{-\infty}^{\infty} \int_{-\infty}^{\infty} \exp i\{-(\sigma_1 + \sigma_2)\tau + (\vec{k}_1 + \vec{k}_2) \cdot \vec{r}\} \cdot s[\vec{k}_1, \sigma_1] \cdot \\ & \cdot s[\vec{k}_2, \sigma_2] \cdot {}^H[\sigma_1, \sigma_2; \vec{k}_1, \vec{k}_2] d\vec{k}_1 d\vec{k}_2 d\sigma_1 d\sigma_2 \quad (6.4) \end{aligned}$$

Formally, the Fourier transform of the autocovariance function yields the spectral density function. Thus, multiplying both sides of Eq. (6.4) by $\exp i\{-\omega\tau + \vec{k} \cdot \vec{r}\}$ and integrating over time and space yields

$$\begin{aligned} & \int_{-\infty}^{\infty} \int_{-\infty}^{\infty} \gamma(\tau, \vec{r}) \exp i\{-\omega\tau + \vec{k} \cdot \vec{r}\} d\tau d\vec{r} = \\ & = \int_{-\infty}^{\infty} \int_{-\infty}^{\infty} s[\vec{k}, \sigma] \cdot \exp i\{-(\sigma + \omega)\tau + (\vec{k} + \vec{k}) \cdot \vec{r}\} d\vec{k} d\sigma d\tau d\vec{r} + \\ & + \int_{-\infty}^{\infty} \int_{-\infty}^{\infty} \int_{-\infty}^{\infty} s[\vec{k}_1, \sigma_1] \cdot s[\vec{k}_2, \sigma_2] \cdot {}^H[\sigma_1, -\sigma_1; \vec{k}_1, -\vec{k}_1] \cdot \\ & \cdot {}^H[\sigma_2, -\sigma_2; \vec{k}_2, -\vec{k}_2] \cdot \exp i\{-\omega\tau + \vec{k} \cdot \vec{r}\} d\vec{k}_1 d\vec{k}_2 d\sigma_1 d\sigma_2 d\tau d\vec{r} + \end{aligned}$$

(continued)

$$\begin{aligned}
 & + \underset{-\infty}{\overset{\infty}{\iint \iint \iint}} s[\vec{k}_1, \sigma_1] \cdot s[\vec{k}_2, \sigma_2] \cdot {}^H h^2[\sigma_1, \sigma_2; \vec{k}_1, \vec{k}_2] \cdot \\
 & \cdot \exp i\{-(\sigma_1 + \sigma_2 + \omega)\tau + (\vec{k}_1 + \vec{k}_2 + \vec{k}) \cdot \vec{r}\} d\vec{k}_1 d\vec{k}_2 d\sigma_1 d\sigma_2 d\tau d\vec{r} \quad (6.5)
 \end{aligned}$$

Inverting the order of integration over the wave number and frequency differentials with the time and space differentials results in integrals equivalent to the Dirac delta distribution given by Eqs. (2.13) for the spatial integration and a similar identity for the temporal integration. Substituting these identities for the Dirac delta distribution, the following expression is obtained:

$$\begin{aligned}
 & \underset{-\infty}{\overset{\infty}{\iint \iint}} \gamma(\tau, \vec{r}) \exp i\{-\omega\tau + \vec{k} \cdot \vec{r}\} d\tau d\vec{r} = \\
 & = (2\pi)^3 \underset{-\infty}{\overset{\infty}{\iint \iint}} s[\vec{k}, \sigma] \cdot \delta(\vec{k} + \vec{k}) \cdot \delta(\sigma + \omega) d\vec{k} d\sigma + \\
 & + (2\pi)^3 \underset{-\infty}{\overset{\infty}{\iint \iint \iint}} s[\vec{k}_1, \sigma_1] \cdot s[\vec{k}_2, \sigma_2] \cdot {}^H h[\sigma_1, -\sigma_1; \vec{k}_1, -\vec{k}_1] \cdot \\
 & \cdot {}^H h[\sigma_2, -\sigma_2; \vec{k}_2, -\vec{k}_2] \cdot \delta(\omega) \delta(\vec{k}) d\vec{k}_1 d\vec{k}_2 d\sigma_1 d\sigma_2 + \\
 & + 2(2\pi)^3 \underset{-\infty}{\overset{\infty}{\iint \iint \iint}} s[\vec{k}_1, \sigma_1] \cdot s[\vec{k}_2, \sigma_2] \cdot {}^H h^2[\sigma_1, \sigma_2; \vec{k}_1, \vec{k}_2] \cdot \\
 & \cdot \delta(\sigma_1 + \sigma_2 + \omega) \cdot \delta(\vec{k}_1 + \vec{k}_2 + \vec{k}) d\vec{k}_1 d\vec{k}_2 d\sigma_1 d\sigma_2 \quad (6.6)
 \end{aligned}$$

Dividing both sides by $(2\pi)^3$ and comparing the expression for the generalized Fourier transform pair for the spectral density functions yields the following:

$$S[\omega, \vec{k}] = \frac{1}{(2\pi)^3} \underset{-\infty}{\overset{\infty}{\iint \iint}} \gamma(\tau, \vec{r}) \exp i\{-\omega\tau + \vec{k} \cdot \vec{r}\} d\tau d\vec{r}$$

The first integral in Eq. (6.6) gives

$${}_1 S[\omega, \vec{k}] = s[\omega, \vec{k}] \quad (6.7)$$

which is the spectral density for the linear Gaussian estimate. The second integral vanishes identically because the argument of the Dirac delta distribution is not in the domain of the integral. Integrating the third integral and using the shifting property of the Dirac delta distribution gives

$${}_2S[\vec{k}, \omega] = \underset{-\infty}{\overset{\infty}{\iint}} s[\vec{k}_1, \sigma_1] \cdot s[\vec{k} - \vec{k}_1, \omega - \sigma_1] \cdot \\ \cdot H^2[\sigma_1, \omega - \sigma_1; \vec{k}_1, \vec{k} - \vec{k}_1] \cdot d\vec{k}_1 d\sigma_1 \quad (6.8)$$

Equation (6.8) is the important result first given by Tikh [123] for a continuous spectrum of deep water waves and later by Longuet-Higgins [79] for a discrete spectrum of deep water waves that the second order spectrum which results only from first and second perturbation order contributions is a convolution of products of all first order spectral densities whose sums and differences in frequencies contribute to the same frequency of the second order spectral density. Equation (6.8) is a general expression for the second order spectral density for both time and space lags. The hydrodynamic relationship which restricts the spectrum of the random measure to those values in the σ, k plane given by the linear dispersion equation has not been invoked.

The simulation of a time series for a random sea requires that the spectral density be given in the frequency domain vice the wave number domain. The spectral density has been given in the wave number domain as a result of solving the spatial boundary value problem in Section 4. The transformation from wave number space to frequency space will be considered next.

CHAPTER 3

APPLICATIONS OF NONLINEAR RANDOM SEA SIMULATIONS

Section 1 transforms the directional random measure expressed in wave number space for the linear Gaussian random sea into the spectral density expressed in frequency space. Section 2 discusses the fast Fourier transform algorithm and its application to synthesizing random sea realizations. Section 3 introduces the Bretschneider spectrum, evaluates the two constant parameters required to represent measured hurricane generated wave spectra, and discusses the application of the Phillips equilibrium spectrum in the simulation of nonlinear random seas. Section 4 briefly describes the measured hurricane generated wave and pressure force realizations recorded by Wave Project II during Hurricane Carla in the Gulf of Mexico. Section 5 compares the distributions and spectra of measured sea surface realizations from four hurricane generated records with the simulated linear and nonlinear random sea surface realizations. Section 6 derives the equations required in the application of the digital linear filter technique to predict wave pressure forces from random sea surface realizations. Section 7 compares the distributions and spectra of the measured and predicted wave pressure forces at the 55.3 feet dynamometer elevation on a vertical piling located in 99 feet of water.

1. Fourier Series Approximations of the Random Measure

Although the nonlinear interaction kernels for water of finite depth computed by Tick [125] and by Hasselmann [54] have been available for several years, no successful attempts to employ these kernels to construct second order nonlinear sea simulations have been published. Tick [125] attributed this to the computational difficulties involved in applying the theory.

The availability of the Fast Fourier Transform (FFT) algorithm [37] now makes the simulation of nonlinear random seas correct to second order in the perturbation parameter relatively simple. Moreover, the retention of complex phase angles by the FFT algorithm makes it possible to compute the spectral densities correct to second order entirely in the frequency domain and to make one inversion to the time domain for the final sea surface realization. Although no simultaneous temporal simulations of the sea surface at varying horizontal spatial locations were made in this study, the extension of the technique developed in this chapter is trivial as will become obvious later. These simultaneous simulations at varying horizontal spatial locations are required for the dynamic analysis of multilegged pile-supported platforms.

Simulation by digital computer of nonlinear random seas correct to second order using Eq. (4.43), Chapter 2, Section 4, requires that the exact Fourier-Stieltjes integrals be approximated by Fourier series. The process of transforming the

Fourier-Stieltjes integrals requires first that the spectral distribution function have density:

$$dF[\vec{k}(\sigma)] = F[\vec{k}(\sigma)] \cdot d\vec{k} \quad (1.1)$$

The spectrum of the random measure, $F[\vec{k}(\sigma)]$, is in wave number space as a result of solving a spatial boundary value problem in Chapter 2 and a transformation to frequency space is required in order to simulate a time series. The transformation from rectangular cartesian coordinates to polar coordinates is given by

$$k_x = |\vec{k}| \cos \theta \quad (1.2a)$$

$$k_y = |\vec{k}| \sin \theta \quad (1.2b)$$

with the following change of variables Jacobian:

$$\begin{aligned} \left| J \left(\frac{\partial(k_x, k_y)}{\partial(|\vec{k}|, \theta)} \right) \right| &= \begin{vmatrix} \cos \theta & \sin \theta \\ -|\vec{k}| \sin \theta & |\vec{k}| \cos \theta \end{vmatrix} \\ &= |\vec{k}| = k \end{aligned} \quad (1.3)$$

Substituting this change of variables yields the following discrete polar spectral representation:

$$F[\vec{k}(\sigma)] \cdot d\vec{k} = F[k, \theta] \cdot k \cdot dk \cdot d\theta \quad (1.4)$$

Finally, the transformation from the scalar wave number space, k , to wave frequency space, σ , is made via the linear dispersion equation to obtain the following:

$$F[k, \theta] \cdot k \cdot dk \cdot d\theta = F[\sigma, \theta] \cdot |J\{\frac{\partial k}{\partial \sigma}\}| \cdot d\sigma \cdot d\theta \quad (1.5)$$

where the Jacobian of the change of variables is the following:

$$|J\{\frac{\partial k}{\partial \sigma}\}| = \{C_g\}^{-1} = \{\frac{C}{2} [1 + \frac{2|\vec{k}|h}{\sinh\{2|\vec{k}|h\}}]\}^{-1} \quad (1.6)$$

The determination of the directional dependency of a general three-dimensional random process is not trivial even for a linear Gaussian estimate. A good description of the theoretical derivation is given by Longuet-Higgins [78] which is based on the theories of Raleigh [105] and Rice [109]. Additional insight into the directional spectrum problem with some specific applications is given by Kinsman [72; Ch. 8]. Applications to directional wave arrays are given by Borgman [19] and Snyder and Smith [121]. Snyder and Smith [121] outline an extension of the linear directional spectrum to a nonlinear directional spectrum for the case of an array of wave recorders. Hasselmann et al. [57] give a nonlinear application for the determination of the directional spread from a single pressure realization. These references reflect the complexities involved in describing the directional dependency of the spectral representation of a random sea.

For the simulation of a time series of a random sea, the horizontal spatial coordinates may be considered as fixed and the directional dependency may be expressed implicitly in the random measure by the following integral:

$$F[\sigma] = \int_0^{2\pi} k \frac{F[\sigma, \theta]}{C_g} \cdot \exp i\{-k(\cos(\theta)x_1 + \sin(\theta)y_1)\} d\theta \quad (1.7)$$

where x_1, y_1 are fixed values of the horizontal spatial coordinates.

The approximation of the stochastic integral representation of a random sea realization by a Fourier series requires that the discrete stochastic amplitude of the approximating series represent the equivalent energy content as that contained in the exact integral representation over a differential interval, $d\sigma$, i.e.,

$$|F_1(n)|^2 = |F[n\Delta\sigma]|^2 \cdot \Delta\sigma \quad (1.8)$$

Including the directional dependency implicitly through the complex phase of the stochastic amplitude, $F_1(n)$, the stochastic integrals given by Eq. (4.41) in Chapter 2, Section 4, may be approximated by the following series:

$$\begin{aligned} n(t) &= \sum_{n=-\infty}^{\infty} F_1(n) \exp{i\{n\sigma t\}} + \\ &+ \frac{1}{2g} \sum_{n=-\infty}^{\infty} \sum_{m=-\infty}^{\infty} F_1(n) F_1(m) H[m, n; k_n, k_m] \cdot \\ &\cdot \exp i\{(n+m)\sigma t\} \end{aligned} \quad (1.9)$$

The simulation by digital computer of the random process represented by the stochastic series in Eq. (1.9) requires the evaluation of a suitable expression for the stochastic random function, $F_1(n)$, and also requires that this function represent a Gaussian random process. Descriptions of various stochastic amplitudes which may be used to simulate the random

linear sea are given by Birkhoff and Kotik [14], St. Denis [117,118], Le Mehaute [74], Kinsman [72], *inter alios*. Techniques for simulating by digital computer a random Gaussian realization utilizing these stochastic amplitudes or deterministic amplitudes are given by Mihram [89] and Borgman [20,23].

The technique selected for simulating linear Gaussian random seas for the purpose of this study is the following:

- (1) Generate a sequence of random numbers which are uniformly distributed between {0,1}.
- (2) Multiply the uniformly distributed random number sequence by 2π in order to obtain a random phase angle which is uniformly distributed between $\{0, 2\pi\}$.
- (3) Form a complex number of unit amplitude via Euler's equation using the uniformly distributed random phase angle as the argument.
- (4) Multiply the complex number computed in (3) by the square root of the differential energy content given by the Bretschneider spectrum.

Following this simulation procedure, the stochastic complex amplitude in Eq. (1.9) may be expressed by the following two-sided Fourier spectrum:

$$F_1(n) = \sqrt{S_{BB}(n) \cdot \frac{\pi}{T_R}} \cdot [\exp i\{-\psi(n)\}] \quad (1.10)$$

where $S(n)$ is the value of the one-sided Bretschneider spectrum at frequency $n \cdot 2\pi/T_R$, T_R is the length of simulated record, and $\psi(n)$ is the random phase angle generated in procedure (2) above.

This procedure may be shown to be equivalent to filtering Gaussian white noise. Details may be found in Bendat [5], Davenport and Root [38], Laning and Battin [73], *inter alios*.

By referencing the horizontal spatial coordinate to a fixed location, ($x=0$, say), the complex stochastic amplitude for the random sea simulation may be computed by initializing the complex coefficients of the fast Fourier transform with the linear stochastic values given in Eq. (1.10) plus the second order contributions given by the double summation in Eq. (1.9). In order to understand this method better, a brief description of the fast Fourier transform algorithm is needed and will be presented next.

2. Fast Fourier Transform (FFT)

The fast Fourier transform algorithm used to simulate the random nonlinear sea surface profile is the Subroutine NLØGN written by Robinson [110]. Since most FØRTRAN compilers do not admit zero or negative subscripts for arrays, the notation used by Robinson [110] and by Borgman [21] has been modified to correspond to the subscripts values acceptable to FØRTRAN compilers. The Subroutine NLØGN approximates the Fourier integral transform pair by the following discrete

Fourier series approximation:

$$\eta(n) = \Delta f \sum_{m=1}^{LX} X(m) \cdot \exp i\{2\pi(m-1)(n-1)/LX\} \quad (2.1a)$$

$$X(m) = \Delta t \sum_{n=1}^{LX} \eta(n) \cdot \exp i\{-2\pi(m-1)(n-1)/LX\} \quad (2.1b)$$

where the time sequence, $\eta(n)$, is given at LX discrete values of time which are partitioned into equal intervals of Δt seconds and the Fourier spectral sequence, $X(m)$, is given at LX discrete values of frequency which are partitioned into equal intervals of Δf Hertz. In order for the inverse transform to be exact, the following relationship between the time and frequency intervals must hold:

$$\Delta t \cdot \Delta f = 1/LX \quad (2.2)$$

and LX must be equal to 2 raised to an integer power.

The complex Fourier spectral sequence represented by Eq. (2.1b) represents a two-sided spectrum with one-half of the spectral sequence contained in the complex array elements

$$2 \leq m \leq (LX+2)/2 \quad (2.3)$$

and the complex conjugate spectral sequence contained in the complex array elements

$$(LX+2)/2 \leq m \leq LX \quad (2.4)$$

The mean value of the time sequence is represented by the first array element ($m=1$). The time sequence, $\eta(n)$, is real

and, therefore, the following complex conjugate relationship for the complex spectral sequence holds:

$$X(LX+2-m) = X^*(m) \quad (2.5)$$

This equality may be demonstrated by substituting $m = (LX+2-m)$ into Eq. (2.1b) to obtain

$$X(LX+2-m) = \Delta t \sum_{n=1}^{LX} \eta(n) \cdot \exp i\{-2\pi(LX-m+1)(n-1)/LX\} \quad (2.6)$$

The exponential argument reduces to the following:

$$\text{ARG} = i\{2\pi(m-1)(n-1)/LX\} - i\{2\pi(n-1)\} \quad (2.7)$$

which gives Eq. (2.5) as a result of the following identity:

$$\exp i\{-2\pi(n-1)\} \equiv 1 ; \quad n=1, 2, 3, \dots, LX \quad (2.8)$$

The norming constant, LX , is associated with the time sequence in the Subroutine NL \varnothing GN (cf. Robinson [110], pp. 62-64) vice with the frequency sequence established in the standardized notation presented in Chapter 2. Consequently, the complex Fourier coefficients for the linear random sea given by Eq. (1.10) were initialized by the following complex expression:

$$X(m) = F(m) \cdot (LX)$$

$$= (LX) \cdot \sqrt{S(m\Delta\sigma)} \cdot \pi/T_R \cdot \exp i\{-\psi(m)\} \quad (2.9)$$

where $\psi(m)$ is the random phase angle generated by the process described in Section 1 and $S(m\Delta\sigma)$ is the value of the BB

Bretschneider spectral component at frequency, $m \cdot 2\pi / T_R$. The IBM Subroutine RANDU was used to generate the random number sequence required for the computation of the random phase angles uniformly distributed in the interval $\{0, 2\pi\}$. A description of the simulation of a linear Gaussian sea using uniformly distributed phase angles is given by Borgman [20, 23] and by Brown [31].

3. The Bretschneider Spectrum and the Phillips Equilibrium Spectrum

Bretschneider [28] has developed the following spectral representation for a linear sea:

$$S(\sigma)_{BB} = \frac{\alpha g^2}{\sigma^5} \exp\left\{-0.675 \left[\frac{T}{T}\right]^4\right\} \quad (3.1)$$

where α and T are parametric constants. This one-sided spectrum is completely defined by these two parameters. In order to compare Eq. (3.1) with spectra from random seas obtained from measured hurricane records, it is necessary to transform these two constant parameters into parameters which are measurable from the hurricane records. This may be accomplished by (1) requiring that the Bretschneider spectrum and the measured spectrum have equal variance and (2) that the frequency of the well-defined peak of the Bretschneider spectrum agree in a best least-squares sense with the frequency of the often ill-defined "peak" of the measured spectrum. As measured spectra frequently differ in the number and the magnitudes of "peaks" present depending, *inter alia*, on the

degree of smoothing used, a resort to a best least-squares agreement between the frequencies of the measured and Bretschneider "peaks" is required.

The variance of a measured spectrum may be computed either from the mean square of the recorded realization,

$$E_f = \frac{1}{T_R} \int_{-T_R/2}^{T_R/2} n^2(t) dt \quad (3.2)$$

where T_R is the length of the measured record or, equivalently, from the integral of the one-sided spectral density function

$$E_f = \int_0^\infty S(\sigma) d\sigma \quad (3.3)$$

The frequency at which the peak of the Bretschneider spectrum occurs may be determined by equating to zero the derivative with respect to the angular frequency of the spectral density function and evaluating the resulting algebraic equation at the frequency at which the peak of the spectrum occurs; i.e.,

$$\frac{\partial S(\sigma)}{\partial \sigma} = 0 ; \quad \sigma = \sigma_0 \quad (3.4)$$

Equations (3.3) and (3.4) yield two equations which allow the two constant parameters given by Bretschneider to be transformed into two measurable constant parameters, i.e.,

$$\{\alpha, T\} \rightarrow \{E_f, \sigma_0\} \quad (3.5)$$

Integrating the Bretschneider spectrum is most easily done by first making the following change of variables:

$$\frac{T}{\bar{T}} = \frac{\bar{\sigma}}{\sigma} \quad (3.6a)$$

$$v = \exp\{-0.675(\frac{\bar{\sigma}}{\sigma})^4\} \quad (3.6b)$$

$$dv = \frac{2.7}{\bar{\sigma}} (\frac{\bar{\sigma}}{\sigma})^5 \exp\{-0.675(\frac{\bar{\sigma}}{\sigma})^4\} \quad (3.6c)$$

Making these change of variables and integrating, the following expression for the variance of the spectrum is obtained:

$$E_f = \frac{\alpha g^2}{2.7(\bar{\sigma})^4} \int_0^\infty dv = \frac{\alpha g^2}{2.7(\bar{\sigma})^4} \exp\{-0.675(\frac{\bar{\sigma}}{\sigma})^4\} \Big|_0^\infty$$

$$E_f = \frac{\alpha g^2}{2.7(\bar{\sigma})^4} \quad (3.7)$$

Differentiating Eq. (3.1) with respect to the angular frequency, σ , equating the result to zero, and evaluating the resulting expression at the frequency of the peak in the spectrum yields the following:

$$\frac{\partial S(\sigma)}{\partial \sigma}_{BB} = \left\{ -\frac{5}{\sigma_0} + \frac{2.7}{\bar{\sigma}} \left(\frac{\bar{\sigma}}{\sigma_0}\right)^5 \cdot \frac{\alpha g^2}{(\sigma_0)^5} \exp\{-0.675(\frac{\bar{\sigma}}{\sigma_0})^4\} \right\}; \sigma = \sigma_0$$

$$= 0 \quad (3.8)$$

Equations (3.7) and (3.8) finally determine the following two constant parameters:

$$\alpha = \frac{2.7 E_f}{g^2} (\bar{\sigma})^4 \quad (3.9a)$$

$$(\bar{\sigma})^4 = \frac{5}{2.7} (\sigma_0)^4 \quad (3.9b)$$

Substituting these two parameters into Eq. (3.1) results in

the following form for the Bretschneider spectrum:

$$S(\sigma) = \frac{5 E_f}{\sigma_0} \left(\frac{\sigma_0}{\sigma} \right)^5 \exp \left\{ -1.25 \left(\frac{\sigma_0}{\sigma} \right)^4 \right\} \quad (3.10)$$

The best least-squares estimate for the "peak frequency," σ_0 , may be computed by the application of the linear Taylor differential correction technique (cf. Marquardt [86] or McCalla [87]). In this technique, a mean square error between the measured and predicted spectra at the M_c discrete frequencies sampled is formed as follows:

$$\epsilon^2 = \frac{1}{M_c} \sum_{m=1}^{M_c} \left\{ S(m) - \frac{S(m)}{BB} \right\}^2 \quad (3.11)$$

where M_c corresponds to the cutoff frequency above which the measured spectral estimates are negligible.

The Bretschneider spectral distribution function is expanded in a Taylor series about the best estimate of the peak frequency in terms of the linear differential correction to the peak frequency, i.e.,

$$\epsilon^2 = \frac{1}{M_c} \sum_{m=1}^{M_c} \left\{ S(m) - \frac{S(m)}{BB} - \frac{\partial S(m)}{\partial \sigma_0} (\delta \sigma_0) - 0 (\delta \sigma_0)^2 \right\}^2 \quad (3.12)$$

Retaining only the linear corrections, the mean square error is differentiated with respect to the differential correction to the peak frequency, $\delta \sigma_0$, and the result equated to zero, i.e.,

$$\frac{\partial \varepsilon^2}{\partial (\delta \sigma_o)} = - \frac{2}{M_C} \sum_{m=1}^{M_C} \left\{ S(m) - S(m) - \frac{\partial S(m)}{\partial \sigma_o} \cdot \frac{BB}{BB} \right\} \cdot \frac{\partial S(m)}{\partial \sigma_o} = 0 \quad (3.13)$$

which yields the following algebra equation for $\delta \sigma_o$:

$$\delta \sigma_o = \frac{\sum_{m=1}^{M_C} \left[\left\{ S(m) - S(m) \right\} \frac{\partial S(m)}{\partial \sigma_o} \right]}{\sum_{m=1}^{M_C} \left(\frac{\partial S(m)}{\partial \sigma_o} \right)^2} \quad (3.14)$$

This equation may be iterated for the $(j+1)$ correction to the j^{th} estimate for $\delta \sigma_o$ as follows:

$$(\delta \sigma_o)^{(j+1)} = \frac{\sum_{m=1}^{M_C} \left[\left\{ S(m) - S^{(j)}(m) \right\} \frac{\partial S(m)}{\partial (\sigma_o)} \right]}{\sum_{m=1}^{M_C} \left(\frac{\partial S^{(j)}(m)}{\partial \sigma_o} \right)^2} \quad (3.15)$$

The iteration is terminated when successive corrections are acceptably small. Table 3.1 demonstrates the results of fitting four measured spectra from Hurricane Carla with a best least-squares estimate for the peak frequency. The fit and number of iterations to convergence are the poorest for the very narrow spectrum represented by Record No. 06886/2. The number of spectral estimates, M_C , used from the measured spectra was equal to 305 and corresponded to a cut-off frequency equal to 2.34 rad/sec or 0.37 Hertz for Record Nos. 06885/1, 06886/1 and /2, and to 2.92 rad/sec or 0.47 Hz for Record No. 06887/1.

Table 3.1

Rate of Convergence and Final RMS Error Computed for the Best Least-Squares Fit to Measured Spectra from Hurricane Carla for $M_c = 305$

Record No.	Initial σ_o [rad/sec]	Final σ_o [rad/sec]	Last $(\delta\sigma_o)$ [rad/sec]	No. of Iterations	RMS Error [ft 2 /(rad/sec)]	E_f [ft 2]
06885/1	0.5200	0.4990	-6x10 $^{-6}$	5	5.29	22.30
06886/1	0.5000	0.5187	-1x10 $^{-6}$	4	5.83	28.76
06886/2	0.5000	0.4847	-97x10 $^{-6}$	9	12.23	24.96
06887/1	0.5000	0.5199	4x10 $^{-6}$	5	6.52	28.63

A note of caution is in order with regard to the application to design of the Bretschneider spectrum expressed as a function of the two parameters of variance, E_f , and peak frequency, σ_0 . Bretschneider [27,28] correlated his spectrum with the two parameters of wind speed and fetch length and there is no satisfactory guarantee of preventing high frequency instabilities indicated by breaking waves in the simulation of random nonlinear sea realizations when the total energy content and peak frequency of the spectrum are used. In the absence of a detailed stability analysis, the equilibrium spectrum developed by Phillips [99] from a dimensional analysis was employed to limit the energy content in the high frequency region. Although the validity of the equilibrium spectrum has been questioned [42,52,62,80,109], its validity for application to engineering design appears to be appropriate.

Phillips (cf. [100], Ch. 4.5, pp. 109-119) reasoned by similarity conditions that the spectral components in frequency space for frequencies greater than the peak frequency should decay according to

$$S(\sigma) = \beta \cdot g^2 / \sigma^5 ; \quad \sigma > \sigma_0 \quad (3.16)$$

Phillips and others [99,100,104] have found the constant β to have a value of $0.0117 \pm 10\%$ for σ expressed in radians per second. If the frequency is expressed in Hertz, the requirement that the energy content of equivalent differential spectral densities remain constant implies that

$$\frac{S(\sigma_m)}{\eta\eta} \cdot d\sigma = \frac{S(m/T_R)}{\eta\eta} \cdot d(1/T_R) \quad (3.17)$$

which yields

$$\frac{\beta \cdot g^2 \cdot 2\pi \cdot (1/T_R)}{[2\pi \cdot m \cdot (1/T_R)]^5} = \frac{\beta' \cdot g^2 \cdot (1/T_R)}{[m \cdot (1/T_R)]^5} \quad (3.18)$$

so that

$$\beta' = \frac{\beta}{[2\pi]^4} = 7.51 \times 10^{-6} \pm 10\% \quad (3.19)$$

This constant for the equilibrium spectrum given in Hertz differs from that given by Phillips [100; p. 114], which appears to be inverted. The nonlinearization procedure includes a test for high frequency saturation using the equilibrium spectrum of Phillips. None of the spectra from the nonlinear simulations of the measured hurricane spectra exceeded the equilibrium spectrum.

4. Hurricane Carla Data (September 8-10, 1961)

Wave Force Project II (WPII) recorded the instantaneous sea surface elevations and wave pressure forces on a vertical piling which supported an instrumented drilling platform at a location in the Gulf of Mexico with a water depth of approximately 100 feet. The data recorded during WPII have been made available to the public through the National Oceanographic Data Center. Thrasher and Aagaard [122] provide details of the storms recorded and other information relative to these data. Hurricane Carla was recorded during the period

September 8-10, 1961. The continuous records which are available from this period of WPII contain some of the highest and most forceful waves recorded during WPII. One wave, in particular, had an average trough to crest wave height of almost forty feet. These data contain four records from Hurricane Carla with continuous sea surface elevations and pressure forces recordings each covering approximate lengths of time from eleven to fourteen minutes. The data are digitized at uneven intervals of time ranging approximately from 0.12 to 0.24 seconds. Calibration information and equations for transforming the data into engineering units are given by Blank [16]. Table 3.2 contains the characteristics of the four hurricane records used in the comparison with simulated realizations. The data were redigitized for the comparison analysis by linear interpolation after applying the calibration equations given by Blank [16] in order to obtain records which could be analyzed by the Fast Fourier Transform (FFT) algorithm. No time shift was used to effect coincidence between the sea surface realizations recorded by the wave staff and the pressure forces recorded on the instrumented pile because the separation distance between the wave staff and center-line of the pile was only approximately 55 inches. Using linear wave theory, a wave with a period of ten seconds traveling in an ocean of uniform depth of one hundred feet would travel the straight-line distance between the center of the wave staff and the center of the pile in approximately 0.10 seconds. Waves incident from directions other than along

Table 3.2
Characteristics of Hurricane Carla Records

Record No.	Date	Time	Record Length (min.)	LX	Δt
06885/1	Sept. 9, 1961	2100	13.67	4096	0.20
06886/1	Sept. 10, 1961	0000	15.01	4096	0.20
06886/2	Sept. 10, 1961	0030	36.88	4096	0.20
06887/1	Sept. 10, 1961	0300	11.00	4096	0.16

this straight-line would require less travel time and, therefore, the time shift was neglected. The effect on wave-induced pressure forces of neglecting the spatial separation between a wave staff and the center-line of an instrumented vertical piling is demonstrated in Appendix C by the application of kinematics from linear wave theory in the Morison equation.

The pressure forces for each individual dynamometer elevation are given in orthogonal components which are approximately aligned with the platform axes (cf. Blank [16] for dimensional and azimuthal details). The pressure forces recorded by the dynamometer at the 55.33 foot elevation were used in the comparison analysis since this elevation was continuously submerged during the passage of waves and was located near enough to the free surface to have recorded the effects of the smaller high frequency waves whose influence decays with depth. The data recorded at the 78.17 foot elevation would have been preferable for the hydrodynamics acting at this elevation but the low resolution of the Y force component resulted in measured values changing only by increments of approximately $30 \text{ lbs}/\text{ft}^2$ and was felt to be less accurate than the data at the 55.33 foot elevation. The comparison between measured and simulated pressure forces involved the resultant forces as defined by Dean and Aagaard [41]. The waves were assumed to be collinear and to propagate in a direction $\theta_0 = 125^\circ$ relative to the platform coordinate system. The resultant force at time $n\Delta t$ was obtained by the following

expression :

$$\frac{P(n)}{55} = sgn\{\Delta\theta(n)\} \cdot \sqrt{F_X^2(n) + F_Y^2(n)} \quad (4.1)$$

where $F_X(n)$ and $F_Y(n)$ are the orthogonal pressure force components relative to the platform axes digitized at time $n\Delta t$ and the *signum* function is determined by the following:

$$sgn\{\Delta\theta(n)\} = \begin{cases} + & \text{for } |\theta(n) - \theta_0| < 90^\circ \\ - & \text{for } |\theta(n) - \theta_0| > 90^\circ \end{cases} \quad (4.2)$$

where

$$\theta(n) = \text{ARCTAN} \left(\frac{F_Y(n)}{F_X(n)} \right) \quad (4.3)$$

The effect of the approximately -4° angular misalignment with respect to the platform coordinate axes of the dynamometer at the 55.33 foot elevation was not included in the determination of the direction of the resultant force.

5. Comparison of Sea Surface Realizations

The measured spectra from four Hurricane Carla records were used to simulate realizations of random hurricane-generated waves correct to second perturbation order for two different input spectra. The smoothed measured spectra of these four records are shown in Figs. 3.1, 3.2, 3.3, and 3.4. Also shown on these figures are the Bretschneider spectra with equal variance and best least-squares fit to the peak frequency as determined by the procedure discussed in Section 3.

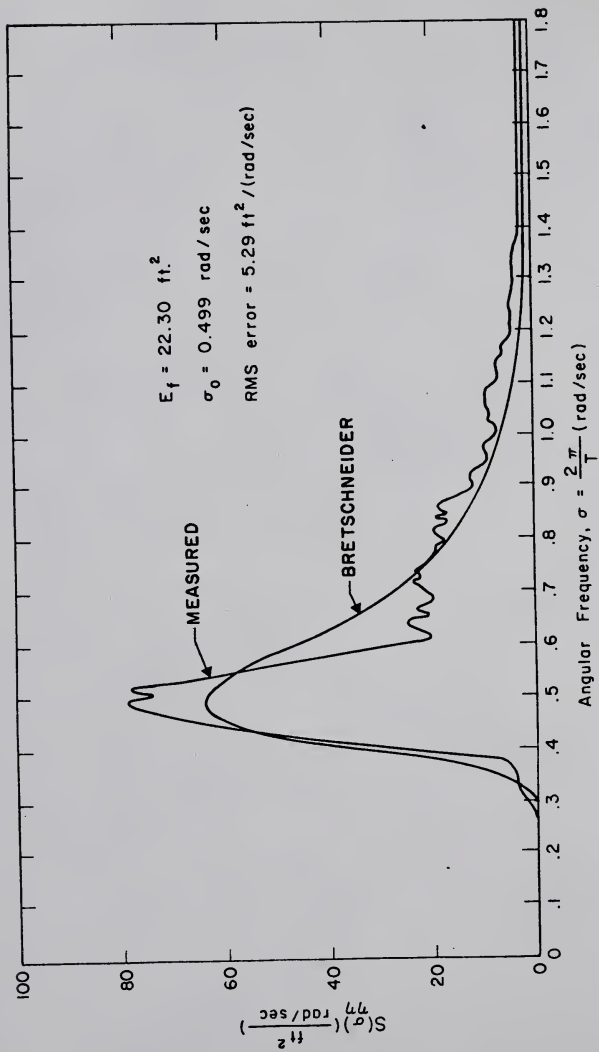


Figure 3.1. Smoothed Measured Spectrum and Bretschneider Spectrum of Equal Variance and Best Least-Squares Fit to Peak Frequency for $M_C = 305$ for Record No. 06885/1.

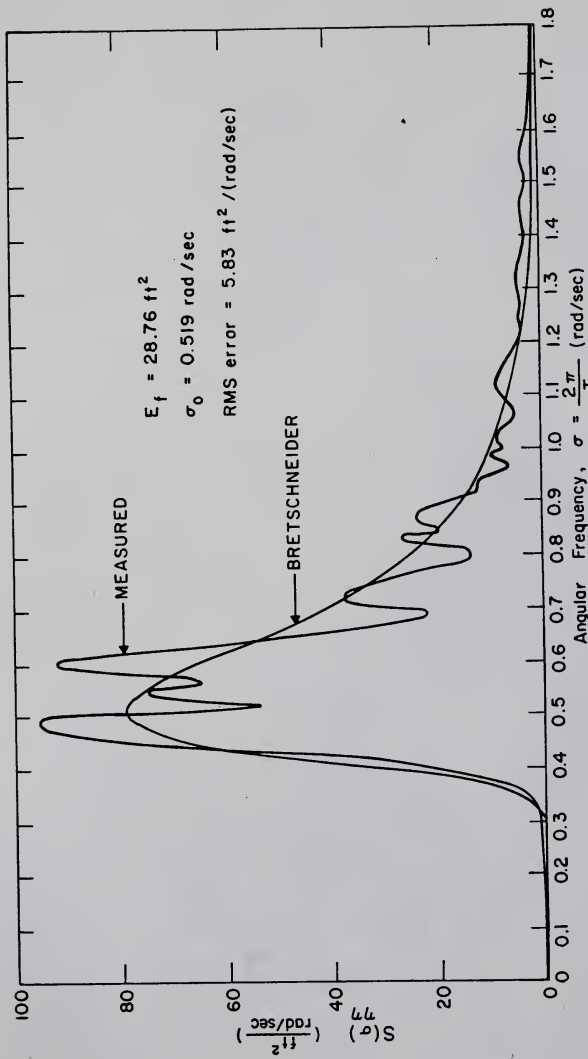


Figure 3.2. Smoothed Measured Spectrum and Bretschneider Spectrum of Equal Variance and Best Least-Squares Fit to Peak Frequency for $M_c = 305$ for Record No. 06886/1.

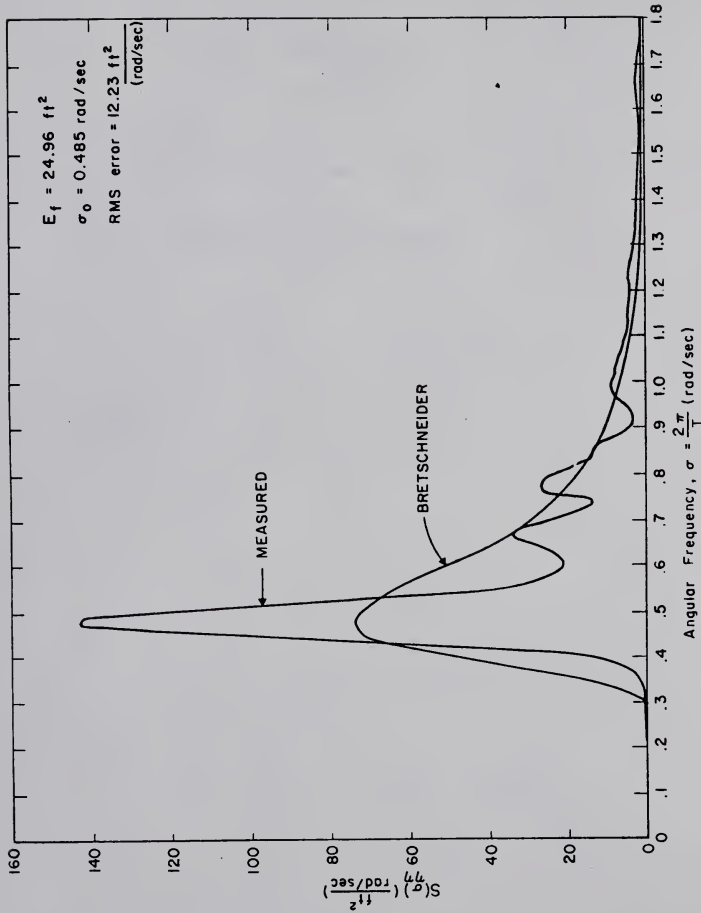


Figure 3.3.

Smoothed Measured Spectrum and Bretschneider Spectrum of Equal Variance and Best Least-Squares Fit to Peak Frequency for $M_c = 305$ for Record No. 06886/2.

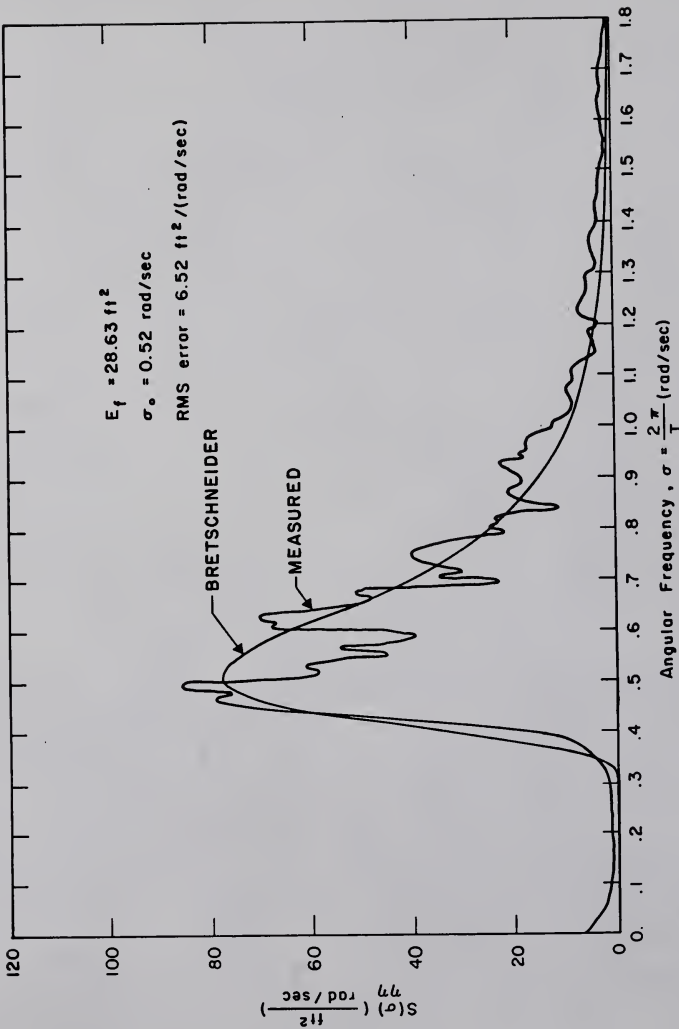


Figure 3.4. Smoothed Measured Spectrum and Bretschneider Spectrum of Equal Variance and Best Least-Squares Fit to Peak Frequency for $M_C = 305$ for Record No. 06887/1.

The measured spectra were smoothed by block averaging over an interval of nine spectral values. This type of smoothing filter was determined by Borgman [21] to be approximately equal to the Gaussian smoothing which he used to investigate the chi-squared confidence intervals of these same records (cf. also Bendat and Piersol [6]). Nine spectral components were block averaged vice the eight components used by Borgman in order that the averaging would be symmetrical. The block averaging was obtained from the following:

$$S(m) = \sum_{n=-4}^{4} S'(m+n)/9 \quad (5.1)$$

where $S(m)$ is the smoothed measured spectral estimate at frequency $m\Delta f$ and S' is the raw spectral estimate. The discrete smoothed spectral estimates have been connected by a continuous curve to aid in reading the figures.

Although the curve which connects the smoothed measured spectral estimates appears to be reasonably smooth, the erratic nature of the raw spectral estimates caused by large differences in the magnitudes of adjacent estimates and by outlier estimates is still evident. The raw spectral estimates oscillate rapidly and these oscillations are especially prevalent in the raw spectra near the best least-squares peak estimates where several large outlier estimates were computed from the FFT coefficients.

The variance of the four measured records varied from $22.3-28.76 \text{ ft}^2$ and the best least-squares estimate of the peak

frequency varied from 0.485-0.520 rad/sec. The root-mean-square errors were computed from the discrete smoothed measured spectral estimates and the discrete Bretschneider spectral values by the following:

$$\text{RMS error} = \sqrt{\frac{1}{M_c} \sum_{m=1}^{M_c} \frac{\{S(m) - S_{BB}(m)\}^2}{n\eta}} \quad (5.2)$$

where M_c is the total number of spectral estimates used. Borgman [21] determined that the magnitudes of the raw spectral estimates became negligible after three hundred and five (305) values and a value of $M_c = 305$ was selected for this comparison analysis. The RMS errors varied between 5.29-12.23 ft²/(rad/sec) with the largest error occurring for the relatively narrow spectral representation for Record No. 06886/2. All of the measured spectra demonstrated several "peaks" and, except for Record No. 06886/2, there are two "peaks" of nearly equal amplitudes very near the best least-squares estimate of maximum peak.

From each of the measured and Bretschneider spectra representing one measured record, six realizations were simulated. Three linear and three nonlinear realizations for both the smoothed measured and the Bretschneider spectra were simulated using the IBM Scientific Subroutine Program RANDU to generate the random numbers required to compute the random phase angles. The same three "seed" numbers required to initialize the RANDU random number generator were used for each of the four records. These three seeds were chosen

since they generally demonstrated the following three different linear measures of skewness: (1) negative, (2) positive, and (3) nearly zero. The realizations from the linear simulation which were generated using this method would have demonstrated zero skewness measure had the random number generator realized a purely Gaussian process.

The cumulative probability distributions from each of the four records showing all six simulated realizations in addition to the measured realization are shown in Figs. 3.5, 3.6, 3.7, and 3.8. Realizations from the unsmoothed measured spectrum would have demonstrated exactly the same distribution as the measured data represented by the open circles if the identical measured phase angles had been used as a result of the exact inverse relationship in the FFT algorithm. The variations between the distributions from the measured spectrum demonstrate the importance of these phase angles in determining the distribution of any realization. The straight line represents a normal distribution having the identical mean and standard deviation as the realizations.

All realizations demonstrate close agreement to a Gaussian process between two normalized standard deviations. The ordinate values have been normalized by the standard deviation of the simulated or measured record; i.e.,

$$\eta(i) = \frac{\eta_{\min} + (i-1) \cdot \Delta\eta}{\sigma_N} \quad i=1, 2, \dots, 31 \quad (5.3)$$

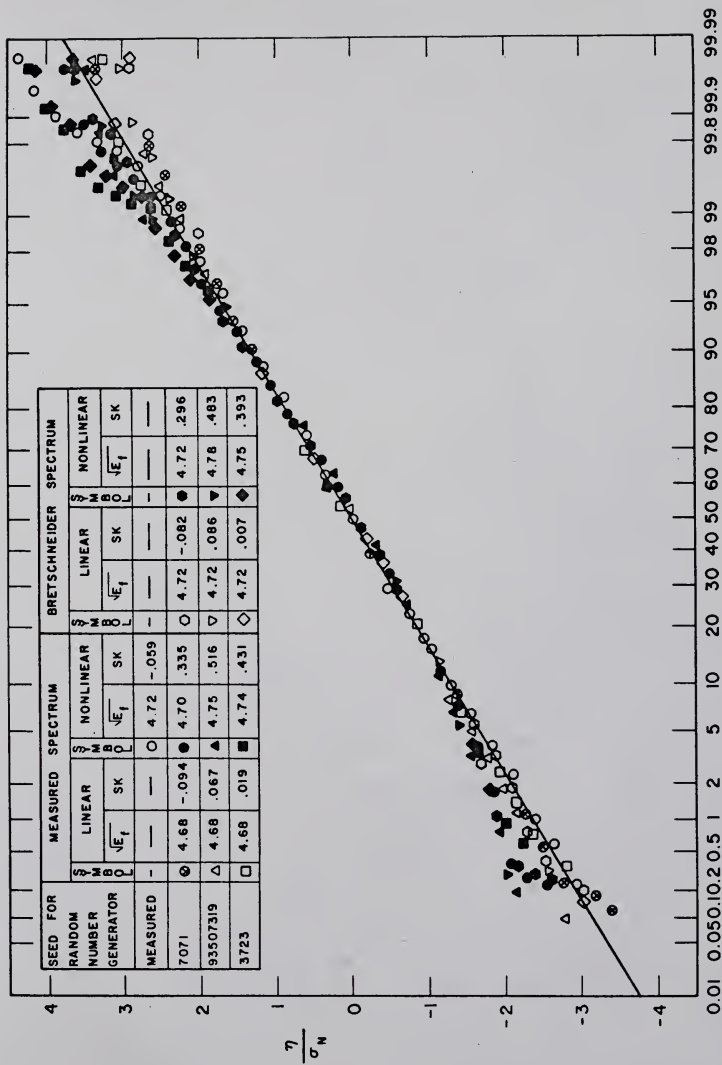


Figure 3.5. Cumulative Probability Distributions for the Normalized Measured Realization and the Linear and Nonlinear Simulated Realizations for Record No. 06885/1.

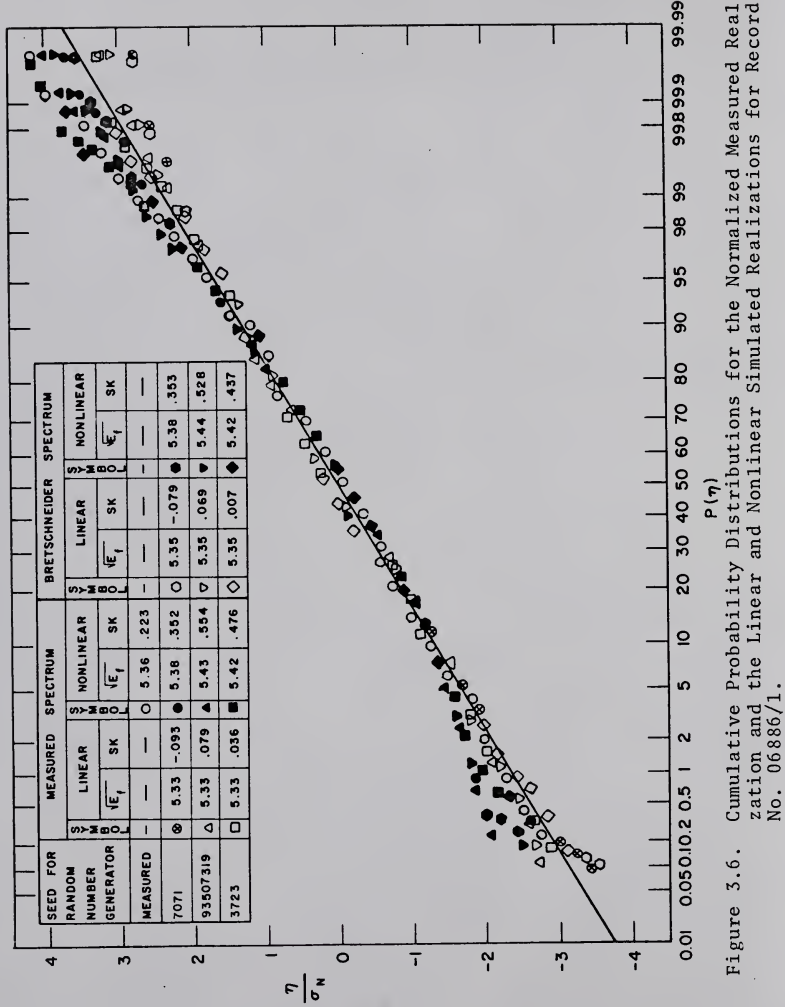


Figure 3.6. Cumulative Probability Distributions for the Normalized Measured Realization and the Linear and Nonlinear Simulated Realizations for Record No. 06886/1.

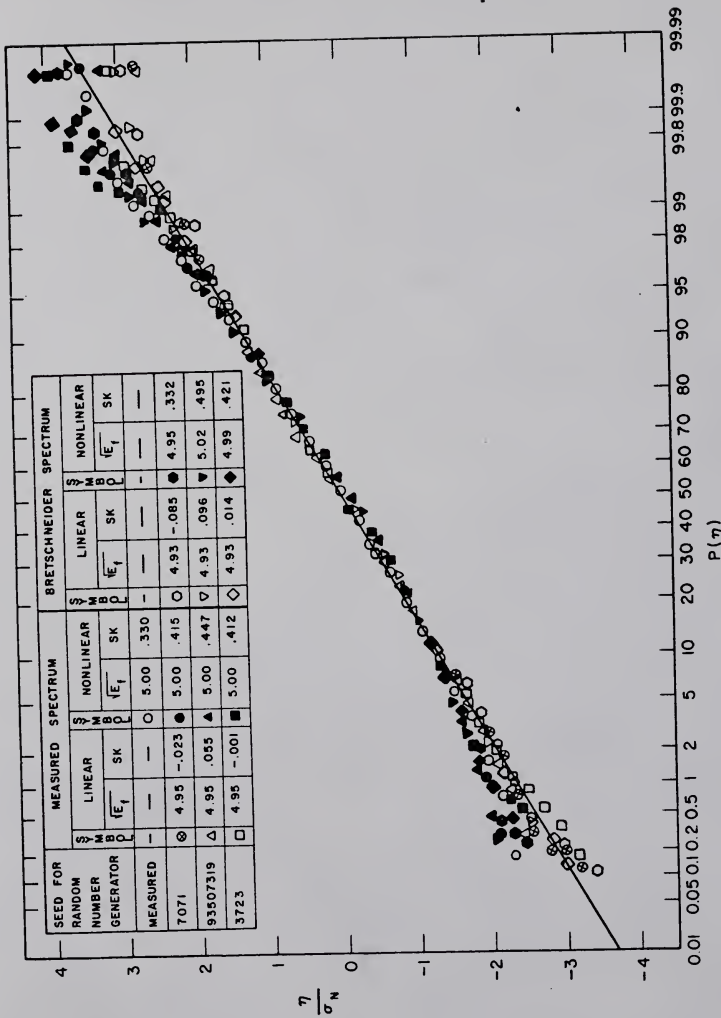


Figure 3.7. Cumulative Probability Distributions for the Normalized Measured Realization and the Linear and Nonlinear Simulated Realizations for Record No. 06886/2.

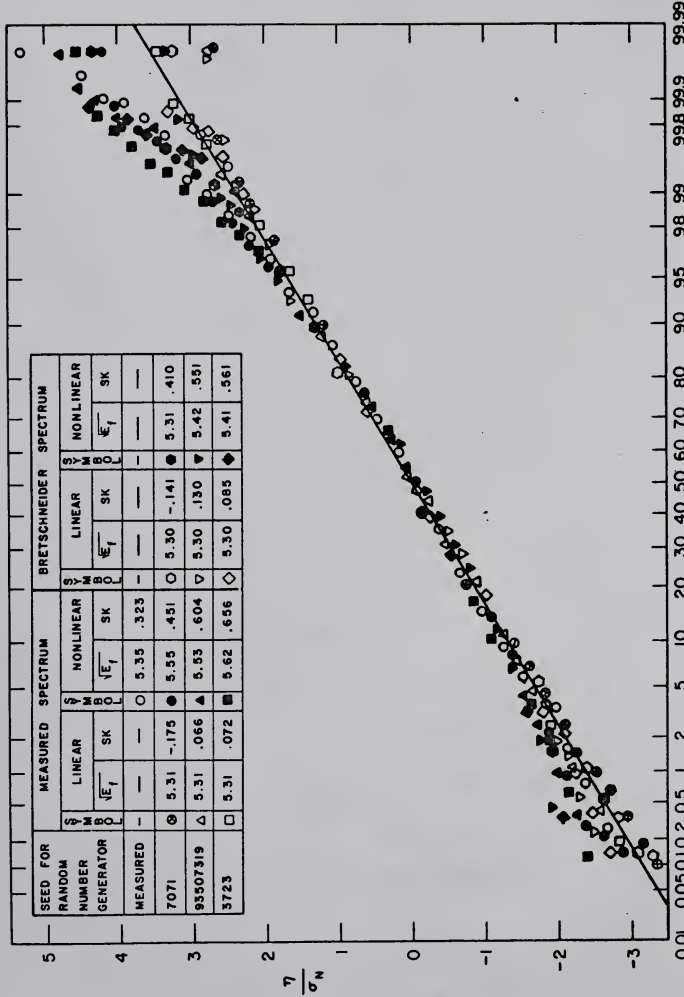


Figure 3.8. Cumulative Probability Distributions for the Normalized Measured Realization and the Linear and Nonlinear Simulated Realizations for Record No. 06887/1.

where $\eta(i)$ is the value of the i^{th} discrete cumulative interval, σ_N is the standard deviation of the measured or simulated realization; and

$$\Delta\eta = [\eta_{\max} - \eta_{\min}] / 30 \quad (5.4)$$

where η_{\max} is the maximum value of the sea surface realization and η_{\min} is the minimum value. The mean of the measured or simulated record was subtracted from the value of each realization and the variance was computed by

$$\sigma_N^2 = \frac{1}{(LX-1)} \sum_{n=1}^{LX} \{\eta(n) - \bar{\eta}\}^2 \quad (5.5)$$

where $\bar{\eta}$ is the mean of the realization determined by

$$\bar{\eta} = \frac{1}{LX} \sum_{n=1}^{LX} \eta(n) \quad (5.6)$$

and LX is the number of time values in the random sequence. The largest values of the sea surface, η , from the nonlinear simulations are seen from these figures to be approximately 0.5-1.5 standard deviations greater than the corresponding largest realizations from the linear simulations.

Figures 3.9, 3.10, 3.11, and 3.12 demonstrate the second order spectra, $S_{\eta\eta}(\sigma)$, computed for both the smoothed measured and Bretschneider spectra. Theoretically, these spectra may be added linearly to the first order spectra as a consequence of the Gaussian assumption and the resulting total energy, E_f , would be statistically identical for all nonlinear realizations from the same initial linear spectra. The final value

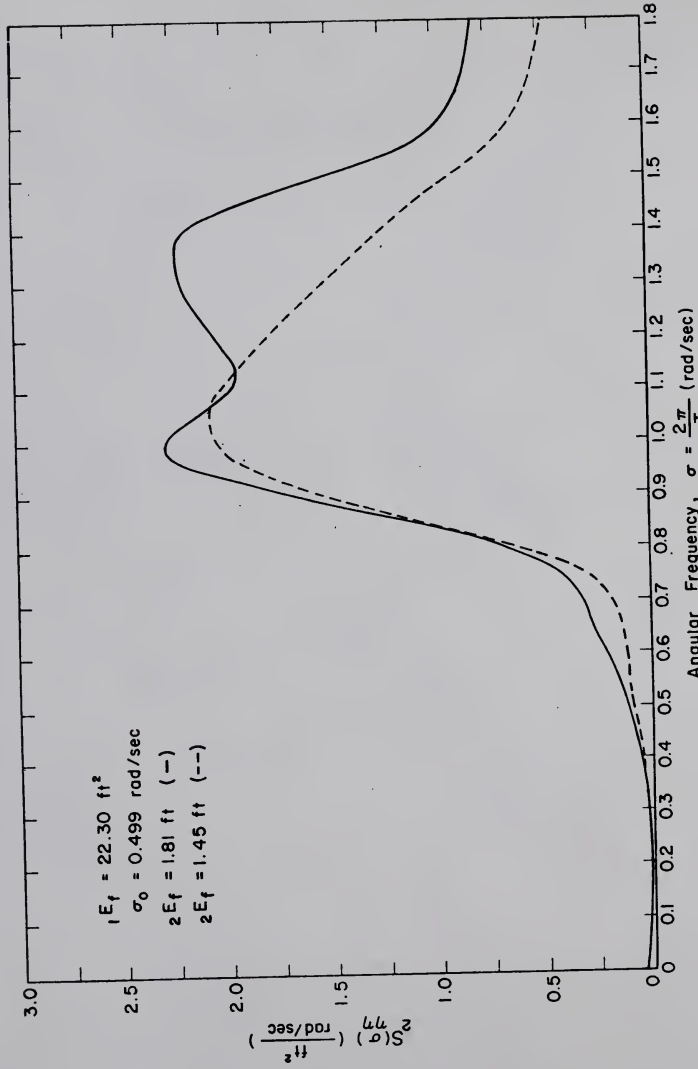


Figure 3.9.

Second Order Spectra Computed from Smoothed Measured Spectrum (—) and from Bretschneider Spectrum (---) for Record No. 06885/1.

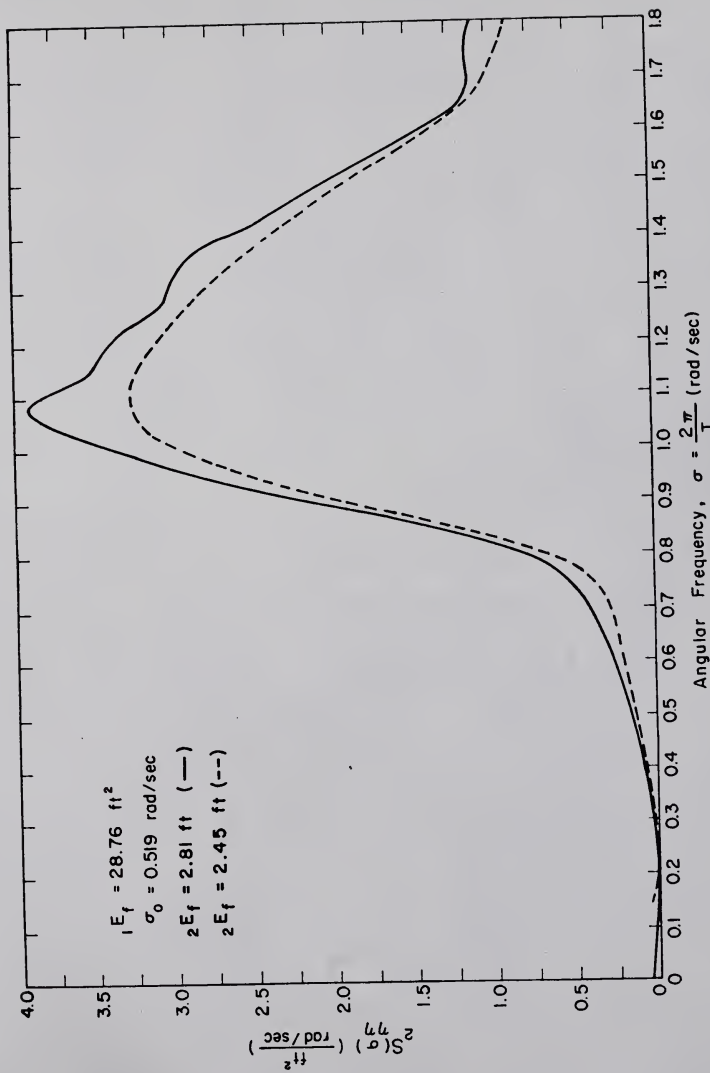


Figure 3.10. Second Order Spectra Computed from Smoothed Measured Spectrum (—) and from Bretschneider Spectrum (- -) for Record No. 06886/1.

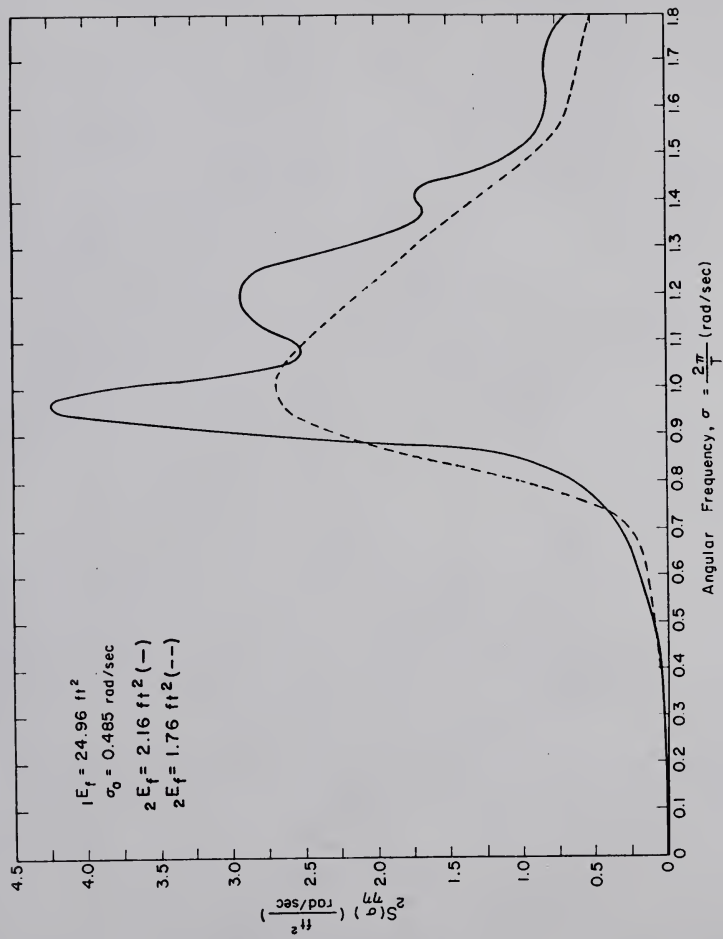


Figure 3.11. Second Order Spectra Computed from Smoothed Measured Spectrum (—) and from Bretschneider Spectrum (---) for Record No. 06886/2.

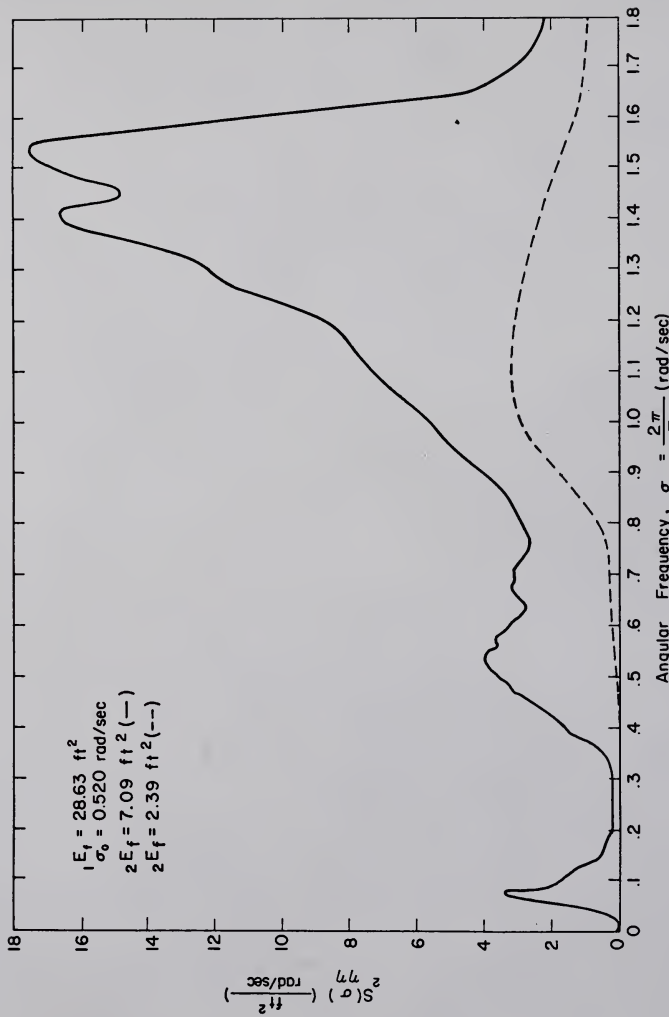


Figure 3.12. Second Order Spectra Computed from Smoothed Measured Spectrum (—) and from Bretschneider Spectrum (--) for Record No. 06887/1.

of the total energy for each realization from the same initial spectrum varies as a result of the nonvanishing three-product second order statistical moment between the first and second perturbation orders for the random sea surface, i.e., the linear first perturbation order solution is not strictly Gaussian and

$$\mathbb{E}\{1\eta(t) \cdot 2\eta(t+\tau) + 2\eta(t) \cdot 1\eta(t+\tau)\} \neq 0 \quad (5.7)$$

The discrete second order spectra may be computed from the continuous first order spectra given by Eq. (6.8) in Chapter 2, Section 6, by replacing the integral with a discrete sum; i.e.,

$${}_2S_{\eta\eta}(m) = 2 \sum_{\ell=1}^{\infty} S(\ell-m) \cdot S(m) \cdot H^2[(\ell-m), m] \cdot \Delta\sigma \quad (5.8)$$

where

$$\Delta\sigma = \frac{2\pi}{T_R} \quad (5.9)$$

Substituting the FFT expressions for the spectra yields

$${}_2S_{\eta\eta}(m) = \frac{4\Delta t}{(LX)^3 \pi} \sum_{\ell=1}^{M_c} X(\ell-m) \cdot X(m) \cdot X^*(\ell-m) \cdot X^*(m) \quad (5.10)$$

where M_c is the maximum number of discrete FFT coefficients required to represent the energy spectrum.

The second order spectra from both the smoothed measured and Bretschneider spectra consistently indicate a peak at approximately $2\sigma_0$. The peak spectral values from the smoothed measured spectra are consistently larger in magnitude than

the spectral values of the peak estimates from the Bretschneider spectra. While the Bretschneider spectra contain only one second order peak, the measured spectra generally contain more than one. These second order peaks reflect the nonlinearities of the self-interactions. The contributions to the nonlinear realization from these self-interactions indicate the importance of the outlier spectral estimates which are capable of generating large self-interaction values. Both the smoothed measured spectra and the Bretschneider spectra contain smoothly varying spectral estimates and the possibility of large nonlinear self-interaction contributions has been eliminated as a result of this smoothness.

Ensembles from three linear and nonlinear realizations from the smoothed measured spectra are shown in Figs. 3.13, 3.14, 3.15, and 3.16. Ensembles from three linear and nonlinear realizations from the Bretschneider spectra are shown in Figs. 3.17, 3.18, 3.19, and 3.20. The time intervals of the measured realizations shown at the top of these ensembles were selected because the largest waves measured were recorded during these intervals. The simulated ensembles generally did not contain the largest waves in the simulated realization and the figures of cumulative distributions must be examined in order to determine the extreme values which were realized for any particular simulation.

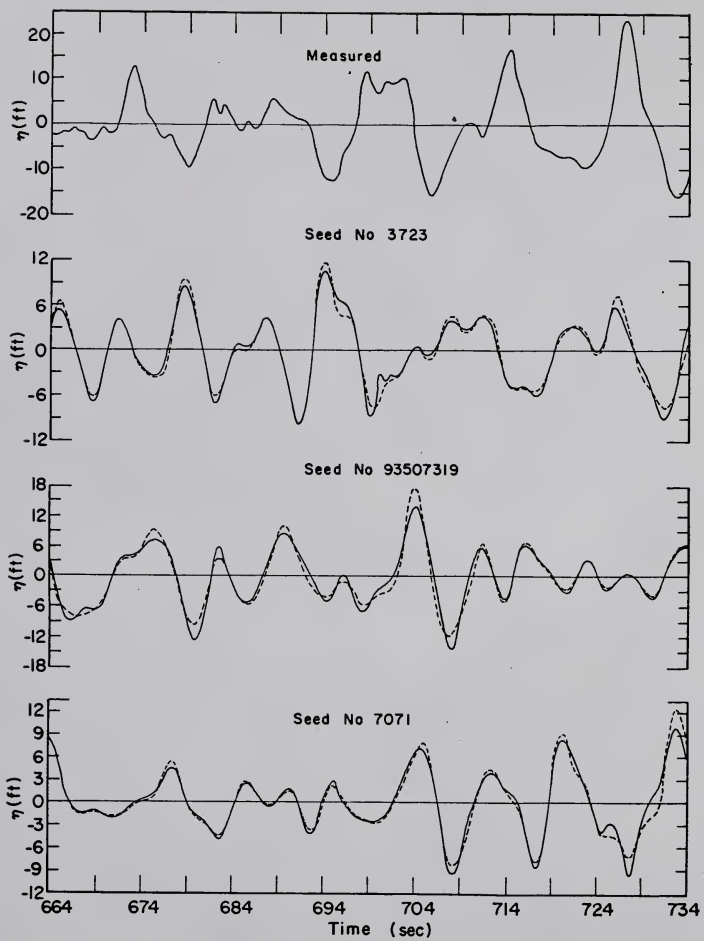


Figure 3.13. Ensemble Comparison Between Measured Realization and Linear and Nonlinear Realizations Simulated from Smoothed Measured Spectrum from Record No. 06885/1.

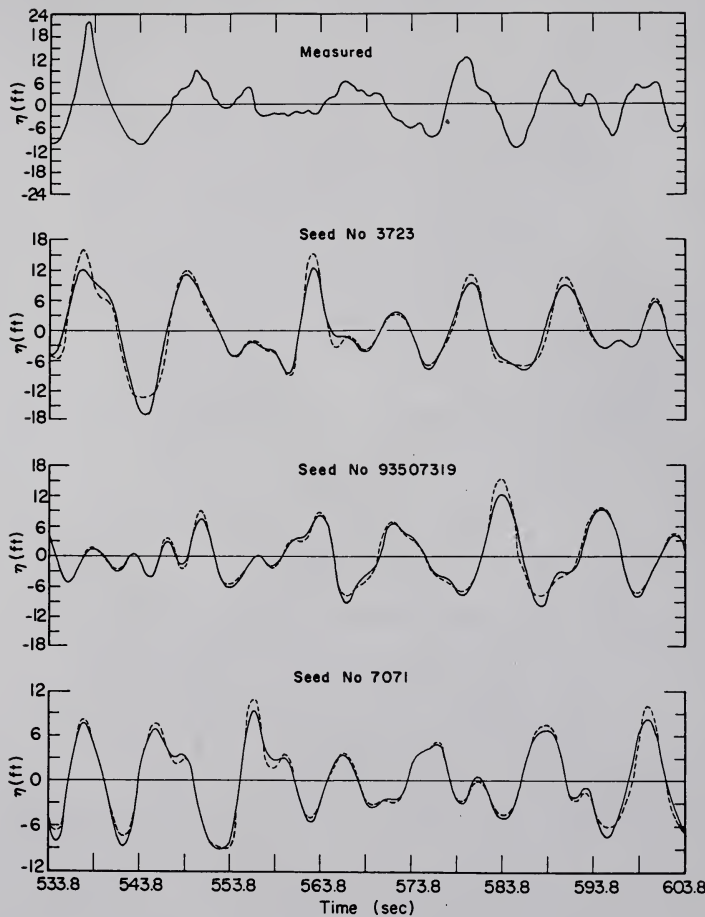


Figure 3.14. Ensemble Comparison Between Measured Realization and Linear and Nonlinear Realizations Simulated from Smoothed Measured Spectrum from Record No. 06886/1.

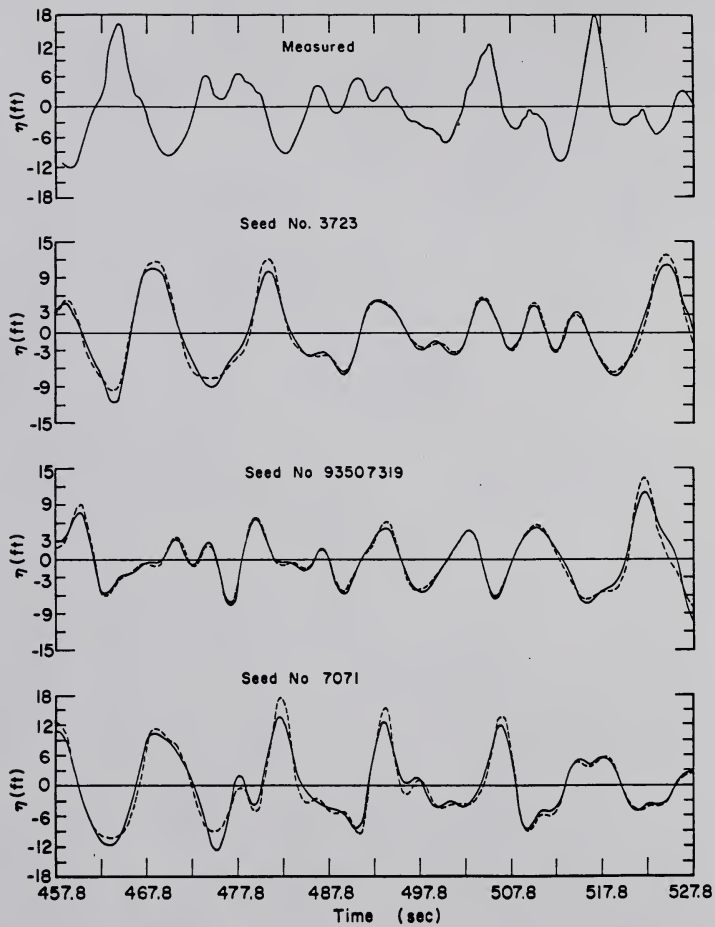


Figure 3.15. Ensemble Comparison Between Measured Realization and Linear and Nonlinear Realizations Simulated from Smoothed Measured Spectrum from Record No. 06886/2.

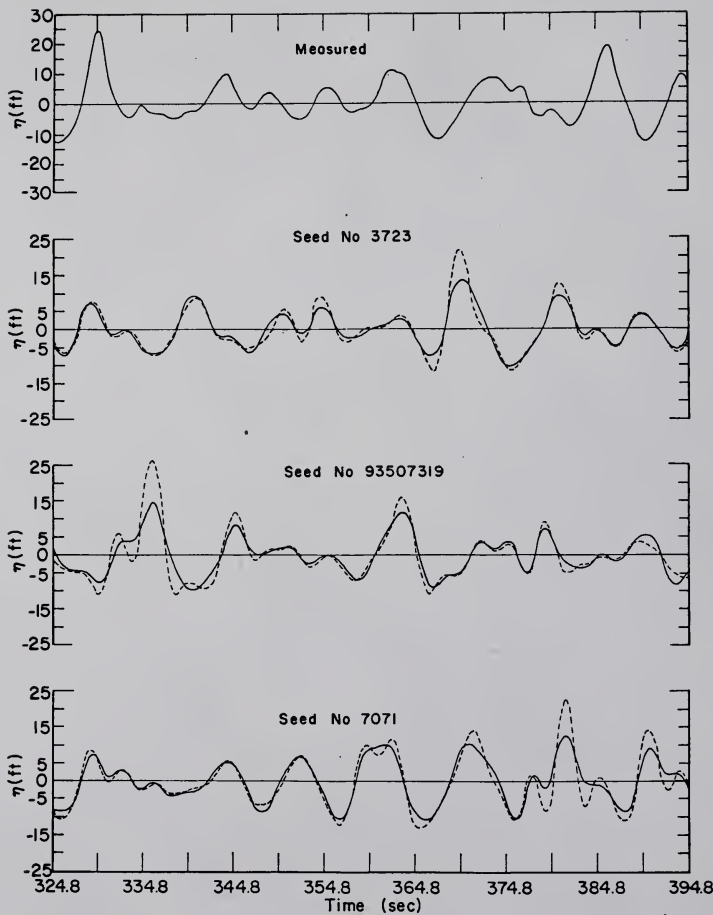


Figure 3.16. Ensemble Comparison Between Measured Realization and Linear and Nonlinear Realizations Simulated from Smoothed Measured Spectrum from Record No. 06887/1.

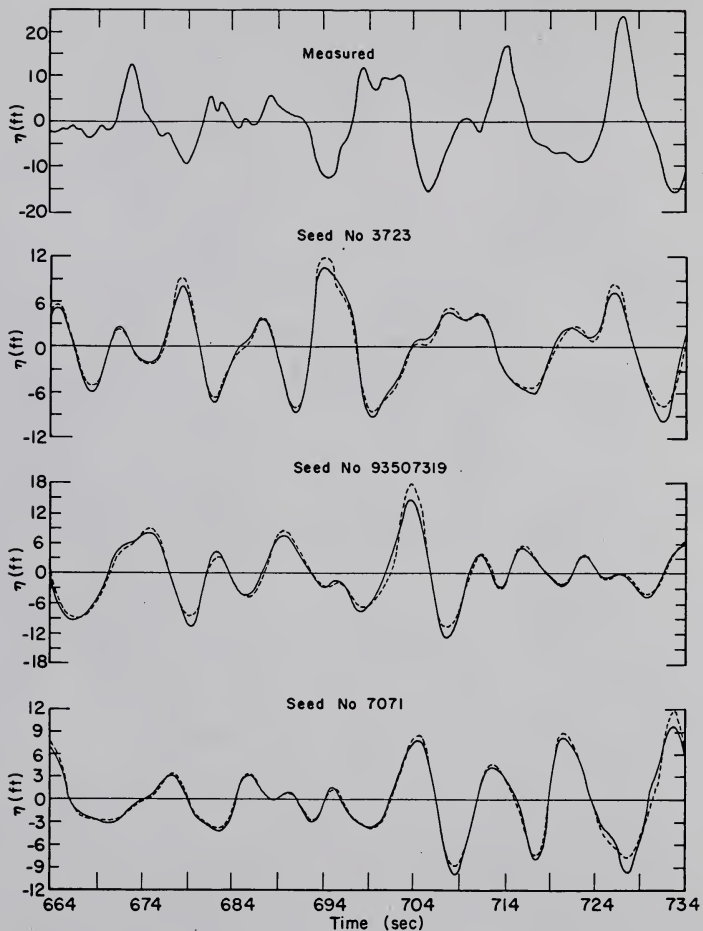


Figure 3.17. Ensemble Comparison Between Measured Realization and Linear and Nonlinear Realizations Simulated from Bretschneider Spectrum from Record No. 06885/1.

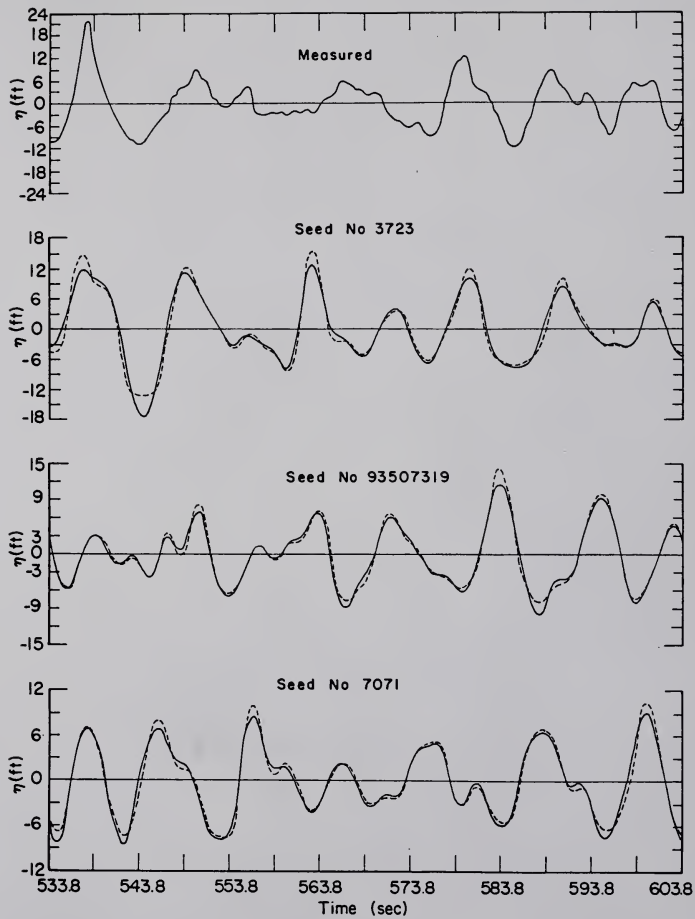


Figure 3.18. Ensemble Comparison Between Measured Realization and Linear and Nonlinear Realizations Simulated from Bretschneider Spectrum from Record No. 06886/1.

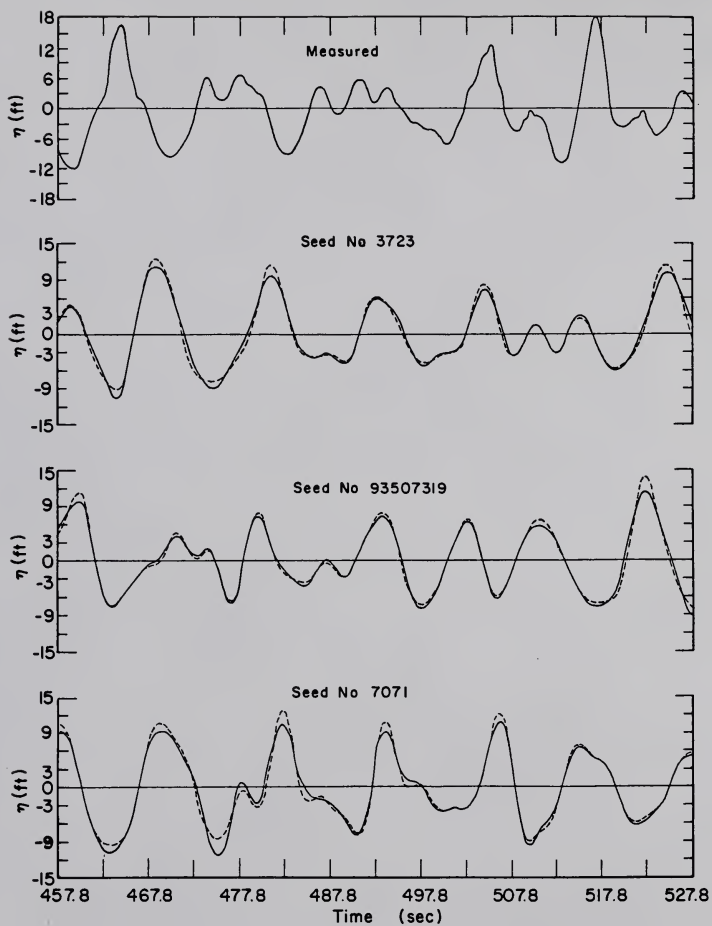


Figure 3.19. Ensemble Comparison Between Measured Realization and Linear and Nonlinear Realizations Simulated from Bretschneider Spectrum from Record No. 06886/2.

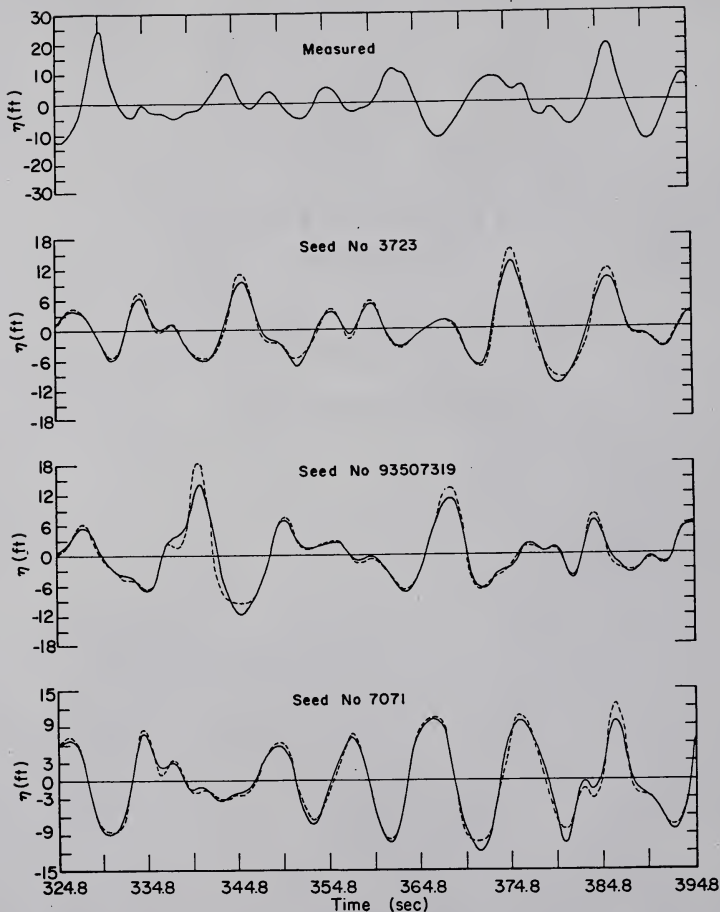


Figure 3.20. Ensemble Comparison Between Measured Realization and Linear and Nonlinear Realizations Simulated from Bretschneider Spectrum from Record No. 06887/1.

6. Digital Linear Filter

The digital linear filter technique is a method by which certain wave fields may be computed by the convolution of an impulse response function with a time sequence of the sea surface. Reid [106] developed the technique to compute kinematic fields for predicting wave forces on piles. Grooves [53] has tabulated a number of frequency response functions using linear wave theory which will compute several wave fields by this general convolution method. Wheeler [129] applied the technique developed by Reid [106] to hurricane-generated wave data recorded by Wave Project II during Hurricane Carla and computed drag and inertia force coefficients which varied with the vertical depth of pressure force correlation. A succinct and lucid description of the technique which is applicable to wave force predictions has been given by Borgman [22].

As applied in the prediction of wave forces on piles, the digital linear filter technique assumes that the kinematic wave fields may be computed from linear wave theory and that the sea surface realizations represent an irregular long-crested wave field which is the result of the superposition of linear waves. The application which is derived in this section departs from the descriptions given by Reid [106] and by Borgman [22] in the following areas:

- (1) a "stretched" vertical coordinate is to be utilized.

- (2) the horizontal acceleration field is to be computed by numerical differentiation of the horizontal velocity field vice by the convolution method.

The stretching of the vertical coordinate in the argument of the vertical coordinate dependent function in the expression for the linear velocity potential has been employed with some success [67,129] to ensure that this function does not become excessively large in magnitude whenever kinematic fields are evaluated for wave crest phase values at elevations above the still water level. For kinematic predictions required at a vertical elevation, s , above the bottom, the stretching function results in the computations actually being made at a stretched elevation, s' , above the bottom; i.e.,

$$s'(\alpha, s) = \alpha(h, t, x) \cdot s \quad (6.1)$$

where the vertical stretching function, $\alpha(h, t, x)$, is given by the following:

$$\alpha(h, t, x) = \frac{h}{h + \eta(t, x)} \quad (6.2)$$

A linear velocity potential when modified by this stretching term becomes

$$\Phi(x, z, t, s') = -i \frac{H}{2} \frac{g}{\sigma} \frac{\cosh\{k \cdot s'(\alpha, s)\}}{\cosh\{kh\}} \exp i(\sigma t - kx) \quad (6.3)$$

Substituting Eq. (6.3) into the equation of continuity yields

$$\Phi_{xx} + \Phi_{zz} = 0\{\Phi_s, \cdot s' \cdot n_x\} \quad (6.4)$$

where the terms $0\{\cdot\}$ are of higher order in wave slope, $Hk/2$, than the two derivatives on the left side. Eq. (6.4) demonstrates that the linear velocity potential modified by a stretched vertical coordinate no longer satisfies exactly the equation of continuity; however, the modified velocity potential does satisfy the equation of continuity to first order in wave slope and is, therefore, consistent with the perturbation expansion which is assumed to be valid for linear wave theory. Additional expressions which may be utilized to extend the wave pressure field computed by linear wave theory above the still water level are given by Borgman [18], Chakrabarti [33], and Nath and Felix [93].

The following brief derivation of the linear filter technique which is applicable to computing horizontal kinematic flow fields in a stretched vertical coordinate follows closely the derivations given by Reid [106] and by Borgman [22] and is included only for convenience.

From the following aperiodic linear velocity potential

$$\Phi(x, s', t) = -i \int_{-\infty}^{\infty} F(\sigma) \cdot \frac{g}{\sigma} \frac{\cosh\{ks'\}}{\cosh\{kh\}} \exp i\{\sigma t - kx\} d\sigma \quad (6.5)$$

and linear dispersion equation

$$\sigma^2 = gk \tanh\{kh\} \quad (6.6)$$

With $k(-\sigma) = -k(\sigma)$, the following horizontal kinematic fields and scalar sea surface realization for a fixed horizontal

spatial value for x ($x=0$, say) may be easily computed correct to first order in wave slope:

$$u(s', t) = \int_{-\infty}^{\infty} F(\sigma) \sigma \frac{\cosh\{ks'\}}{\sinh\{kh\}} \exp i\{\sigma t\} d\sigma \quad (6.7a)$$

$$u_t(s', t) = i \int_{-\infty}^{\infty} F(\sigma) \sigma^2 \frac{\cosh\{ks'\}}{\sinh\{kh\}} \exp i\{\sigma t\} d\sigma \quad (6.7b)$$

$$n(t) = \int_{-\infty}^{\infty} F(\sigma) \exp i\{\sigma t\} d\sigma \quad (6.7c)$$

The spectral density of the sea surface, $F(\sigma)$, is obtained by the following Fourier inversion:

$$F(\sigma) = \frac{1}{2\pi} \int_{-\infty}^{\infty} n(t) \exp i\{-\sigma t\} dt \quad (6.8)$$

The spectral response functions for the horizontal kinematic fields are seen by inspection of Eqs. (6.7a,b) to be the following:

$$g_u(\sigma, s') = \sigma \frac{\cosh\{ks'\}}{\sinh\{kh\}} \quad (6.9a)$$

$$g_{u_t}(\sigma, s') = \sigma^2 \frac{\cosh\{ks'\}}{\sinh\{kh\}} \quad (6.9b)$$

which are symmetric and antisymmetric functions, respectively, of the frequency, σ , provided that $k(-\sigma) = -k(\sigma)$.

These spectral response functions may be expanded in generalized Fourier series (cf. Lighthill [75], Papoulis [96], or Titchmarsh [126]) where the interval of periodicity must be greater than or equal to the maximum frequency of measurable energy in the spectrum of the sea surface, $F(\sigma)$. Reid [106] did not employ a stretched vertical coordinate and truncated

the frequency response functions at a cut-off frequency which was less than the frequency of periodicity. Wheeler [129] used a stretching function and let the value of the cut-off frequency equal the periodic interval. The cut-off frequency must be less than or equal to the Nyquist frequency which is determined by the spacing used in digitizing the measured record; i.e.,

$$\sigma_c \leq \frac{\pi}{\Delta t} \quad (6.10)$$

where Δt is the digitizing interval and σ_c is the cut-off angular frequency.

Expanding the frequency response functions given by Eq. (6.9a,b) in generalized finite Fourier series which are periodic in frequency space over the interval of periodicity, $\{2\pi/\tau_0\}^{-1}$, the following series result:

$$g_u(\sigma, s') = \sum_{m=-M}^M C_m \exp i\{-\sigma m \tau_0\} \quad (6.11a)$$

$$g_{u_t}(\sigma, s') = i \sum_{m=-M}^M C'_m \exp i\{-\sigma m \tau_0\} \quad (6.11b)$$

where M is the maximum number of coefficients required to fit the series to the frequency response function, $\{2\pi/\tau_0\}^{-1}$ is the interval of periodicity, and the reality requirements for symmetric and antisymmetric expansions are given by the following relationships:

$$C_{-m} = C_m \quad (\text{symmetric}) \quad (6.12a)$$

$$C'_{-m} = -C'_m \quad (\text{antisymmetric}) \quad (6.12b)$$

The generalized Fourier transforms of Eqs. (6.11a,b) (cf. Lighthill [75], Papoulis [96], or Titchmarsh [126]) are given by the following impulse response functions:

$$g_u(\tau, s') = \int_{-\infty}^{\infty} g_u(\sigma, s') \exp i\{\sigma\tau\} d\sigma \quad (6.13a)$$

$$g_{u_t}(\tau, s') = \int_{-\infty}^{\infty} g_{u_t}(\sigma, s') \exp i\{\sigma\tau\} d\sigma \quad (6.13b)$$

Substitution of the Fourier series approximations for the frequency response functions given by Eqs. (6.11a,b) into Eqs. (6.13a,b) yields the following:

$$g_u(\tau, s') = \sum_{m=-M}^{M} C_m \int_{-\infty}^{\infty} \exp i\{\sigma(\tau-m\tau_0)\} d\sigma \quad (6.14a)$$

$$g_{u_t}(\tau, s') = i \sum_{m=-M}^{M} C'_m \int_{-\infty}^{\infty} \exp i\{\sigma(\tau-m\tau_0)\} d\sigma \quad (6.14b)$$

The integrals in Eqs. (6.14a,b) are seen to be equal to the Dirac delta distribution in the time domain by their similarity to Eq. (2.12), Chapter 2, Section 2, which defines the shifting property in the spatial domain. Therefore, the impulse response functions are seen to be a comb of Dirac delta distributions in the time domain and are proportional to the Fourier series coefficients which approximate the continuous frequency response functions, i.e.,

$$g_u(\tau, s') = 2\pi \sum_{m=-M}^{M} C_m \delta(\tau-m\tau_0) \quad (6.15a)$$

$$g_{u_t}(\tau, s') = 2\pi i \sum_{m=-M}^{M} C'_m \delta(\tau-m\tau_0) \quad (6.15b)$$

The expressions for the Fourier transform of the sea surface spectral density, $F(\sigma)$, given by Eq. (6.8) and the expressions for the frequency response functions given by Eqs. (6.9a,b) may be substituted into the equations for the aperiodic horizontal kinematic flow fields given by Eqs. (6.7a,b) to yield the following:

$$u(s', t) = \int_{-\infty}^{\infty} G_u(\sigma, s') \cdot \exp i\{\sigma t\} \cdot \frac{1}{2\pi} \int_{-\infty}^{\infty} n(\tau) \exp i\{-\sigma\tau\} d\tau d\sigma \quad (6.16a)$$

$$u_t(s', t) = i \int_{-\infty}^{\infty} G_{u_t}(\sigma, s') \cdot \exp i\{\sigma t\} \cdot \frac{1}{2\pi} \int_{-\infty}^{\infty} n(\tau) \exp i\{-\sigma\tau\} d\tau d\sigma \quad (6.16b)$$

Inverting the order of integration and rearranging terms results in the following:

$$u(s', t) = \int_{-\infty}^{\infty} n(\tau) \cdot \left\{ \frac{1}{2\pi} \int_{-\infty}^{\infty} G_u(\sigma, s') \exp i\{\sigma(t-\tau)\} d\sigma \right\} d\tau \quad (6.17a)$$

$$u_t(s', t) = i \int_{-\infty}^{\infty} n(\tau) \cdot \left\{ \frac{1}{2\pi} \int_{-\infty}^{\infty} G_{u_t}(\sigma, s') \exp i\{\sigma(t-\tau)\} d\sigma \right\} d\tau \quad (6.17b)$$

Comparing the expressions in brackets $\{\cdot\}$ in Eqs. (6.17a,b) with the expressions for the impulse response functions given by Eqs. (6.13a,b), it may be seen that these bracketed terms are the impulse response functions shifted by $(t-\tau)$. Replacing τ with $(t-\tau)$ in the equivalent expression for the impulse response function given by Eqs. (6.15a,b) and substituting for the bracketed terms in Eqs. (6.17a,b), the following are obtained:

$$u(s', t) = \sum_{m=-M}^{M} C_m \int_{-\infty}^{\infty} n(\tau) \cdot \delta[t - (\tau + m\tau_0)] d\tau \quad (6.18a)$$

$$u_t(s', t) = - \sum_{m=-M}^{M} C'_m \int_{-\infty}^{\infty} n(\tau) \cdot \delta[t - (\tau + m\tau_0)] d\tau \quad (6.18b)$$

The following change of variables substitution

$$\tau' = t - \tau \quad (6.19)$$

results in the final convolution expressions for the horizontal kinematic fields:

$$u(s', t) = \sum_{m=0}^{M-1} C_m \int_{-\infty}^{\infty} \eta(t - \tau') [\delta(\tau' - m\tau_0) + \delta(\tau' + m\tau_0)] d\tau' \quad (6.20a)$$

$$u_t(s', t) = \sum_{m=1}^{M-1} C'_m \int_{-\infty}^{\infty} \eta(t - \tau') [\delta(\tau' + m\tau_0) - \delta(\tau' - m\tau_0)] d\tau' \quad (6.20b)$$

The convolutions given by Eqs. (6.20a,b) are the weighted sums of products of the sea surface sequence with the Fourier coefficients of the spectral response functions.

These spectral response functions are a function of time through the stretching function. Consequently, the spectral response function for the horizontal velocity was partitioned into ten even intervals of constant elevation, s' , given by

$$s'_{\ell} = \ell \cdot s' / 10 \quad \ell = 0, 1, \dots, 10 \quad (6.21)$$

and the instantaneous horizontal velocity was computed at the eleven contours of constant elevation, s'_{ℓ} , from Eq. (6.20a). The instantaneous horizontal velocity at the desired elevation, s , was then computed by linear interpolation between contours of constant elevation, s'_{ℓ} .

The previous applications of the vertical "stretching" function involved predicting pressure forces only for maximum peak forces [129] or only for forces recorded during the crest

portion of a wave [67]. The advantages of extending the kinematics of linear theory to vertical elevations above the still water level by Eq. (6.2) are not achieved, however, without a corresponding deleterious effect of amplifying kinematic field predictions in the trough region of a wave compared to predictions from unstretched linear theory. Since a continuous time sequence of predicted pressure forces are required for simulation, this overprediction by the stretching function in the trough region of waves can be as important as the overprediction in the crest region by the unmodified linear theory. A demonstration and discussion of this effect may be found in Section 7 of this chapter.

In the application to the WPII data, the cut-off frequency of 0.3125 Hz and the filter spacing of 1.60 seconds used by Wheeler [129] were adopted. The instantaneous horizontal velocity for a desired elevation was computed from the convolution given by Eq. (6.20a) using the weighting coefficients for contours of constant elevation shown in Table 3.3 and by linear interpolation between these contours of constant elevation. The instantaneous horizontal acceleration was computed by numerically differentiating the horizontal velocity at contours of constant elevation, s_ℓ^t , according to the following formula:

$$u_t(s_\ell^t, n) = \frac{u[s_\ell^t, n+1] - u[s_\ell^t, n-1]}{2\Delta t} \quad (6.22)$$

Table 3.3

Impulse Response Coefficients for Horizontal Velocity
Field with Stretched Vertical Coordinate ($h = 99$ ft.)

$m \setminus s_i$	0.0	0.1	0.2	0.3	0.4	0.5	0.6	0.7	0.8	0.9	1.0
0	0.12773	0.12888	0.13248	0.13895	0.14919	0.16485	0.18902	0.22798	0.29477	0.41853	0.66767
1	0.09130	0.09143	0.09179	0.09220	0.09229	0.09123	0.08721	0.07616	0.04854	-0.01873	-0.18331
2	0.02839	0.02771	0.02562	0.02193	0.01636	0.00854	-0.00173	-0.01392	-0.02480	-0.02297	0.02695
3	-0.00213	-0.00229	-0.00273	-0.00329	-0.00367	-0.00339	-0.00170	0.00225	0.00862	0.01397	0.00094
4	-0.00359	-0.00347	-0.00310	-0.00250	-0.00171	-0.00089	-0.00036	-0.00073	-0.00269	-0.00556	-0.00141
5	-0.00014	-0.00012	-0.00005	0.00005	0.00014	0.00025	0.00046	0.00104	0.00247	0.00478	0.00421
6	0.00052	0.00050	0.00044	0.00035	0.00022	0.00003	-0.00030	-0.00096	-0.00232	-0.00471	-0.00651
7	0.00011	0.00010	0.00009	0.00007	0.00007	0.00011	0.00026	0.00071	0.00182	0.00411	0.00725
8	-0.00007	-0.00007	-0.00006	-0.00006	-0.00006	-0.00010	-0.00023	-0.00060	-0.00158	-0.00378	-0.00772

Note: Cut-off frequency, $f_c = 0.3125$ Hz.

and the value of the horizontal velocity at the desired elevation, s , was determined by numerical interpolation between contours of constant elevation. The resultant horizontal pressure on a vertical pile at elevation, s , was computed from the Morison equation utilizing these two kinematic fields and the modified Dean and Aagaard resultant force coefficients from Table 3.4 (cf. [67]). The Reynolds number was computed using a value for the kinematic viscosity equal to 1.4×10^{-5} ft 2 /sec and for a piling diameter equal to 3.71 ft. The density of the sea water was assumed to be 2.0 slugs/ft 3 .

Table 3.4

Drag and Modified Inertia Force Coefficients
for Resultant Pressure Forces
(from Dean and Aagaard [41])

Reynolds No. ($\times 10^5$)	$Re < 3$	$3 \leq Re < 10$	$10 \leq Re$
C_D	1.34	0.98	0.92
C_M	1.18	1.18	1.18

7. Comparison of Pressure Forces

To reiterate, the main purpose of the nonlinear random sea simulation is to provide a random forcing function to be employed in the stochastic analysis of deep water pile-

supported platforms. The principal comparisons between the random sea simulations and the measured realizations which were previously discussed involved only the statistics of the random waves. Borgman [17] has developed a theory for determining wave forces on a pile from a narrow band spectrum of random waves. Wells [128] offered constructive comments relative to the second order nonlinearities omitted in the theory. Pierson and Holmes [102] later developed a probability density function for random wave forces using Gaussian assumptions and compared both the probability densities and cumulative probability distributions of their model with measured force data. The advantages and disadvantages of the model were discussed by several writers [40,90,107] in addition to the closure by the authors [103].

No attempt has been made in this study to derive the probability density function of the pressure force distributions obtained by filtering the nonlinear random realizations as this is a most complex problem due to the nonlinearities involved. One simulated realization from each of the four measured hurricane-generated continuous records, however, was selected as a random input for the digital linear filter technique in order to compute pressure forces for comparison and demonstration of the force realizations which may be expected in applications. The same seed number for the random number generator was used for each simulated realization since the sea surface realizations computed from the same seed number represented varying degrees of fits to distributions

of the measured sea surface realizations from each measured record and, therefore, did not always give the best agreement with the measured realizations.

The stretching function, $\alpha(h,t,x)$, introduced in Section 6 is inversely proportional to the instantaneous value of the sea surface, η . This fact introduces a negative bias into the computation of horizontal kinematics by the digital linear filter technique which results in the overprediction of kinematics in the trough region of the waves compared to predicted kinematic values from unstretched linear theory.

Figures 3.21 and 3.22 illustrate this effect for two strictly periodic waves. The nonlinear wave shown by the dotted line is a dimensional example of the Dean Stream Function CASE 7-C and represents a nondispersive progressive wave having a wave height which is three-fourths of the breaking wave height for a water depth of 99 feet and a wave period of 10 seconds. The solid line represents a linear wave with the equivalent wave period and total energy as the dimensional form of the Stream Function CASE 7-C. The horizontal velocities were computed using the filter coefficients given in Table 3.3 and the horizontal accelerations were computed by numerical differentiation using Eq. (6.22). The pressure forces were computed by the Morison equation using the modified Dean and Aagaard coefficients from Table 3.4. The values of the kinematic viscosity, sea water density, and piling diameter required to compute the Reynolds number and pressure forces are given in Section 6. The negative bias in the

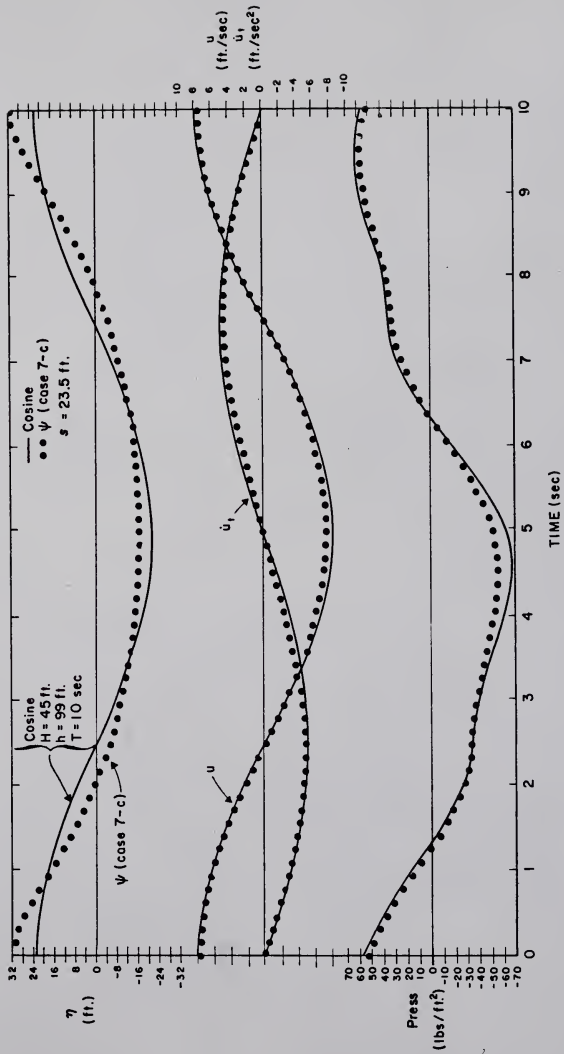


Figure 3.21. Comparison of Horizontal Kinematic Fields and Pressure Forces Computed by Digital Linear Filter Technique from Skewed (---) and Nonskewed (•••) Periodic Waves.

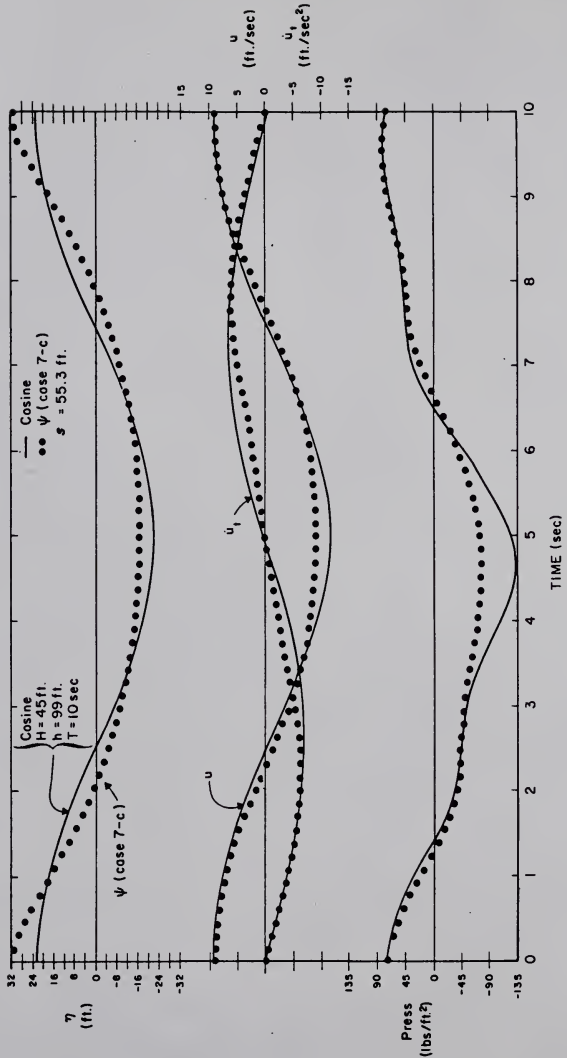


Figure 3.22. Comparison of Horizontal Kinematic Fields and Pressure Forces Computed by Digital Linear Filter Technique from Skewed (•) and Nonskewed (—) Strictly Periodic Waves.

pressure force is noticeable in both examples with the more dramatic effect demonstrated at the 55.3 foot elevation. The effect of the skewed Stream Function profile appears to be lower velocity values compared with the value computed by filtering the unskewed linear profile in the trough regions of the two profiles.

Figures 3.23, 3.24, 3.25, and 3.26 each contain four pressure force spectra from the dynamometer located at the 55.3 foot elevation. The four spectra represent the following: (1) measure pressure force spectra; (2) pressure force spectrum computed from filtering a nonlinear simulated realization synthesized from the measured amplitude spectrum; (3) pressure force spectrum computed from filtering a nonlinear simulated realization synthesized from the Bretschneider spectrum; and (4) pressure force spectrum computed from filtering the measured sea surface realization.

Table 3.5 demonstrates the comparisons of mean square pressures determined by these four methods for each of the four measured records. None of the predicted mean square pressures exceeded the measured values. The mean square pressures computed from the measured realizations, $\sqrt{P_{Pn}^2}$, were consistently greater than the other predicted values. The mean square pressures predicted from realizations simulated from the Bretschneider spectrum, $\sqrt{P_{PB}^2}$, were consistently greater than the values from realizations simulated from the smoothed measured spectrum, $\sqrt{P_{PM}^2}$; however, these differences were not great.

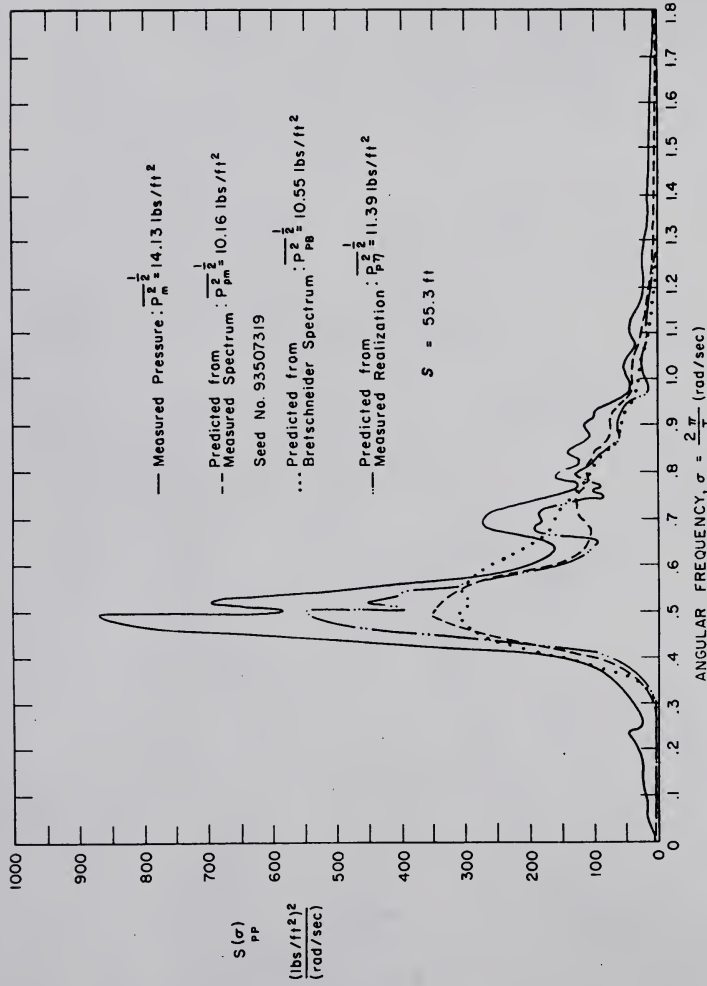


Figure 3.23. Comparison Between Measured and Predicted Pressure Force Spectra from Record No. 06885/1.

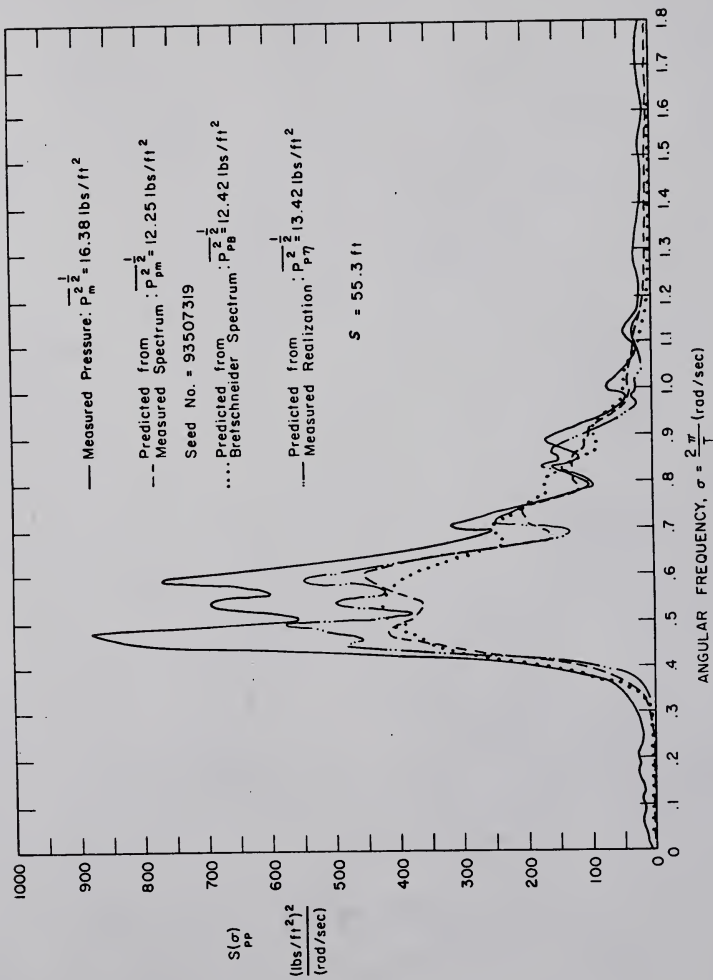


Figure 3.24. Comparison Between Measured and Predicted Pressure Force Spectra from Record No. 06886/1.

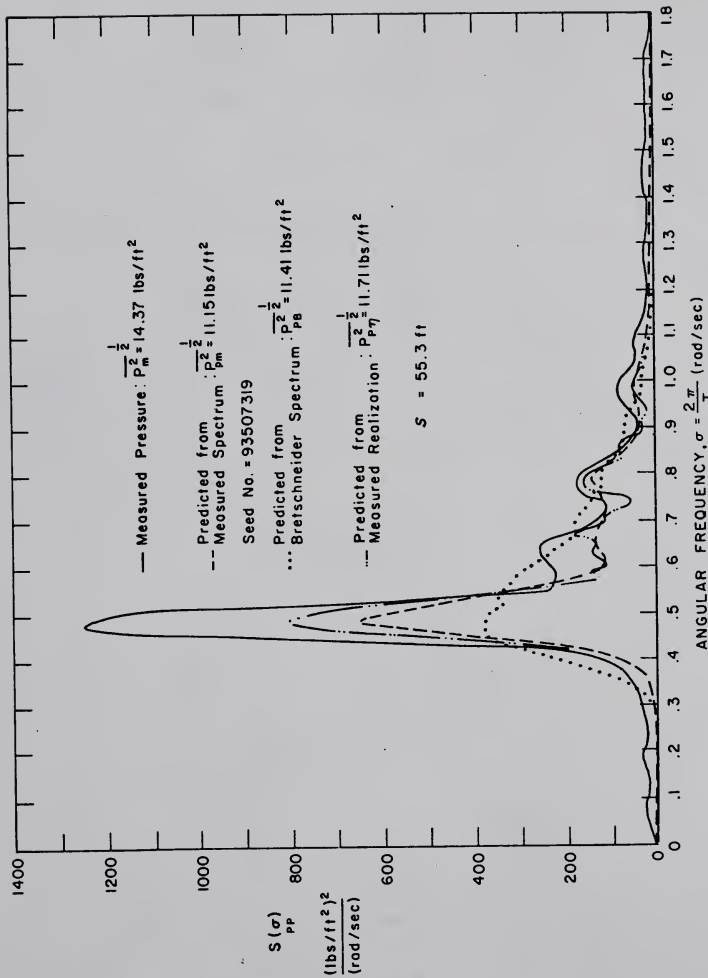


Figure 3.25. Comparison Between Measured and Predicted Pressure Force Spectra
from Record No. 06886/2.

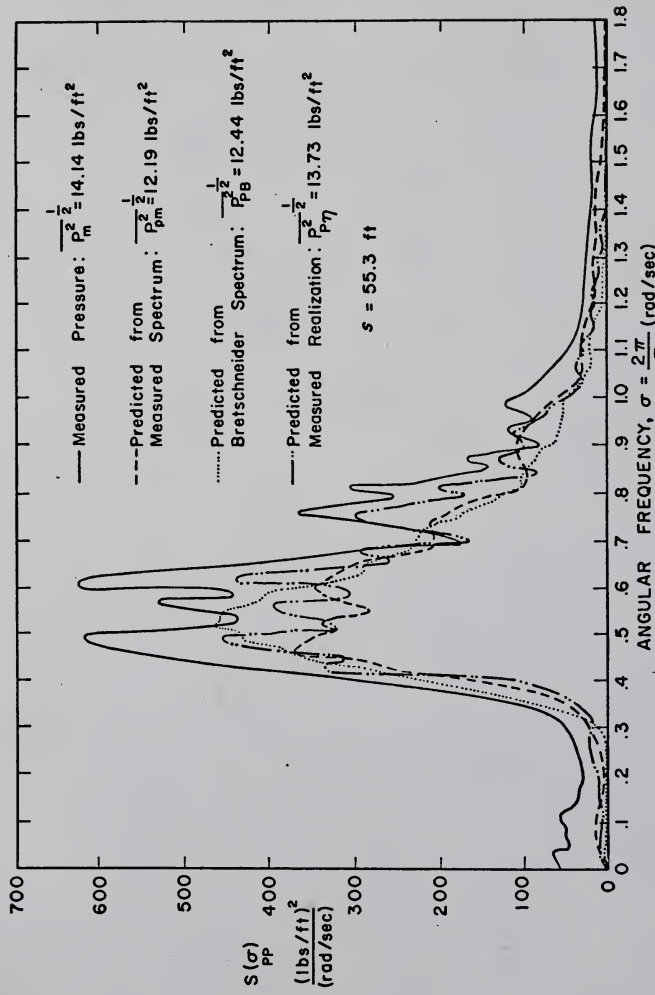


Figure 3.26. Comparison Between Measured and Predicted Pressure Force Spectra
from Record No. 06887/1.

Table 3.5

Comparison Between Measured and Simulated Pressure Forces
at 55 foot Dynamometer Elevation from Hurricane Carla

Record No.	η	$\overline{P}_M^{1/2}$	$\overline{P}_{PM}^{1/2}$	$\overline{P}_{PB}^{1/2}$	$\overline{P}_{P\eta}^{1/2}$	ϵ_{MPM}	ϵ_{MPB}	$\epsilon_{P\eta P\eta}$	ϵ_{PBPB}
	(ft ²)	(lbs./ft ²)	(lbs./ft ²)	(lbs./ft ²)	(lbs./ft ²)	(%)	(%)	(%)	(%)
06885/1	22.30	14.13	10.16	10.55	11.39	28.10	25.34	19.39	7.37
06886/1	28.76	16.38	12.25	12.42	13.42	25.21	24.18	18.07	7.45
06886/2	24.96	14.37	11.15	11.41	11.71	22.41	20.60	18.51	2.56
06887/1	28.63	14.14	12.19	12.44	13.73	12.43	12.02	2.48	9.79
									2.01

$$\text{Note: } \epsilon_{ij} = \frac{\overline{P}_i^{1/2} - \overline{P}_j^{1/2}}{\overline{P}_i^{1/2}} \times 100\%$$

In general, the shape of the spectra computed from filtering the measured realization approximated very closely that of the measured sea realization and force spectra. This similarity was noticed by Wiegel and led Borgman [18] to develop his linear spectral model. It is possible that an adjustment of the force coefficients could bring these predicted pressure force spectra into near perfect agreement with the measured pressure force spectra. In any event, it is evident that the force spectra computed from the measured realizations agree very well with the measured force spectra.

Figures 3.27, 3.28, 3.29, and 3.30 demonstrate the pressure force distributions from the following four types of measured and simulated realizations: (1) measured; (2) predicted from filtering the measured sea surface realization; (3) predicted from filtering both the linear and nonlinear simulated realization synthesized from the smoothed measured spectrum; and (4) predicted from filtering both the linear and nonlinear simulated realizations synthesized from the Bretschneider spectrum. Again, the same seed number for the random number generator was used for all simulations. As was noted with the distributions of the random sea surface realizations, the measured pressure force data and the pressure forces computed from simulated realizations agree very well between two normalized standard deviations. The ordinate values in these figures have been normalized by the standard deviation of the realization by the following expression:

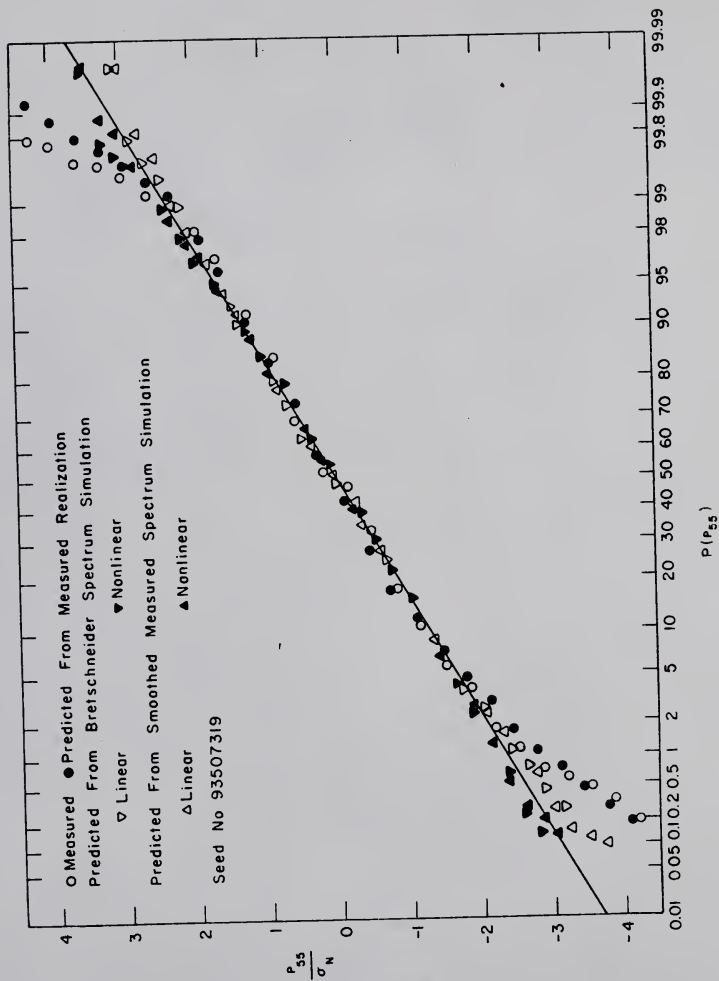


Figure 3.27. Cumulative Probability Distributions of Measured and Predicted Pressure Force Realizations from Record No. 06885/1.

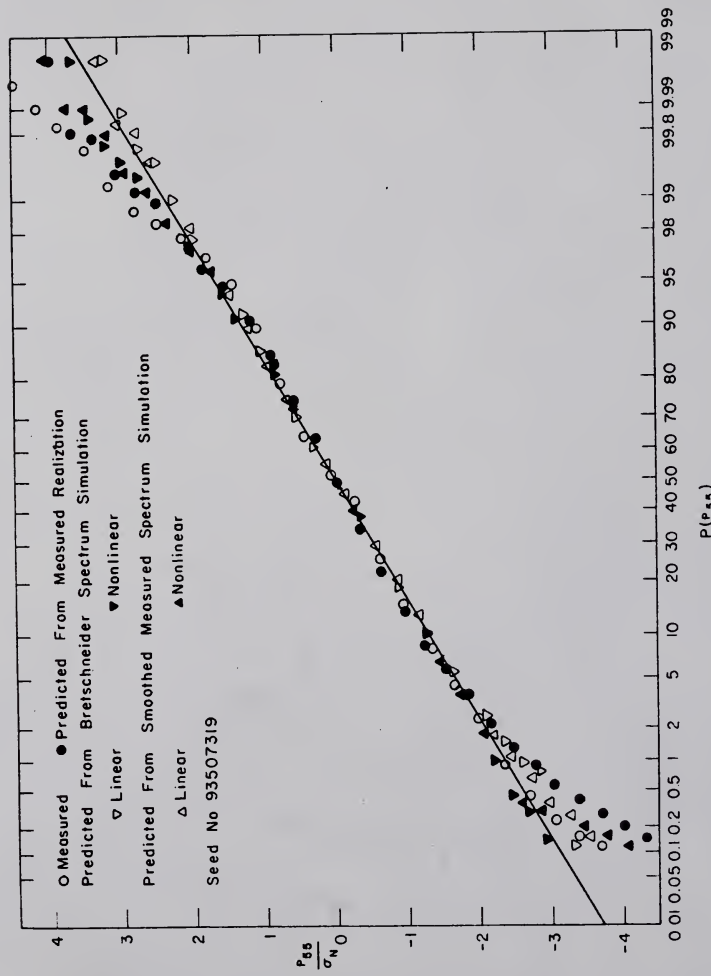


Figure 3.28. Cumulative Probability Distributions of Measured and Predicted Pressure Force Realizations from Record No. 06886/1.

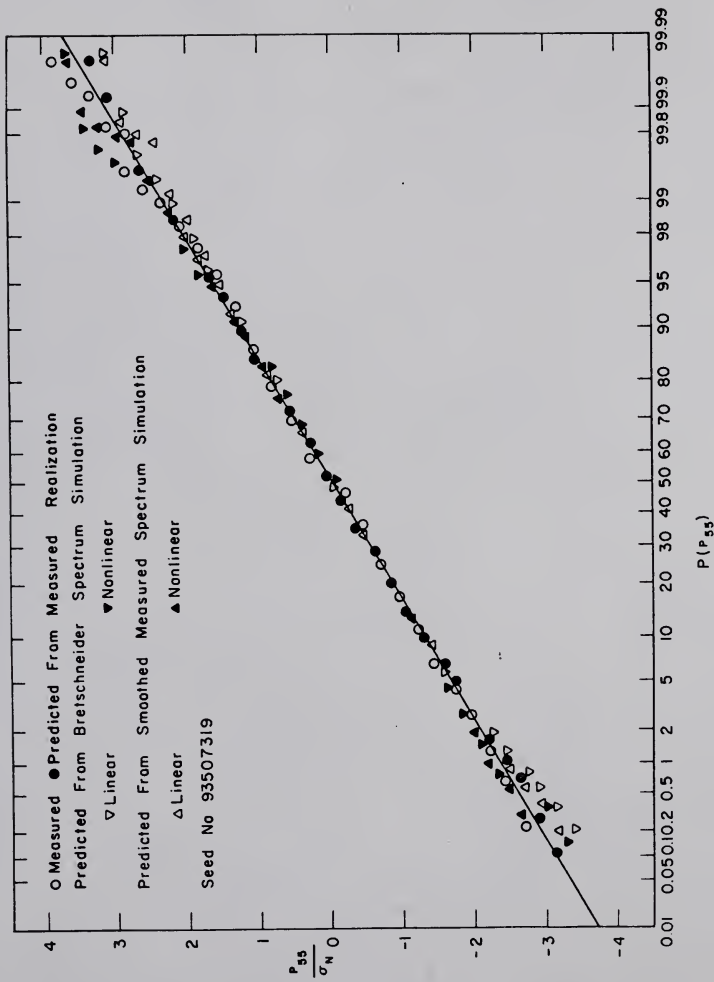


Figure 3.29. Cumulative Probability Distributions of Measured and Predicted pressure Force Realizations from Record No. 06886/2.

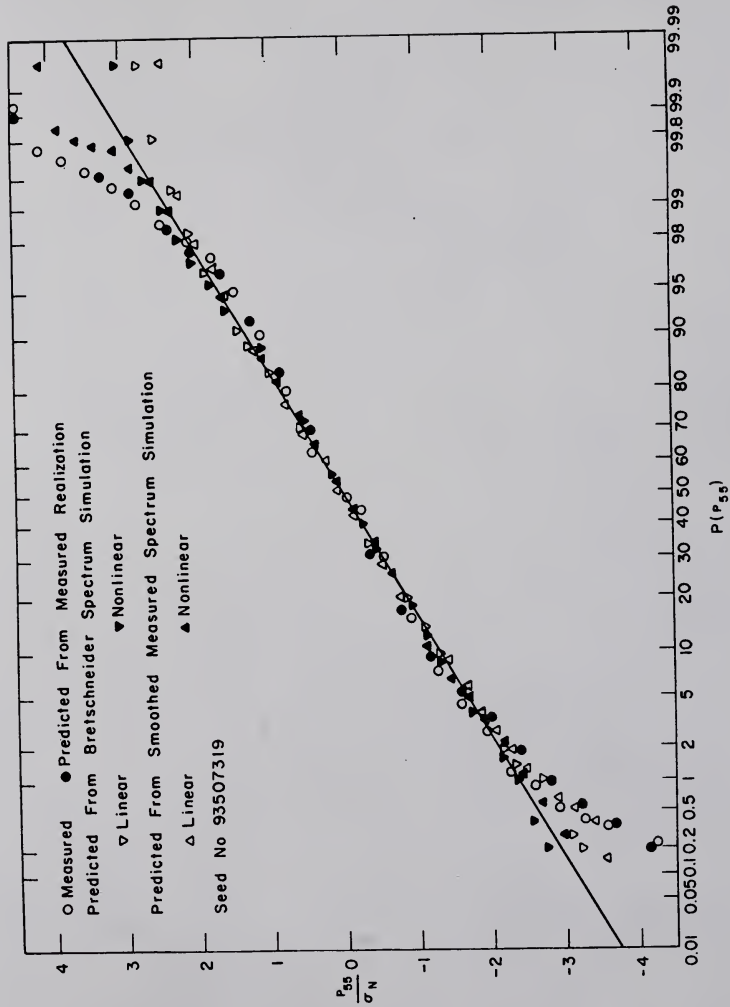


Figure 3.30. Cumulative Probability Distributions of Measured and Predicted Pressure Force Realizations from Record No. 06887/1.

$$P_{55}(i) = \frac{(P_{55})_{\min} + (i-1) \cdot \Delta P_{55}}{\sigma_N} ; \quad i = 1, 2, \dots, 31 \quad (7.1)$$

where $P_{55}(i)$ is the normalized value of the i^{th} discrete cumulative pressure force interval, σ_N is the variance of the measured or simulated pressure force realization at the 55.3 foot dynamometer elevation, and

$$\Delta P_{55} = [(P_{55})_{\max} - (P_{55})_{\min}] / 30 \quad (7.2)$$

where $(P_{55})_{\max}$ is the maximum pressure force and $(P_{55})_{\min}$ is the minimum pressure force measured or predicted at the 55.3 foot dynamometer elevation. The mean of the pressure force time sequence was subtracted from the value of each sequence and the variance was determined from the following:

$$\sigma_N^2 = \frac{1}{(LX-1)} \sum_{n=1}^{LX} [P_{55}(n) - \bar{P}_{55}]^2 \quad (7.3)$$

where \bar{P}_{55} is the mean of the sequence determined from

$$\bar{P}_{55} = \frac{1}{LX} \sum_{n=1}^{LX} P_{55}(n) \quad (7.4)$$

and LX is the total number of values in the random sequence.

Table 3.6 contains the statistical measures from each of the four pressure force time sequences obtained from the four measured records. The skewness of each of the four measured records was less than 0.2. Record No. 06885/1 demonstrates a negative skewness measure for both the sea surface and pressure force realizations. Three of the measured pressure force records demonstrate kurtosis measures greater than 1.40.

Table 3.6

Statistics of Measured and Simulated Pressure Force
Spectra from Hurricane Carla

Record No.	Statistical Measures	Measured Resultant Pressure	Resultant Pressures Computed by Filtering Realizations					
			Measured Realization		Measured Spectrum*		Bretschneider Spectrum*	
			Linear	Nonlinear	Linear	Nonlinear	Linear	Nonlinear
06885/1	Mean	-0.17	-0.53	-0.14	0.03	-0.16	0.03	
	Std. Dev.	14.13	11.39	10.25	10.16	10.60	10.55	
	Skewness	-0.19	-0.41	-0.19	0.12	-0.13	0.16	
	Kurtosis	2.27	1.92	0.14	0.02	0.07	0.03	
06886/1	Mean	0.28	-0.52	-0.28	-0.04	-0.29	-0.04	
	Std. Dev.	16.38	13.42	12.34	12.25	12.56	12.42	
	Skewness	0.19	-0.15	-0.19	0.16	-0.21	0.15	
	Kurtosis	1.44	1.74	0.21	0.12	0.26	0.11	
06886/2	Mean	-0.18	-0.29	-0.16	0.03	-0.17	0.05	
	Std. Dev.	14.37	11.71	11.22	11.15	11.42	11.41	
	Skewness	0.02	-0.08	-0.17	0.13	-0.13	0.21	
	Kurtosis	-0.06	0.14	-0.05	-0.07	0.22	*	0.18
06887/1	Mean	0.90	0.00	-0.39	-0.12	-0.26	-0.05	
	Std. Dev.	14.14	13.73	12.25	12.19	12.49	12.44	
	Skewness	0.01	-0.07	-0.29	0.10	-0.17	0.13	
	Kurtosis	2.14	2.83	0.28	0.50	0.19	0.00	

*Seed number for random number generator = 93507319.

The low negative kurtosis measure came from the relatively narrow band spectrum representing Record No. 06886/2.

Both the skewness and kurtosis measures of the pressure forces computed by filtering the measured sea surface realizations agree favorably with these same measures from the measured pressure force time series. This agreement is another indication of the accuracy of the digital linear filter technique in predicting pressure forces provided the appropriate nonlinear random realization is filtered.

A comparison of the predictions from simulated realizations indicates that the predictions from the linear simulations demonstrate consistently negative skewness measures whose magnitudes were relatively unaffected by the shape of the spectrum used for the simulation. None of the nonlinear predictions demonstrate negative skewness measures. This is another manifestation of the negative bias in the prediction of pressure forces in the trough region of waves which is introduced by the stretching of the vertical coordinate dependent function. Neither the linear nor the nonlinear simulations resulted in pressure force sequences with kurtosis measures greater than 0.50. The low measures of both the skewness and kurtosis indicate that, statistically, the simulated pressure force sequences are almost Gaussian in contrast to the measured values which generally demonstrate low skewness measures but significantly higher than Gaussian kurtosis measures.

Finally, the changes in the standard deviation and kurtosis resulting from the transformations from the linear to nonlinear realizations were, with one exception, negative while the changes in the skewness were consistently positive.

CHAPTER 4

CONCLUSIONS AND RECOMMENDATIONS

1. Random Sea Simulations Correct to Second Perturbation Order

The nonlinear boundary value problem which describes the propagation of irregular random surface gravity waves in water of finite depth has been solved correct to second perturbation order. The expansion of the random velocity potential in a perturbation power series was assumed to be valid for both continuous and discrete spectra. The linear first order solution was determined from a well posed Sturm-Liouville problem in the vertical coordinate which resulted from the separation of variables in a rectangular cartesian coordinate system. The homogeneous Neumann-type bottom boundary condition (BBC) and homogeneous mixed boundary condition representing the combined free surface boundary condition (CFSBC) resulted in a deterministic eigenvalue problem from the linear spectral operator which is unique to within an arbitrary multiplicative constant.

The second order solution was found to be a function of the linear solution through the combined free surface boundary condition. The separation constant for the second order solution was found to be the sums and differences of the linear

eigenvalue spectrum. The spectral operator for the second order solution was computed and was found to be nonsingular. The trivariate function was shown to be the best measure of the second order correction to the linear solution. The coarse measure of the trivariate function, the skewness, was used to determine the measure of the second order corrections as well as the non-Gaussian nature of the linear simulation. Recognizing that the second statistical moment is not closed to the second perturbation order, the second order spectrum was computed and found to be the convolution of first order Gaussian spectral densities. This important result for a linear Gaussian first order spectrum has been given by Tick [123] and Longuet-Higgins [79].

Random realizations of four measured hurricane wave records were simulated correct to second order. Each of the four measured records was simulated using the smoothed measured spectrum and the Bretschneider spectrum with an equivalent variance and best least-squares fit to the peak frequency. Three linear and three nonlinear random realizations for each measured hurricane record were simulated from both the smoothed measured spectrum and the Bretschneider spectrum. The root-mean-square error between the measured and Bretschneider spectra were lowest for three relatively broad spectra and was the highest for the one relatively narrow spectrum.

Each of the linear realizations was found to be slightly non-Gaussian. Each of the second perturbation order

realizations made a positive contribution to the linear skewness measures. The cumulative probability distributions from the simulations demonstrated good agreement with both the measured distributions and a Gaussian distribution with the same mean and variance within two standard deviations. Outside of two standard deviations, the agreement varied considerably. The largest value of the nonlinear realizations were approximately 0.5 to 2.0 standard deviations greater than the corresponding largest values from the linear simulations. Distributions of realizations synthesized from the smoothed measured spectra demonstrated the same variability outside two standard deviations as distributions of realizations synthesized from the Bretschneider spectra. This indicates the importance of the random phase angles in the distributions of random surface gravity waves and the importance of outlier spectral components in nonlinear interactions.

In general, the distributions of nonlinear realizations from the Bretschneider spectrum were as good as those from the smoothed measured spectrum and indicates that it is valid for design use in simulating nonlinear hurricane waves correct to second order.

2. Wave Induced Pressure Forces on a Vertical Piling Computed by Digital Linear Filter with "Stretched" Vertical Coordinate

Three different types of random realizations were used as inputs to the digital linear filter technique to predict the kinematics required to estimate pressure forces using the

Morison equation. The three types of realizations were: (1) the measured sea surface realization; (2) the linear and nonlinear realizations simulated from the smoothed measured spectra; and (3) the linear and nonlinear realizations simulated from the Bretschneider spectra having an equivalent variance and best least-squares fit to the smoothed measured spectra. None of the values of the root-mean-square pressure from the three predicted pressure force realizations were equal to or exceed the measured pressure force values. The predicted pressure force sequences computed from the measured sea surface realizations using the modified Dean and Aagaard force coefficients always yielded the highest predicted root-mean-square pressures and demonstrated a spectral shape which approximated very closely that of the measured pressure force spectra. This indicates that the digital linear filter technique is appropriate for analysis and design for waves with amplitudes that are at least one-half the breaking amplitude provided the appropriate random realization is filtered.

The realizations simulated from the Bretschneider spectrum using only one seed number for the random number generator consistently yielded root-mean-square pressure forces which were slightly higher than those realized from the smoothed measured spectra. The skewness of the pressure force sequence computed from the linear realizations from both the smoothed measured and Bretschneider spectra were consistently negative. This negative bias is the result of the vertical coordinate stretching function. The skewness

measure of the pressure force sequence computed from the nonlinear realizations from both spectra were consistently slightly positive. This indicates that the positive skewness of nonlinear sea surface realizations tends to compensate for the negative skewness introduced by the vertical coordinate stretching function. Pressure force simulations using the digital linear filter in conjunction with the vertical coordinate stretching function should be obtained from nonlinear realizations with a positive skewness measure in order to ensure that the pressure force sequences are not negatively biased.

Three of the measured pressure force sequences demonstrated slightly positive skewness measures. The one sequence with a slightly negative pressure force skewness measure was obtained from a record with a slightly negatively skewed sea surface realization. Although the skewness measure should theoretically be positive for slightly non-Gaussian processes, the sign of the skewness of the measured pressure force sequence corresponded to the sign of skewness of the measured sea surface realization.

The kurtosis of the measured pressure force sequences from the relatively narrow band Record No. 06886/2 was found to be platykurtic (i.e., $K < 3$), while the three measured pressure force time sequences were found to be leptokurtic (i.e., $K > 3$). The measured pressure force sequences were found to be nearly Gaussian between two standard deviations as were the sea surface simulations. The simulated pressure

forces synthesized from the two types of spectra were found to agree with the measured pressure force realizations between two standard deviations. For values outside two standard deviations, the agreement varied considerably.

3. Recommendations for Additional Applications

Chu and Mei [35,36] have shown that the application of the method of multiple scales (cf. Neyfeh [95]) to slowly varying Stokes waves introduces a correction to the dispersion equation (and, therefore, to the eigenvalues) at second order in the perturbation expansions. The extension of the nonlinearization procedure for simulating nonlinear random waves by the application of the method of multiple scales to a spectrum of random waves would offer the advantage of introducing a nonlinear correction to the second order interaction matrix through the second order corrections to the eigenvalues. The extension would be more complicated since the nonlinear boundary value problem would have to be solved correct to third order (cf. Chu and Mei [35,36]). In addition, the spectral amplitudes and phases would become slowly varying functions of time and, consequently, nonstationary. Nonstationary spectral analyses involve more complex evolutionary spectral techniques (cf. Brown [31]).

Hasselmann [60] has developed a general solution for the nonlinear interaction of shear currents and surface gravity waves. This general solution assumes that the fluid is

inviscid and that the velocity field may be decomposed into rotational and irrotational components. The vertical vorticity distribution is expanded in a complete orthonormal set over the finite depth, h , given, e.g., by the following series:

$$\phi_r = \sqrt{\frac{2}{h}} \sum_n A_n \cdot f(t) \cdot \sin\left\{\frac{2n\pi}{h}(h+z)\right\} \exp i\{\vec{k} \cdot \vec{x}\} \quad (3.1)$$

The modifications of the Bernoulli equation due to the presence of the shear current are given by Hasselmann in Appendix C to [60]. In addition, the Eulerian equations for nonlinear gravity waves-shear current perturbations are reduced to the general Hamiltonian equations by Hasselmann [60] and some of the difficulties encountered in applications are discussed. The nonlinearization procedure developed in this study could be extended to include shear currents by this method but the algebraic details may prove to be quite complex.

The stretching function utilized to evaluate the horizontal kinematic fields introduced a negative bias compared to values computed from the unmodified linear theory velocity potential. Alternate stretching functions should be investigated and compared with the kinematic field values predicted for vertical elevations above the mean sea level computed by a Taylor series expansion similar to the method described by Reid [106].

The "peak enhancement factor" (cf. Hasselmann et al. [62]) was not employed for the random simulations synthesized from the Bretschneider spectrum. The application of this factor would be of value in realizing larger nonlinear self-

interaction contributions from the enhanced spectral amplitudes near the peak frequency of the spectrum compared to the nonlinear self-interaction contributions from a Bretschneider spectrum having equal variance. The application of the peak enhancement factor results in transforming the Bretschneider spectrum from a two-parameter spectrum to a five-parameter spectrum. The correlation of these five parameters with parameters measurable from measured spectra has not been completed (cf. Hasselmann *et al.* [62]). The transformation to a five-parameter spectral representation still results in a smoothly continuous spectrum from which outlier spectral estimates which are capable of large self-interaction contributions have been effaced.

Finally, Green's functions have been extremely useful in determining pressure forces on fixed and floating obstacles for the linear deterministic boundary value problem (cf. Hildebrand [65] and Wehausen [127]). Free space Green's functions have also been useful in evaluating wave propagation problems for random boundary value problems (cf. Boyce [26] and Frisch [51]). The random linear velocity potential may be expressed as a spatial integral over the boundaries with the Green's function as the resolvent kernel of the integral. If this linear integral solution could be successfully employed in the inhomogeneous forcing terms of the second order combined free surface boundary condition, the result would be an extension of the Green's function to second order and would be extremely useful in radiation, scattering and diffraction problems.

APPENDIX A
THE FOUR-PRODUCT MOMENT FOR A GAUSSIAN VARIATE

The factoring of the fourth order statistical moment of a jointly normal Gaussian variate was used by Tipp [123] and Longuet-Higgins [79] to obtain irreducible products of covariances. Parzen [98; p. 93] and Middleton [88; p. 343] give different methods for obtaining this important and useful result. The derivation given below is included for convenience.

The four-product moment of the four random variables z_1 , z_2 , z_3 , and z_4 is to be evaluated from the following expression:

$$\begin{aligned} E\{z_1 z_2 z_3 z_4\} = & E\{z_1 z_2\} \cdot E\{z_3 z_4\} + E\{z_1 z_3\} \cdot E\{z_2 z_4\} + \\ & + E\{z_1 z_4\} \cdot E\{z_2 z_3\} \end{aligned} \quad (\text{A.1})$$

Consider the random variable Z as a four-element column vector given by

$$Z = \begin{pmatrix} z_1 \\ z_2 \\ z_3 \\ z_4 \end{pmatrix} \quad (\text{A.2})$$

with vector matrix transpose given by

$$Z^T = [z_1, z_2, z_3, z_4] \quad (\text{A.3})$$

and with zero mean

$$E\{Z\} = 0 \quad (A.4)$$

The characteristic function, $\phi(u)$, is the Fourier-Stieltjes transform of the distribution function of the random variable, i.e.,

$$\begin{aligned}\phi_Z(u) &= \int_{-\infty}^{\infty} \exp i\{u^T z\} dP(z) \\ \phi_Z(u) &= E\{\exp i\{u^T Z\}\} \\ \phi_Z(u) &= \exp\{-\frac{1}{2} u^T P_Z u\}\end{aligned} \quad (A.5)$$

where P_Z is the covariance matrix

$$P_Z = E\{ZZ^T\}$$

$$P_Z = \begin{pmatrix} E\{Z_1 Z_1\} & E\{Z_2 Z_1\} & E\{Z_3 Z_1\} & E\{Z_4 Z_1\} \\ E\{Z_1 Z_2\} & E\{Z_2 Z_2\} & E\{Z_3 Z_2\} & E\{Z_4 Z_2\} \\ E\{Z_1 Z_3\} & E\{Z_2 Z_3\} & E\{Z_3 Z_3\} & E\{Z_4 Z_3\} \\ E\{Z_1 Z_4\} & E\{Z_2 Z_4\} & E\{Z_3 Z_4\} & E\{Z_4 Z_4\} \end{pmatrix} \quad (A.6)$$

Upon carrying out the matrix multiplication, the following result is obtained:

$$\phi(u_1, u_2, u_3, u_4) = \exp\{-\frac{1}{2} \sum_{i=1}^4 \sum_{j=1}^4 u_i u_j E\{Z_i Z_j\}\} \quad (A.7)$$

The four-product moment may be computed by differentiating the characteristic function with respect to its four arguments and evaluating the result with the argument set equal to zero, i.e.,

$$\mathbb{E}\{z_1 z_2 z_3 z_4\} = \frac{\partial^4}{\partial u_1 \partial u_2 \partial u_3 \partial u_4} \phi_{z_1, z_2, z_3, z_4}^{(0, 0, 0, 0)} \quad (\text{A.8})$$

Note that, in general,

$$\frac{\partial \phi(u_\ell=0)}{\partial u_\ell} = - \sum_{i \neq \ell} u_i \mathbb{E}\{z_\ell z_i\} \quad (\text{A.9a})$$

so that

$$\frac{\partial \phi(0, u_2, u_3, u_4)}{\partial u_1} = - \sum_{\ell=2}^4 u_\ell \cdot \mathbb{E}\{z_1 \cdot z_\ell\} \cdot \phi(0, u_2, u_3, u_4) \quad (\text{A.9b})$$

$$\frac{\partial^2 \phi(0, 0, u_3, u_4)}{\partial u_1 \partial u_2} = [-\mathbb{E}\{z_1 z_2\} + \sum_{\ell=3}^4 u_\ell \mathbb{E}\{z_2 z_\ell\} \cdot \sum_{k=3}^4 u_k \mathbb{E}\{z_1 z_k\}] \cdot$$

$$\cdot \phi(0, 0, u_3, u_4) \quad (\text{A.9c})$$

$$z_1, z_2, z_3, z_4$$

$$\frac{\partial^3 \phi(0, 0, 0, u_4)}{\partial u_1 \partial u_2 \partial u_3} = \left(\begin{array}{l} u_4 \mathbb{E}\{z_1 z_2\} \cdot \mathbb{E}\{z_3 z_4\} + u_4 \mathbb{E}\{z_2 z_3\} \mathbb{E}\{z_1 z_4\} \\ + u_4 \mathbb{E}\{z_2 z_4\} \cdot \mathbb{E}\{z_1 z_3\} - u_4^3 \mathbb{E}\{z_2 z_4\} \cdot \mathbb{E}\{z_1 z_4\} \cdot \mathbb{E}\{z_3 z_4\} \end{array} \right).$$

$$\cdot \phi(0, 0, 0, u_4) \quad (\text{A.9d})$$

$$z_1, z_2, z_3, z_4$$

$$\frac{\partial^4 \phi(0, 0, 0, 0)}{\partial u_1 \partial u_2 \partial u_3 \partial u_4} = \mathbb{E}\{z_1 z_2\} \cdot \mathbb{E}\{z_3 z_4\} + \mathbb{E}\{z_2 z_3\} \cdot \mathbb{E}\{z_1 z_4\} +$$

$$+ \mathbb{E}\{z_2 z_4\} \cdot \mathbb{E}\{z_1 z_3\} \quad (\text{A.9e})$$

which is the desired formula. The vanishing of the three-product moment for a Gaussian variate may be obtained from Eq. (A.9d) by setting $u_4 \equiv 0$.

APPENDIX B

ALTERNATE QUADRATIC FILTER

The realizations correct to second perturbation order shown in the figures in Chapter 3 were synthesized from a convolution and linear summation in the frequency domain in order to exploit the spectral representation of differential operators of the perturbed set of linear problems by means of the fast Fourier transform.

The general applications of nonlinear filtering methods in the time domain for frequency modulated problems have been given by Wiener [132]. A discussion relating to the general quadratic filtering problem was given by Tick [124]. The application to the simulation of nonlinear random surface gravity waves by a quadratic filter which is derived in this appendix was suggested by Borgman [25].

The time series realization for the sea surface may be expressed by the following:

$$\eta(t) = h_0 + \int_{-\infty}^{\infty} h_1(\tau) \cdot \zeta(t-\tau) d\tau + \iint_{-\infty}^{\infty} h_2(\tau_1, \tau_2) \cdot \\ \cdot \eta(t-\tau_1) \cdot \eta(t-\tau_2) d\tau_1 d\tau_2 \quad (B.1)$$

where $\zeta(t-\tau)$ is a Gaussian white noise process such that

$$\zeta(t) \sim N(0, 1) \quad (B.2)$$

and 1^n is the first order realization given by the first integral. The value of the zeroeth order kernel, h_0 , is determined by requiring that the process have zero mean, i.e.,

$$\begin{aligned} E\{\eta(t)\} &= h_0 + \int_{-\infty}^{\infty} h_1(\tau) \cdot E\{\zeta(t-\tau)\} d\tau + \iint_{-\infty}^{\infty} h_2(\tau_1, \tau_2) \cdot \\ &\quad \cdot E\{1^n(t-\tau_1) \cdot 1^n(t-\tau_2)\} d\tau_1 d\tau_2 \\ &= 0 \end{aligned} \quad (\text{B.3})$$

which reduces to

$$h_0 = - \int_{-\infty}^{\infty} d\tau_1 \int_{-\infty}^{\infty} h_2(\tau_1, \tau_2) \cdot \gamma(\tau_1 - \tau_2) d\tau_2 \quad (\text{B.4})$$

$$1^n 1^n$$

by virtue of Eq. (B.2).

The first order kernel is the impulse response function of the deterministic spectral representation given by

$$h_1(\tau) = 2\pi \sum_{m=-M}^{M} C_m \delta(\tau - m\tau_0) \quad (\text{B.5})$$

where the Fourier coefficients are determined from

$$C_m = \frac{1}{\pi} \int_0^{\sigma_c} \sqrt{S(\sigma)} \Delta\sigma \cdot \exp i\{m\sigma\tau_0\} d\sigma \quad (\text{B.6})$$

and σ_c is the cut-off frequency.

The second order kernel requires a double Dirac delta comb and is given by

$$h_2(\tau_1, \tau_2) = 4\pi^2 \sum_{n=-M}^{M} \sum_{m=-M}^{M} C_{n,m} \delta(\tau_1 - n\tau_0) \cdot \delta(\tau_2 - m\tau_0) \quad (\text{B.7})$$

where the Fourier coefficients are determined by

$$C_{n,m} = \frac{1}{\pi^2} \int\limits_0^{\sigma_c} \int\limits_0^{\sigma_c} H(\sigma_1, \sigma_2) \cdot \exp i\{n\sigma_1 \tau_o + m\sigma_2 \tau_o\} d\sigma_1 d\sigma_2 \quad (B.8)$$

Substituting the appropriate impulse response functions, the random sea realization correct to second perturbation order becomes:

$$\begin{aligned} \eta(t) = & 2\pi \sum_{m=-M}^M C_m \cdot \int_{-\infty}^{\infty} \zeta(t-\tau) \cdot \delta[\tau - m\tau_o] d\tau + \\ & + 4\pi^2 \sum_{n=-M}^M \sum_{m=-M}^M C_{n,m} \int_{-\infty}^{\infty} \int_1^n \eta(t-\tau_1) \cdot \eta(t-\tau_2) \cdot \delta[\tau_1 - n\tau_o] \cdot \\ & \cdot \delta[\tau_2 - m\tau_o] d\tau_1 d\tau_2 \end{aligned} \quad (B.9)$$

The convolution given by Eq. (B.9) may now be computed in the time domain from the appropriate known Fourier series expansions of the energy density spectrum and the nonlinear interaction kernel derived in Section 4, Chapter 2. The linear first order realization given by the first integral in Eq. (B.9) must be evaluated first and then the convolution of this realization with the Fourier coefficients representing nonlinear interaction matrix is computed and the two time series added in accordance with Eq. (B.9).

APPENDIX C

EFFECT OF THE HORIZONTAL SPATIAL SEPARATION BETWEEN WAVE STAFF AND INSTRUMENTED PILING ON THE EVALUATION OF PRESSURE FORCE COEFFICIENTS

The effect of the horizontal spatial separation between a wave staff and an instrumented platform piling on the evaluation of pressure force coefficients by a regression of the measured and predicted values can be most significant.

Figure C.1 indicates the geometry for the wave staff and instrumented piling for the Wave Project II data acquisition system. The coordinate axes are aligned with the platform. The measured force may be expressed by the Morison equation as

$$F_m = K_D \cdot u |u| + K_I \cdot u_t \quad (C.1)$$

where K_D is a constant representing the drag coefficient sea water density, and piling geometry and K_I is an inertia constant representing the inertia coefficient and sea water density, and piling geometry. The predicted pressure force may also be given by the Morison equation as follows:

$$F_p = K'_D \cdot u' |u'| + K'_I u'_t \quad (C.2)$$

Assuming that kinematics from linear wave theory are approximately correct, the horizontal velocity and acceleration for

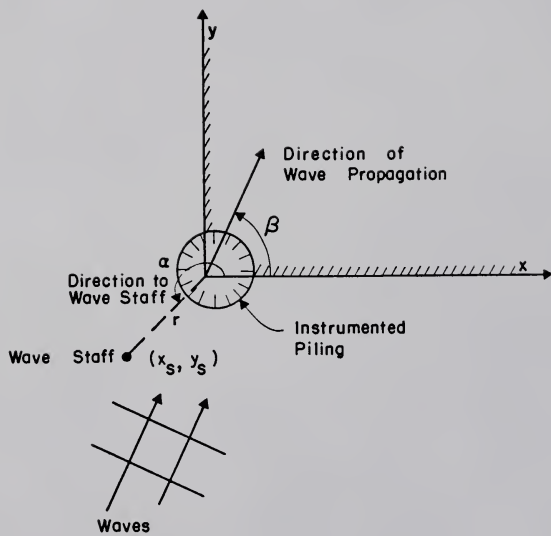


Figure C.1. Orientation of Wave Staff and Instrumented Piling for Wave Project II.

the measured force are

$$u = \sqrt{A_z} \cdot \cos\{\sigma t\} \quad (\text{C.3a})$$

$$u_t = -\sqrt{A_z} \cdot \sin\{\sigma t\} \quad (\text{C.3b})$$

and for the predicted force are

$$u' = \sqrt{A_z} \cdot \cos\{\sigma t - (k_x \cdot x_s + k_y \cdot y_s)\} \quad (\text{C.4a})$$

$$u'_t = -\sqrt{A_z} \cdot \sin\{\sigma t - (k_x \cdot x_s + k_y \cdot y_s)\} \quad (\text{C.4b})$$

where x_s, y_s are the coordinates of the wave staff, k_x, k_y are the wave numbers referenced to the platform coordinates, and $\sqrt{A_z}, \sqrt{A_z}$ are functions of the vertical coordinate along the pile and the wave amplitude.

The spatial phase shift may be related to the angular frequency through the orthogonal components of the wave celerity referenced to the platform coordinate system to yield

$$k_x \cdot x_s + k_y \cdot y_s = \sigma \cdot \left\{ \frac{x_s}{C_x} + \frac{y_s}{C_y} \right\} = \sigma \cdot t' \quad (\text{C.5})$$

The square of the error between the measured and predicted forces during the passage of a wave crest may be expressed by

$$\epsilon^2 = \int_{-T/4}^{T/4} \{F_m - F_p\}^2 dt \quad (\text{C.6})$$

The presence of the absolute value of the horizontal velocity in the drag force term requires that the integral be decomposed into two intervals according to the value of the sign

of the trigonometric term containing the phase shifted argument. The cosine becomes negative when

$$t-t' < -T/4 \quad \text{for } t \geq -T/4 \quad (\text{C.7})$$

and becomes positive when

$$t-t' > -T/4 \quad \text{for } t \leq T/4 \quad (\text{C.8})$$

Therefore, the integral in Eq. (C.6) may be decomposed into the following two integrals:

$$\begin{aligned} \epsilon^2 = & \int_{-T/4}^{-T/4+t'} \{-K_D \cdot A_z \cos^2(\sigma t) - K_I \sqrt{A_z} \sin(\sigma t) - \\ & [-K_D' A_z \cos^2\{\sigma(t-t')\} - K_I' \sqrt{A_z} \sin\{\sigma(t-t')\}]\}^2 dt + \\ & \int_{-T/4+t'}^{T/4} \{K_D \cdot A_z \cos^2(\sigma t) - K_I \sqrt{A_z} \sin(\sigma t) - \\ & [K_D' A_z \cos^2\{\sigma(t-t')\} - K_I' \sqrt{A_z} \sin\{\sigma(t-t')\}]\}^2 dt \end{aligned} \quad (\text{C.9})$$

Equation (C.9) is to be minimized with respect to the unknown force constants, K_D' and K_I' . Differentiating Eq. (C.9) first with respect to the drag coefficient, K_D' , and then with respect to the inertia coefficient, K_I' , and equating each result to zero yields the following two equations:

$$\begin{aligned} & \int_{-T/4}^{-T/4+t'} [-K_D \cdot A_z \cdot \cos^2(\sigma t) - K_I \cdot \sqrt{A_z} \cdot \sin(\sigma t) + K_D' \cdot A_z \cdot \cos^2\{\sigma(t-t')\} + \\ & + K_I' \cdot \sqrt{A_z} \cdot \sin\{\sigma(t-t')\}] \cdot \cos^2\{\sigma(t-t')\} dt + \\ & + \int_{-T/4+t'}^{T/4} \left[\begin{array}{l} K_D \cdot A_z \cdot \cos^2(\sigma t) - K_I \cdot \sqrt{A_z} \cdot \sin(\sigma t) \\ - K_D' \cdot A_z \cdot \cos^2\{\sigma(t-t')\} + K_I' \cdot \sqrt{A_z} \cdot \sin\{\sigma(t-t')\} \end{array} \right] \cdot \\ & \cdot \cos^2\{\sigma(t-t')\} dt = 0 \end{aligned} \quad (\text{C.10a})$$

$$\begin{aligned}
 & -T/4 + t' \left[-K_D \cdot A_z \cdot \cos^2(\sigma t) - K_I \cdot \sqrt{A_z} \cdot \sin(\sigma t) \right] \\
 & -T/4 \left[+K'_D \cdot A_z \cdot \cos^2\{\sigma(t-t')\} + K'_I \cdot \sqrt{A_z} \cdot \sin\{\sigma(t-t')\} \right] \cdot \sin\{\sigma(t-t')\} dt \\
 & + \frac{T/4}{-T/4 + t'} \left[K_D \cdot A_z \cdot \cos^2(\sigma t) - K_I \cdot \sqrt{A_z} \cdot \sin(\sigma t) \right] \\
 & -T/4 + t' \left[-K'_D \cdot A_z \cdot \cos^2\{\sigma(t-t')\} + K'_I \cdot \sqrt{A_z} \cdot \sin\{\sigma(t-t')\} \right] \\
 & \cdot \sin\{\sigma(t-t')\} dt = 0 \tag{C.10b}
 \end{aligned}$$

Define the following ratios:

$$\frac{K'_I \cdot \sqrt{A_z}}{K_D \cdot A_z} = \frac{P_I}{P_D} \tag{C.11a}$$

$$\frac{K'_I \cdot \sqrt{A_z}}{K_I \cdot \sqrt{A_z}} = \frac{C'_I}{C_I} \tag{C.11b}$$

$$\frac{K'_D \cdot A_z}{K_D \cdot A_z} = \frac{C'_D}{C_D} \tag{C.11c}$$

After very tedious algebra, the following dimensionless ratio between the computed drag coefficient, C'_D , and the actual drag coefficient may be determined:

$$\begin{aligned}
 \frac{C'_D}{C_D} &= \frac{4}{3\pi} \left\{ \frac{\pi}{2} + \frac{3}{4} \sin\{2\sigma t'\} - \sigma t' - \left[\frac{\sigma t'}{2} - \frac{\pi}{4} \right] \cos(2\sigma t') \right\} + \\
 &+ \frac{|P_I|}{|P_D|} \cdot \frac{32}{9\pi} \sin(\sigma t') \tag{C.12}
 \end{aligned}$$

and the dimensionless ratio between the computed inertia coefficient, C'_I , and the actual inertia coefficient is

$$\frac{C'_I}{C_I} = \cos(\sigma t') - \frac{|P_D|}{|P_I|} \cdot \frac{4}{3\pi} \{ \sin(\sigma t') + 2 \sin(2\sigma t') \} \tag{C.13}$$

For very small separation distances compared to wave period, the following asymptotic values are easily found:

$$\frac{C_D'}{C_D} = 1 + \frac{32}{9\pi} (\sigma t') \frac{|P_I|}{|P_D|} \quad (C.14a)$$

$$\frac{C_I'}{C_I} = 1 - \frac{20}{3\pi} (\sigma t') \frac{|P_D|}{|P_I|} \quad (C.14b)$$

From Fig. C.1, the following identity is obtained:

$$\begin{aligned} \sigma t' &= k_x \cdot x_s + k_y \cdot y_s \\ &= k \cdot \cos \beta \cdot r \cdot \cos \alpha + k \cdot \sin \beta \cdot r \cdot \sin \alpha \\ &= kr \cos(\beta - \alpha) \end{aligned} \quad (C.15)$$

Figures C.2 and C.3 give values of dimensionless drag and inertia coefficient ratios as a function of $\sigma t'$ in terms of the following dimensionless distance for various ratios of drag and inertia pressure force:

$$\frac{r'}{L} = \frac{2\pi}{L} \cdot r \cdot \cos(\beta - \alpha) \quad (C.16)$$

where L is the wave length determined from linear theory.

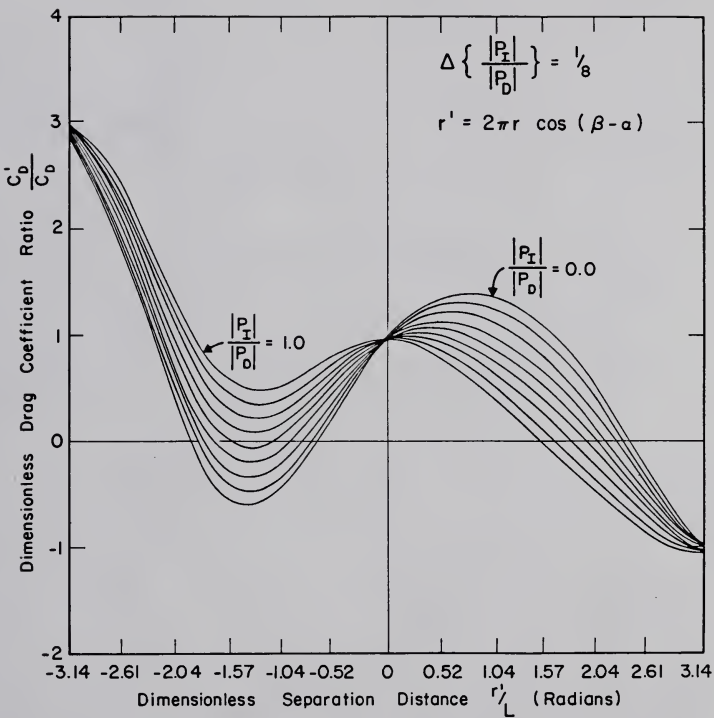


Figure C.2. Effect of Dimensionless Wave Staff-Instrumented Piling Separation Distance on Drag Coefficients Determined from Morison Equation with Linear Theory Kinematics (L = linear theory wavelength).

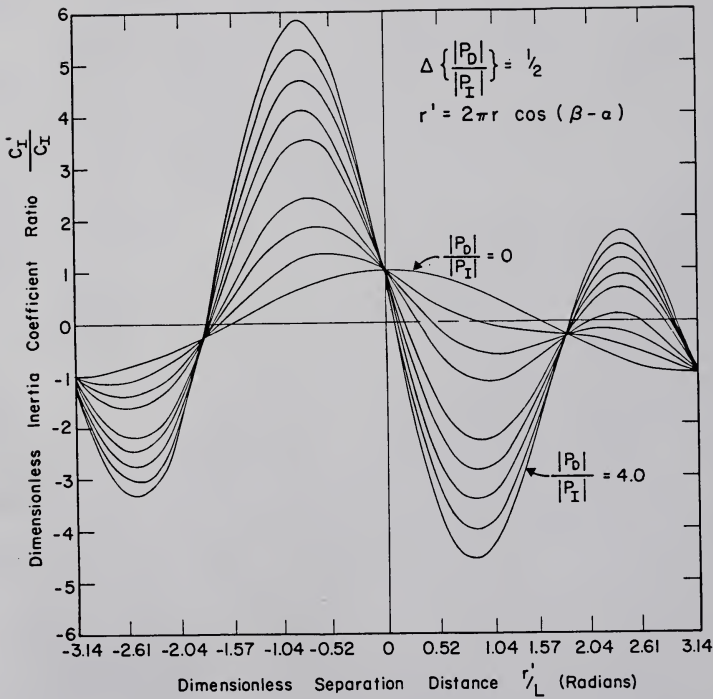


Figure C.3. Effect of Dimensionless Wave Staff-Instrumented Piling Separation Distance on Inertia Coefficients Determined from Morison Equation with Linear Theory Kinematics (L = linear theory wavelength).

LIST OF REFERENCES

1. Ablowitz, M.J. and Benney, D.J., "The Evolution of Multi-Phase Modes for Nonlinear Dispersive Waves," Studies Applied Math., Vol. XLIX, No. 3, Sept. 1970, pp. 225-238.
2. Ablowitz, M.J., "Applications of Slowly Varying Non-linear Dispersive Wave Theories," Studies Applied Math., Vol. L, No. 4, Dec. 1971, pp. 329-344.
3. Bartlett, M.S., Stochastic Processes, Cambridge, England: University Press, 1966.
4. Batchelor, G.K., The Theory of Homogeneous Turbulence, Cambridge, England: University Press, 1953.
5. Bendat, J.S., Principles and Applications of Random Noise Theory, New York: John Wiley and Sons, Inc., 1958.
6. Bendat, J.S. and Piersol, A.G., Measurement and Analysis of Random Data, New York: John Wiley and Sons, Inc., 1966.
7. Benney, D.J. and Saffman, P.G., "Nonlinear Interactions of Random Waves in a Dispersive Medium," Proc. Roy. Soc. London, A, Vol. 289, 1966, pp. 301-320.
8. Benney, D.J., "The Asymptotic Behavior of Nonlinear Dispersive Waves," J. Math. and Phys., Vol. LXVI, No. 2, June 1967, pp. 115-132.
9. Benney, D.J. and Newell, A.C., "The Propagation of Non-linear Wave Envelopes," J. Math. and Phys., Vol. XLVI, No. 2, June 1967, pp. 133-139.
10. Benney, D.J. and Newell, A.C., "Sequential Time Closures for Interacting Random Waves," J. Math. and Phys., Vol. XLVI, No. 4, Dec., 1967, pp. 363-393.
11. Benney, D.J. and Newell, A.C., "Random Wave Closures," Studies Applied Math., Vol. XLVIII, No. 1, March 1969, pp. 29-53.

12. Berge, B. and Penzien, J., "Three-Dimensional Stochastic Response of Offshore Towers to Wave Forces," Preprints 1974 Offshore Technology Conf., Vol. II, Paper No. OTC2050, May 6-8, 1974, pp. 173-190.
13. Bharuchua-Reid, A.T., Random Integral Equations, New York: Academic Press, 1972.
14. Birkhoff, G. and Kotik, J., "Fourier Analysis of Wave Trains," Gravity Waves, Nat'l. Bur. Stds., No. 521, 1951, pp. 221-234.
15. Birkhoff, G., Bona, J. and Kampe de Feriet, J., "Statistically Well-Set Cauchy Problems," in Probabilistic Methods in Applied Mathematics, ed. by A.T. Bharuchua-Reid, Vol. 3, New York: Academic Press, 1973, pp. 2-121.
16. Blank, L.S., "Wave Project II Users Guide," Chevron Oil Field Research Co., August 25, 1969.
17. Borgman, L.E., "Wave Forces on Piling for Narrow-Band Spectra," J. Waterways and Harbors Div., Proc. ASCE, Vol. 91, WW3, 1965, pp. 65-90.
18. Borgman, L.E., "Spectral Analysis of Ocean Wave Forces on Piling," J. Waterways and Harbors Div., Proc. ASCE, Vol. 93, WW2, 1967, pp. 126-156.
19. Borgman, L.E., "Directional Spectra Models for Design Use," Preprint First Offshore Technology Conf., Vol. I, Paper No. OTC 1069, May 1969, pp. 721-747.
20. Borgman, L.E., "Ocean Wave Simulation for Engineering Design," J. Waterways and Harbors Div., Proc. ASCE, Vol. 95, WW4, Nov. 1969, pp. 557-583.
21. Borgman, L.E., "Confidence Intervals for Ocean Wave Spectra," Proc. Thirteenth Coast. Engr. Conf., Vol. I, Ch. 10, July 10-14, 1972, pp. 237-250.
22. Borgman, L.E., "Statistical Models for Ocean Wave Forces," in Adv. in Hydrosciences, ed. by V.T. Chow, New York: Academic Press, 1972, pp. 139-181.
23. Borgman, L.E., "Computer Simulation of Multivariate Normal Vectors Applied to the Reliability of Spectral-Based Calculations," Stat. Lab. Report No. 2007, Univ. Wyoming, 1973.
24. Borgman, L.E., "Spectrum Analysis of Random Data," Stat. Lab. Report No. 2008, Univ. Wyoming, 1973.
25. Borgman, L.E., Private communication, 1974.

26. Boyce, W.E., "Random Eigenvalue Problems," in Probabilistic Methods in Applied Mathematics, ed. by A.T. Bharuchua-Reid, New York: Academic Press, 1968, pp. 1-73.
27. Bretschneider, C.L., "A One-Dimensional Gravity Wave Spectrum," in Ocean Wave Spectra, Englewood Cliffs, N.J.: Prentice-Hall, Inc., 1963, pp. 41-56.
28. Bretschneider, C.L., "Wave Generation by Wind, Deep and Shallow Water," in Estuary and Coastline Hydrodynamics, ed. by A.T. Ippen, New York: McGraw-Hill Book Co., Inc., 1966, pp. 133-196.
29. Brillinger, D.R. and Rosenblatt, M., "Asymptotic Theory of Estimates of k^{th} Order Spectra," in Spectral Analysis of Time Series, ed. by B. Harris, New York: John Wiley and Sons, Inc., 1967, pp. 153-188.
30. Brillinger, D.R. and Rosenblatt, M., "Computation and Interpretation of k^{th} Order Spectra," in Spectral Analysis of Time Series, ed. by B. Harris, New York: John Wiley and Sons, Inc., 1967, pp. 189-232.
31. Brown, L.J., "Methods for the Analysis of Non-Stationary Time Series with Applications to Oceanography," Tech. Report HEL 16-3, Hydraulics Engr. Lab., Univ. Calif., May 1967.
32. Cartwright, D.E. and Longuet-Higgins, M.S., "The Statistical Distribution of the Maxima of a Random Function," Proc. Roy. Soc. London, A, Vol. 237, 1956, pp. 212-232.
33. Chakrabarti, S.K., Discussion of "Dynamics of Single Point Mooring in Deep Water," by J.H. Nath and M.P. Felix, J. Waterways and Harbors Div., Proc. ASCE, Vol. 97, WW3, Aug. 1971, pp. 588-590.
34. Chorin, A.J., "Gaussian Fields and Random Flow," J. Fluid Mech., Vol. 63, 1974, pp. 21-32.
35. Chu, V.H. and Mei, C.C., "On Slowly-Varying Stokes Waves," J. Fluid Mech., Vol. 41, 1970, pp. 873-887.
36. Chu, V.H. and Mei, C.C., "The Non-Linear Evolution of Stokes Waves in Deep Water," J. Fluid Mech., Vol. 47, 1971, pp. 337-351.
37. Cooley, J.W. and Tukey, J.W., "An Algorithm for the Machine Calculation of Complex Fourier Series," Math. of Comput., Vol. 19, April 1965, pp. 297-301.
38. Davenport, W.B. and Root, W.L., Random Signals and Noise, New York: McGraw-Hill Book Co., Inc., 1958.

39. Dean, R.G., "Stream Function Representation of Non-linear Ocean Waves," J. Geophys. Res., Vol. 70, No. 18, Sept. 15, 1965, pp. 4561-4572.
40. Dean, R.G., Discussion of "Irregular Wave Forces on a Pile," by W.J. Pierson and P. Holmes, J. Waterways and Harbors Div., Proc. ASCE, Vol. 92, No. WW4, 1966, pp. 37-40.
41. Dean, R.G. and Aagaard, P.M., "Wave Forces: Data Analysis and Engineering Calculation Method," J. Pet. Tech., March 1970, pp. 368-375.
42. De Leonibus, P.S., Simpson, L.W., and Mattie, M.G., "Equilibrium Range in Wave Spectra Observed at an Open Ocean Tower," J. Geophys. Res., Vol. 79, No. 21, July 20, 1974, pp. 3041-3053.
43. Dunford, N. and Schwartz, J.T., Linear Operators Parts I, II, III, New York: Interscience Publishers, Inc., 1963.
44. Edge, B.L. and Meyer, P.G., "A Stochastic Model for the Response of Permanent Offshore Structures Subject to Soil Restraints and Wave Forces," Water Resources Research Center Report No. WRC-0269, Georgia Institute of Technology, 1969.
45. Finkelstein, A.B., "The Initial Value Problem for Transient Water Waves," Comm. Pure and Applied Math., Vol. X, 1957, pp. 511-522.
46. Foster, T., "Model for Nonlinear Dynamics of Offshore Towers," J. Eng. Mech. Div., Proc. ASCE, Vol. 96, No. EM1, 1970, pp. 41-67.
47. Friedman, A. and Shinbrot, M., "The Initial Value Problem for the Linearized Equations of Water Waves I," J. Math. and Mech., Vol. 17, 1967, pp. 107-180.
48. Friedman, A. and Shinbrot, M., "The Initial Value Problem for the Linearized Equations of Water Waves II," J. Math. and Mech., Vol. 18, 1969, pp. 1177-1193.
49. Friedman, B., Principles and Techniques of Applied Mathematics, New York: John Wiley and Sons, Inc., 1956.
50. Friedrichs, K.O., Perturbation of Spectra in Hilbert Space, Providence, Rhode Island: Am. Math. Soc., 1965.
51. Frisch, U., "Wave Propagation in Random Media," in Probabilistic Methods in Applied Mathematics, ed. by A.T. Bharucha-Reid, New York: Academic Press, 1968, pp. 75-198.

52. Garrett, J., "Some Observations on the Equilibrium Region of the Wind-Wave Spectrum," J. Mar. Res., Vol. 27, No. 3, 1969, pp. 273-277.
53. Groves, G.W., "Note on Computation of Ocean Wave Elements by Convolution Methods," J. Geophys. Res., Vol. 65, No. 3, March 1960, pp. 997-1006.
54. Hasselmann, K., "On the Nonlinear Energy Transfer in a Gravity-Wave Spectrum, Part 1, General Theory," J. Fluid Mech., Vol. 12, 1962, pp. 481-500.
55. Hasselmann, K., "On the Nonlinear Energy Transfer in a Gravity-Wave Spectrum, Part 2, Conservation Theorems, Wave-Particle Correspondence, Irreversibility," J. Fluid Mech., Vol. 15, 1963, pp. 273-281.
56. Hasselmann, K., "On the Nonlinear Energy Transfer in a Gravity-Wave Spectrum, Part 3, Computation of the Energy Flux and Swell-Sea Interaction for a Neumann Spectrum," J. Fluid Mech., Vol. 15, 1963, pp. 383-398.
57. Hasselmann, K., Munk, W., and MacDonald, G., "Bispectra of Ocean Waves," in Time Series Analysis, ed. by M. Rosenblatt, New York: John Wiley and Sons, Inc., 1963, pp. 125-140.
58. Hasselmann, K., "On the Nonlinear Energy Transfer in a Wave Spectrum," in Ocean Wave Spectra, Englewood Cliffs, N.J.: Prentice-Hall, Inc., 1963, pp. 191-197.
59. Hasselmann, K., "A Statistical Analysis of the Generation of Microseisms," Rev. Geophys., Vol. 1, No. 2, 1963, pp. 177-210.
60. Hasselmann, K., "Feynman Diagrams and Interaction Rules of Wave-Wave Scattering Processes," Rev. of Geophys., Vol. 4, No. 1, 1966, pp. 1-32.
61. Hasselmann, K., "Nonlinear Interactions Treated by the Methods of Theoretical Physics (with application to the generation of waves by wind)," Proc. Roy. Soc. London, A, Vol. 299, 1967, pp. 77-100.
62. Hasselmann, K., Barnett, T.P., Bouws, E., Carlson, H., Cartwright, D.E., Enke, K., Ewing, J.A., Gienapp, H., Hasselmann, D.E., Kruseman, P., Meerburg, A., Muller, P., Olbers, D.J., Richter, K., Sell, W., and Walden, H., "Measurements of Wind-Wave Growth and Swell Decay During the Joint North Sea Wave Project (JONSWAP)," UDC 551.466.31; ANE German Bight, Deutsches Hydrographisches Institut, Hamburg, Germany, 1973.

63. Haubrich, R.A., "Earth Noise, 5 to 500 Millicycles per Second," J. Geophys. Res., Vol. 70, No. 6, March 15, 1965, pp. 1415-1427.
64. Hildebrand, F.B., Advanced Calculus for Applications, Englewood Cliffs, N.J.: Prentice-Hall, Inc., 1962.
65. Hildebrand, F.B., Methods of Applied Mathematics, Second Ed., Englewood Cliffs, N.J.: Prentice-Hall, Inc., 1965.
66. Hinch, M.J. and Clay, C.S., "The Application of the Discrete Fourier Transform in the Estimation of Power Spectra, Coherence, and Bispectra of Geophysical Data," Rev. of Geophys., Vol. 6, No. 3, Aug. 1968, pp. 347-363.
67. Hudspeth, R.T., Dalrymple, R.A., and Dean, R.G., "Comparison of Wave Forces Computed by Linear and Stream Function Methods," Preprints 1974 Offshore Technology Conf., Vol. II, Paper No. OTC 2037, May 6-8, 1974, pp. 17-32.
68. Jazwinski, A.H., Stochastic Processes and Filtering Theory, New York: Academic Press, 1970.
69. Jenkins, G.M. and Watts, D.C., Spectral Analysis and Its Applications, San Francisco: Holden Day, 1968.
70. Kampe de Feriet, J., "Introduction to the Statistical Theory of Turbulence," J. SIAM, "Part I," Vol. 2, pp. 1-9, "Part II," Vol. 2, pp. 143-174, "Part III," Vol. 2, pp. 244-271, 1954.
71. Kampe de Feriet, J., "Statistical Fluid Mechanics: Two-Dimensional Linear Gravity Waves," in Partial Differential Equations and Continuum Mechanics, ed. by R.E. Langer, Madison, Wis.: University Wisconsin Press, 1961.
72. Kinsman, B., Wind Waves, Englewood Cliffs, N.J.: Prentice-Hall, Inc., 1965.
73. Lanning, J.L. and Battin, R.N., Random Processes in Automatic Control, New York: McGraw-Hill Book Co., Inc., 1956.
74. Le Mehaute, B., An Introduction to Hydrodynamics and Water Waves, Vol. II, ESSA Technical Report, ERL 118-POL 3-2, July 1969.
75. Lighthill, M.J., Introduction to Fourier Analysis and Generalized Functions, Cambridge: University Press, 1958.

76. Long, R.B., "Scattering of Surface Waves by an Irregular Bottom," J. Geophys. Res., Vol. 78, No. 33, Nov. 30, 1973, pp. 7861-7870.
77. Longuet-Higgins, M.S. and Stewart, R.W., "Radiation Stress and Mass Transport in Gravity Waves, with Applications to Surf Beats," J. Fluid Mech., Vol. 13, 1962, pp. 481-504.
78. Longuet-Higgins, M.S., "The Directional Spectrum of Ocean Waves, and Processes of Wave Generation," Proc. Roy. Soc., A, Vol. 265, 1961, pp. 286-315.
79. Longuet-Higgins, M.S., "The Effects of Non-Linearities on Statistical Distributions in Theory of Sea Waves," J. Fluid Mech., Vol. 17, 1963, pp. 459-480.
80. Longuet-Higgins, M.S., "On Wave Breaking and the Equilibrium Spectrum of Wind-Generated Waves," Proc. Roy. Soc., A, Vol. 310, 1969, pp. 151-159.
81. Lumley, J.L., Stochastic Tools in Turbulence, New York: Academic Press, 1970.
82. MacDonald, G.J.F., "The Bispectra of Atmospheric Pressure Records," Proc. IBM Scientific Symp. on Statistics, White Plains, N.Y., 1963, pp. 247-269.
83. Malhotra, A.K. and Penzien, J., "Response of Offshore Structures to Random Wave Forces," J. Structural Div., Proc. ASCE, Vol. 96, No. ST10, 1970, pp. 2155-2173.
84. Malhotra, A.K. and Penzien, J., "Nondeterministic Analysis of Offshore Structures," J. Engr. Mech. Div., Proc. ASCE, Vol. 96, No. EM6, 1970, pp. 985-1003.
85. Mansour, A.E. and Millman, D., "Dynamic Random Analysis of Fixed Offshore Platforms," Preprints 1974 Offshore Technology Conf., Vol. II, Paper No. OTC 2049, May 1974, pp. 157-172.
86. Marguardt, D.W., "An Algorithm for Least-Squares Estimation of Nonlinear Parameters," J. SIAM, Vol. 11, 1963, pp. 431-441.
87. McCalla, T.R., Introduction to Numerical Methods and FORTRAN Programming, New York: John Wiley and Sons, Inc., 1967.
88. Middleton, D., An Introduction to Statistical Communication Theory, New York: McGraw-Hill Book Co., Inc., 1960.

89. Mihram, G.A., Simulation: Statistical Foundations and Methodology, New York: Academic Press, 1972.
90. Muga, B.J., Discussion to "Irregular Wave Forces on a Pile," by W.J. Pierson and P. Holmes, J. Waterways and Harbors Div., Proc. ASCE, Vol. 92, No. WW3, Aug. 1966, pp. 92-93.
91. Muga, B.J., and Wilson, J.F., Dynamic Analysis of Ocean Structures, New York: Plenum Press, 1970.
92. Nath, J.H. and Harleman, D.R.F., "Dynamics of Fixed Towers in Deep-Water Random Waves," J. Waterways and Harbors Div., Proc. ASCE, Vol. 95, No. WW4, Nov. 1969, pp. 539-556.
93. Nath, J.H. and Felix, M.P., Closure to "Dynamics of Single Point Mooring in Deep Water," J. Waterways and Harbors Div., Proc. ASCE, Vol. 98, No. WW2, May 1972, pp. 272-273.
94. Newell, A.C., "The Closure Problem in a System of Random Gravity Waves," Rev. Geophys., Vol. 6, No. 1, Feb. 1968, pp. 1-31.
95. Neyfeh, A.H., Perturbation Methods, New York: John Wiley and Sons, Inc., 1973.
96. Papoulis, A., The Fourier Integral and Its Applications, New York: McGraw-Hill Book Co., Inc., 1962.
97. Papoulis, A., Probability, Random Variables, and Stochastic Processes, New York: McGraw-Hill Book Co., Inc., 1965.
98. Parzen, E., Stochastic Processes, San Francisco: Holden Day, 1962.
99. Phillips, O.M., "The Equilibrium Range in the Spectrum of Wind-Generated Waves," J. Fluid Mech., Vol. 4, 1958, pp. 426-434.
100. Phillips, O.M., The Dynamics of the Upper Ocean, Cambridge: University Press, 1969.
101. Phillips, O.M., "Wave Interactions," in Nonlinear Waves, ed. by S. Leibovich and A.R. Seebass, Ithaca, N.Y.: Cornell Univ. Press, 1974, pp. 186-211.
102. Pierson, W.J., Jr. and Holmes, P., "Irregular Wave Forces on a Pile," J. Waterways and Harbors Div., Proc. ASCE, Vol. 91, No. WW4, Nov. 1965, pp. 1-10.

103. Pierson, W.J. and Holmes, P., Closure to "Irregular Wave Forces on a Pile," J. Waterways and Harbors Div., Proc. ASCE, Vol. 93, No. WW2, May 1967, pp. 251-252.
104. Plate, E.J. and Nath, J.H., "Modeling Structures Subjected to Wind Waves," J. Waterways and Harbors Div., Proc. ASCE, Vol. 95, No. WW4, Nov. 1969, pp. 491-511.
105. Strutt, J.W. (Baron Rayleigh), The Theory of Sound, 2 Vols., New York: Dover Pub., 1945.
106. Reid, R.O., "Correlation of Water Level Variations with Wave Forces on a Vertical Pile for Nonperiodic Waves," Proc. VI Conf. on Coastal Engr., Univ. Calif., 1958, pp. 749-786.
107. Reid, R.O., Discussion to "Irregular Wave Forces on a Pile," by W.J. Pierson and P. Holmes, J. Waterways and Harbors Div., Vol. 92, No. WW2, May 1966, pp. 55-56.
108. Rellich, F., Perturbation Theory of Eigenvalue Problems, New York: Gordon and Breach Science Publishers, 1969.
109. Rice, S.O., "Mathematical Analysis of Random Noise," Bell Sys. Tech. Jour., Vol. 23, 1944, and Vol. 24, 1945. Reprinted in Selected Papers on Noise and Stochastic Processes, ed. by N. Wax, New York: Dover Pub., Inc., 1954, pp. 133-294.
110. Robinson, E.A., Multichannel Time Series Analysis with Digital Computer Programs, San Francisco: Holden-Day, 1967.
111. Rosenblatt, M., "A Random Model of the Sea Surface Generated by a Hurricane," J. Math. and Mech., Vol. 6, No. 2, 1957, pp. 235-246.
112. Rosenblatt, M., Random Processes, New York: Oxford Univ. Press, 1962.
113. Saffman, P.G., Discussion to "Nonlinear Interactions Treated by the Methods of Theoretical Physics (with application to the generation of waves by wind)," by K. Hasselmann, Proc. Roy. Soc. London, A, Vol. 299, 1967, pp. 101-103.
114. Selna, L. and Cho, D., "Resonant Response of Offshore Structures," J. Waterways, Harbors, and Coastal Engr. Div., Proc. ASCE, Vol. 98, No. WW1, Feb. 1972, pp. 15-24.
115. Sokolnikoff, I.S. and Redheffer, R.M., Mathematics of Physics and Modern Engineering, New York: McGraw-Hill Book Co., 1966.

116. Soong, T.T., Random Differential Equations in Science and Engineering, New York: Academic Press, 1973.
117. St. Denis, M., "On Wind Generated Waves," in Topics in Ocean Engineering, Vol. 1, ed. by C.L. Brotschneider, Houston, Texas: Gulf Publishing Co., 1969, pp. 3-41.
118. St. Denis, M., "Wind and Wave Loads," in Handbook Ocean Engineering, ed. by J.J. Myers, C.H. Holm, and R.F. McAllister, New York: McGraw-Hill Book Co., Inc., 1969, pp. 12:56-12:104.
119. Sveshnikov, A.A., Applied Methods of the Theory of Random Functions, New York: Pergamon Press, 1966.
120. Snyder, R.L., "Covariance Equations for a Linear Sea," J. Mar. Res., Vol. 31, No. 1, 1973, pp. 40-50.
121. Snyder, R.L. and Smith, L., "On the Estimation of Surface Gravity-Wave Field in the Vicinity of an Array of Wave Recorders," J. Mar. Res., Vol. 31, No. 1, 1973, pp. 51-60.
122. Thrasher, L.W. and Aagaard, P.M., "Measured Wave Force Data on Offshore Platforms," Preprints 1969 Offshore Technology Conference, Vol. I, Paper No. OTC1006, May 18-21, 1969, pp. 71-82.
123. Tick, L.J., "A Non-Linear Random Model of Gravity Waves I," J. Math. Mech., Vol. 8, 1959, pp. 643-651.
124. Tick, L.J., "The Estimation of 'Transfer Functions' of Quadratic Systems," Technometrics, Vol. 3, No. 4, Nov. 1961, pp. 563-567.
125. Tick, L.J., "Nonlinear Probability Models of Ocean Waves," in Ocean Wave Spectra, Englewood Cliffs, N.J.: Prentice-Hall, Inc., 1963, pp. 163-169.
126. Titchmarsh, E.C., Introduction to the Theory of Fourier Integrals, 2nd Ed., London: Oxford Univ. Press, 1948.
127. Wehausen, J.V. and Laitone, E.V., Handbook of Physics, Fluid Dynamics III, Vol. IX, Springer-Verlag, 1960, pp. 446-778.
128. Wells, D.R., Discussion to "Wave Forces on Piling for Narrow-Band Spectra," by L.E. Borgman, J. Waterways and Harbors Div., Proc. ASCE, Vol. 92, No. WW1, Feb. 1966, pp. 138-43.

129. Wheeler, J.D., "Method for Calculating Forces Produced by Irregular Waves," Preprints 1969 Offshore Technology Conference, Vol. I, Paper No. OTC1007, May 18-21, 1969, pp. 83-94.
130. Whitham, G.B., "Dispersive Waves and Variational Principles," in Nonlinear Waves, ed. by S. Leibovich and A.R. Seebass, Ithaca, N.Y.: Cornell Univ. Press, 1974, pp. 139-169.
131. Wiener, N., The Fourier Integral and Certain of Its Applications, New York: Dover Pub., Inc., 1958.
132. Wiener, N., Nonlinear Problems in Random Theory, Cambridge, Mass.: The M.I.T. Press, 1958.
133. Wiener, N., Extrapolation, Interpolation, and Smoothing of Stationary Time Series, Cambridge, Mass.: The M.I.T. Press, 1964.
134. Wilks, L.S., Mathematical Statistics, 2nd Ed., New York: John Wiley and Sons, Inc., 1962.
135. Yaglom, A.M., An Introduction to the Theory of Stationary Random Functions, New York: Dover Pub., Inc., 1973.

BIOGRAPHICAL SKETCH

Robert Turner Hudspeth was born 26 November 1940 in Lubbock, Texas. In 1959 he was an honor graduate of the vocational agriculture program of Monterey Senior High School, Lubbock, Texas, and entered the U. S. Naval Academy, Annapolis, Maryland. In 1963 he was graduated with distinction and was commissioned an ensign in the Civil Engineer Corps, U. S. Navy. After a one-year tour as Assistant Resident Officer-in-Charge of Construction, he entered the University of Washington, Seattle, Washington, to begin a two-year study program toward an advanced engineering degree. He received his MSCE in 1966 and began a two-year tour as a company commander in the Seabees in the Republic of Vietnam. After a one-year tour as Aide to the Commander, Naval Facilities Engineering Command, he began a two-year tour in 1969 as Assistant Director, Ocean Engineering Programs, Naval Facilities Engineering Command. During this period, he also served as Assistant Officer-in-Charge and as Engineering Officer for an ocean engineering project in the Azores Islands. In 1971, he entered the University of Florida to begin studying toward a doctorate in Coastal Engineering.

He is married to Heide Barbara, née Bunge, of Köln, Germany, and they are the proud parents of Alexander Robert, to whom their lives and this thesis are dedicated.

I certify that I have read this study and that in my opinion it conforms to acceptable standards of scholarly presentation and is fully adequate, in scope and quality, as a dissertation for the degree of Doctor of Philosophy.

Robert G. Dean
Robert G. Dean, Chairman
Professor of Coastal and
Oceanographic Engineering

I certify that I have read this study and that in my opinion it conforms to acceptable standards of scholarly presentation and is fully adequate, in scope and quality, as a dissertation for the degree of Doctor of Philosophy.

Omar H. Shemdin
Omar H. Shemdin
Professor of Coastal and
Oceanographic Engineering

I certify that I have read this study and that in my opinion it conforms to acceptable standards of scholarly presentation and is fully adequate, in scope and quality, as a dissertation for the degree of Doctor of Philosophy.

Z. R. Pop-Stojanovic
Zoran R. Pop-Stojanovic
Professor of Mathematics

This dissertation was submitted to the Graduate Faculty of the College of Engineering and to the Graduate Council, and was accepted as partial fulfillment of the requirements for the degree of Doctor of Philosophy.

December, 1974

John Arthur
Dean, College of Engineering

Dean, Graduate School

RU 1 26774

#599 See map 24 140